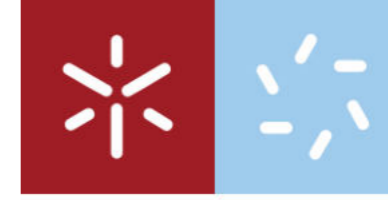




Catarina Pinheiro Macedo

**Development of recombinant protein-
based materials with ability to bind to
cells and to the extracellular matrix**

Universidade do Minho
Escola de Ciências





Universidade do Minho
Escola de Ciências

Catarina Pinheiro Macedo

Development of recombinant protein-based materials with ability to bind to cells and to the extracellular matrix

Dissertação de Mestrado
Mestrado em Genética Molecular

Trabalho efetuado sob a orientação do
Doutor Raul Machado
e do
Doutor André da Costa

junho 2020

DIREITOS DE AUTOR E CONDIÇÕES DE UTILIZAÇÃO DO TRABALHO POR TERCEIROS

Este é um trabalho académico que pode ser utilizado por terceiros desde que respeitadas as regras e boas práticas internacionalmente aceites, no que concerne aos direitos de autor e direitos conexos.

Assim, o presente trabalho pode ser utilizado nos termos previstos na licença abaixo indicada.

Caso o utilizador necessite de permissão para poder fazer um uso do trabalho em condições não previstas no licenciamento indicado, deverá contactar o autor, através do RepositóriUM da Universidade do Minho.



Atribuição-NãoComercial-SemDerivações
CC BY-NC-ND

<https://creativecommons.org/licenses/by-nc-nd/4.0/>

ACKNOWLEDGEMENTS

Aos meus orientadores, Professores André da Costa e Raul Machado, por me terem acolhido no grupo de investigação, por me terem dado a oportunidade de trabalhar neste tema que me entusiasmou desde o início, por toda a ajuda e pelos conselhos que me foram dando durante a execução do trabalho e na escrita da tese.

À Professora Andreia Gomes, pela disponibilidade e pelos conselhos que me deu relativamente à parte relacionada com as experiências com células animais e pela ajuda na interpretação dos resultados obtidos.

Aos colegas do LBM II e do LBA, pela ajuda que me deram ao longo do tempo que passei na bancada. Um agradecimento especial à Maria, à Mafalda e ao Emanuel pelos momentos de boa disposição que ajudaram a superar os momentos menos bons. A todas as pessoas do Departamento de Biologia e do IB-S que, de uma forma ou de outra, me ajudaram quando necessário.

Aos meus amigos, por estarem presentes nos momentos importantes. Um agradecimento especial à Margarida e à Sofia por todos os momentos que passamos juntas ao longo destes anos, pela boa disposição que demonstram sempre, mas também por ouvirem os meus desabafos quando as coisas corriam menos bem.

Aos meus pais, por me terem apoiado incondicionalmente ao longo da minha vida nas escolhas que fui fazendo e por terem tornado possível a realização do mestrado, e ao meu irmão, pelo carinho, apoio e sobretudo pela paciência em me ouvir quando lhe tentava explicar os resultados que obtive. Muito obrigado por tudo.

Ao Pedro, pela paciência, apoio, motivação, mas acima de tudo pelo amor e carinho que tornaram este percurso mais fácil. Obrigada!

Este trabalho foi financiado por fundos nacionais através da FCT – Fundação para a Ciência e a Tecnologia, I.P., no âmbito do projeto "FunBioPlas - Novel synthetic biocomposites for biomedical devices" com referência ERA-IB-2-6/0004/2014.

STATEMENT OF INTEGRITY

I hereby declare having conducted this academic work with integrity. I confirm that I have not used plagiarism or any form of undue use of information or falsification of results along the process leading to its elaboration.

I further declare that I have fully acknowledged the Code of Ethical Conduct of the University of Minho.

ABSTRACT

Development of recombinant protein-based materials with ability to bind to cells and to the extracellular matrix

Tissue engineering is a growing area that primarily targets the creation of functional constructs for tissue repair, using what is known as the triad of tissue engineering: scaffold, cells and signaling molecules. Silk-elastin-like proteins (SELPs) have been gaining interest to be used as scaffolds due to its remarkable properties of biocompatibility, biodegradability and mechanical properties. These genetically engineered biopolymers are composed of tandem repeats of alternated silk- and elastin-like amino acid blocks, combining in the same molecule the tensile strength of silk fibroin with the resilience and water solubility of elastin. In this work, SELP-59-A was genetically engineered to incorporate cell-binding motifs for the formulation of materials with improved cell adhesion ability. Two cell-binding motifs were chosen for the functionalization of SELP-59-A: RGD and C3. The functionalized polymers were used for the production of films by mixing non-functionalized SELP-59-A with different percentages of the functionalized variant. The ability of the films to promote cell adhesion was assessed by culturing cells of the mammalian cell lines HaCaT and SH-SY5Y, for 24 h, on the surface of the materials. The results indicate that adhesion of cells to the films is influenced by factors such as the cell line, adhesion sequence, and concentration of the cell-binding motif. HaCaT adhesion to C3-functionalized films increased with the concentration of cell-binding motif adhesion. On the other hand, the adhesion of HaCaT cells to SELP-59-A_cRGD films showed to increase with adhesion sequence concentration, reaching a maximum at a concentration of 50% of SELP-59-A_cRGD, and remaining stable at higher concentrations. Similarly to HaCaT cells, when incubated on SELP-59-A_nC3 films, the number of SH-SY5Y cells adhered to the films increased with the concentration of cell-binding motif. However, when incubated onto SELP-59-A_cC3 and SELP-59-A_cRGD films, no relation was found between the concentration of adhesion sequence and the number of SH-SY5Y cells adhered to the films. As a whole, the results point to the potential of using SELP-59-A functionalized with cell-binding motifs as biomaterials with improved cell adhesion ability.

Keywords: C3, cell adhesion, recombinant polymer, RGD, SELP

RESUMO

Desenvolvimento de materiais de base proteica com capacidade de ligar a células e à matriz extracelular

A engenharia de tecidos é uma área em crescimento que visa principalmente a criação de construções funcionais para a reparação de tecidos, utilizando aquilo que é conhecido como a tríade da engenharia de tecidos: *scaffold*, células e moléculas sinalizadoras. Os polímeros de seda e elastina (*silk-elastin-like proteins, SELPs*) têm despertado interesse para serem usados como *scaffold* devido às suas propriedades notáveis tais como a biocompatibilidade, biodegradabilidade e propriedades mecânicas. Estes polímeros geneticamente desenhados são compostos por repetições em tandem de blocos de aminoácidos semelhantes à seda e à elastina, combinando na mesma molécula a força tênsil da fibroína da seda com a resiliência e solubilidade em água da elastina. Neste trabalho, o SELP-59-A foi alterado geneticamente para incorporar motivos de adesão celular para a formulação de materiais com maior capacidade de adesão celular. Foram escolhidos dois motivos de adesão para funcionalizar o SELP-59-A: RGD e C3. Os polímeros funcionalizados foram utilizados para a produção de filmes misturando diferentes percentagens de SELP-59-A não funcionalizado com a sua variante funcionalizada. A capacidade dos filmes para promover a adesão celular foi avaliada cultivando células das linhas celulares de mamífero HaCaT e SH-SY5Y, durante 24 h, na superfície dos materiais. Os resultados indicam que a adesão das células aos filmes é influenciada por fatores como a linha celular, a sequência de adesão, e a concentração de motivo de adesão celular. A adesão das HaCaT aos filmes funcionalizados com C3 aumentou com a concentração de motivo de adesão. Por outro lado, a adesão das células HaCaT aos filmes SELP-59-A_cRGD aumentou com a concentração de sequência de adesão, atingindo o valor máximo com a concentração de 50% de SELP-59-A_cRGD, e permanecendo estável em concentrações superiores. Analogamente às células HaCaT, quando incubadas em filmes SELP-59-A_nC3, o número de células SH-SY5Y aderidas aos filmes aumenta com a concentração de motivo de adesão. No entanto, quando incubadas em filmes SELP-59-A_cC3 e SELP-59-A_cRGD, não foi encontrada uma relação entre a concentração de sequência de adesão e o número de células SH-SY5Y aderidas aos filmes. De modo geral, os resultados apontam para o potencial da utilização de SELP-59-A funcionalizado com motivos de adesão celular como biomaterial com maior capacidade de adesão celular.

Palavras-chave: adesão celular, C3, polímero recombinante, RGD, SELP

TABLE OF CONTENTS

ACKNOWLEDGEMENTS	iii
STATEMENT OF INTEGRITY	iv
ABSTRACT.....	v
RESUMO.....	vi
LIST OF FIGURES	ix
LIST OF TABLES	xiii
LIST OF COMMON ABBREVIATIONS.....	xiv
1. INTRODUCTION.....	2
1.1. SCAFFOLDS.....	3
1.1.1. Protein-based polymers.....	5
1.1.1.1. Silk-elastin-like proteins.....	6
1.2. SIGNALING MOLECULES.....	8
1.2.1. Cell adhesion.....	8
1.2.1.1. Cell-cell adhesion.....	9
1.2.1.2. Cell-ECM adhesion.....	10
1.2.1.3. Adhesion sequences.....	12
1.3. CELLS.....	14
2. AIMS	18
3. MATERIALS AND METHODS	20
3.1. BIOLOGICAL MATERIALS.....	20
3.1.1. Microorganisms	20
3.1.2. Mammalian cell lines	21
3.2. CLONING STRATEGY.....	21
3.2.1. pET25b(+) digestion	21
3.2.2. Design and digestion of <i>adapter</i> sequence.....	22
3.2.3. Ligation of the <i>adapter</i> and pET25b(+)	23
3.2.4. Digestion of pET25:: <i>adapter</i>	24
3.2.5. SELP extraction from pDrive:: <i>SELP-59-A</i> plasmid	24
3.2.6. <i>SELP-59-A</i> sequence extension.....	24

3.2.7.	Ligation of pET25:: <i>adapter</i> and <i>SELP-59-A</i>	25
3.2.8.	pET25:: <i>SELP-59-A</i> digestion	25
3.2.9.	Adhesion sequences design and insertion into pET25:: <i>SELP-59-A</i>	26
3.3.	EVALUATION OF PROTEIN PRODUCING LEVELS	27
3.3.1.	SELP-59-A_nRGD production optimization	29
3.4.	PROTEIN PRODUCTION	29
3.5.	PROTEIN PURIFICATION	29
3.6.	PROTEIN PURIFICATION OPTIMIZATION.....	30
3.7.	SOLVENT CASTING AND POST-PROCESSING TREATMENT OF FILMS	30
3.8.	FILM CHARACTERIZATION	31
3.9.	MAMMALIAN CELL LINES STAINING OPTIMIZATION	32
3.10.	EVALUATION OF THE EFFECT OF THE CELL'S FIXATION PROCESS ON FILM STRUCTURE AND STAINING....	33
3.11.	CELL ADHESION ASSAYS	33
4.	RESULTS AND DISCUSSION	36
4.1	CREATION OF RECOMBINANT PROTEIN-BASED POLYMERS BASED ON SILK AND ELASTIN INTEGRATING DIFFERENT CELL BINDING MOTIFS.....	36
4.1.1	Adhesion sequences selection	36
4.1.2	Design of genetic constructions	39
4.2	PRODUCTION AND PURIFICATION OF THE CREATED MATERIALS.....	46
4.2.1	Production of recombinant polymers	46
4.2.2.	Polymer purification	53
4.2.3.	Processing of the polymers	56
4.3	EVALUATION OF CELL AND ECM-BINDING ACTIVITY OF SELP-59-A_CAM FILMS USING MAMMALIAN CELL CULTURES	59
4.3.1	Mammalian cell lines staining optimization	59
4.3.2	Assessment of the effect of the cell's fixation process on film structure and staining.....	63
4.3.3	Cell adhesion assays.....	68
5.	CONCLUSIONS AND FUTURE PERSPECTIVES	77
6.	REFERENCES	80
7.	ANNEXES AND APPENDIXES.....	100

LIST OF FIGURES

FIGURE 1. ENGINEERING STRATEGIES IN TISSUE REGENERATION FOR DIFFERENT TISSUE FORMATION	2
FIGURE 2. REPRESENTATION OF SELP-59-A CONSTRUCT.....	7
FIGURE 3. <i>IN VITRO</i> CELL ADHESION STAGES	9
FIGURE 4. CELL-MATRIX JUNCTIONS MEDIATED BY INTEGRINS	12
FIGURE 5. SCHEMATIC REPRESENTATION OF FILM PREPARATION PROCESS.	31
FIGURE 6. 24-WELL PLATE SCHEME USED FOR CELL STAINING OPTIMIZATION.....	32
FIGURE 7. SCHEMATIC REPRESENTATION OF THE CONSTRUCTIONS DESIGNED.....	39
FIGURE 8. SCHEMATIC REPRESENTATION OF THE ADAPTER DESIGNED, DEPICTING RECOGNITION SEQUENCES FOR RESTRICTION ENZYMES.	40
FIGURE 9. <i>ADAPTER</i> SEQUENCE IN A 1% AGAROSE GEL.....	41
FIGURE 10. pET25:: <i>ADAPTER</i> DIGESTED WITH <i>Ppu21I</i>	41
FIGURE 11. pET25:: <i>ADAPTER</i> PLASMID DIGESTED WITH <i>Eco72I</i>	42
FIGURE 12. pET25:: <i>SELP-59-A</i> DIGESTED WITH <i>Ppu21I</i> AND <i>HindIII</i>	43
FIGURE 13. pET25:: <i>SELP-59-A</i> PLASMID DIGESTED WITH <i>NdeI</i>	43
FIGURE 14. ADHESION SEQUENCES IN A 1% AGAROSE GEL	44
FIGURE 15. LIGATION CONFIRMATION OF THE ADHESION SEQUENCES.....	45
FIGURE 16. SDS-PAGE ANALYSIS OF SELP-59-A PRODUCTION IN <i>E. COLI</i> /BL21 (DE3) pET25:: <i>SELP-59-A</i> TRANSFORMANTS AFTER 22 H AT 200 RPM AND 37 °C IN TBLAC MEDIUM.....	46
FIGURE 17. SDS-PAGE ANALYSIS OF SELP-59-A _{CC3} PRODUCTION IN <i>E. COLI</i> /BL21 (DE3) pET25:: <i>SELP-59-</i> <i>A_{CC3}</i> TRANSFORMANTS AFTER 22 H AT 200 RPM AND 37 °C IN TBLAC MEDIUM.....	47
FIGURE 18. SCREENING OF SELP-59-A _{NC3} PRODUCTION IN SEVERAL COLONIES OF <i>E. COLI</i> /BL21 (DE3) AFTER 22 H AT 200 RPM AND 37 °C IN TBLAC MEDIUM	48
FIGURE 19. PRODUCTION SCREENING OF SELP-59-A _{CRGD} IN <i>E. COLI</i> /BL21 (DE3) pET25:: <i>SELP-59-A_{CRGD}</i> TRANSFORMANTS AFTER 22 H AT 200 RPM AND 37 °C IN TBLAC MEDIUM.....	49
FIGURE 20. SDS-PAGE ANALYSIS OF SELP-59-A _{NRGD} PRODUCTION IN <i>E. COLI</i> /BL21 (DE3) pET25:: <i>SELP-59-</i> <i>A_{NRGD}</i> TRANSFORMANTS AFTER 22 H AT 200 RPM AND 37 °C IN TBLAC MEDIUM	50
FIGURE 21. PRODUCTION SCREENING OF SELP-59-A _{NRGD} IN <i>E. COLI</i> /C43 (DE3) pRARE pET25:: <i>SELP-59-</i> <i>A_{CRGD}</i> TRANSFORMANTS AFTER 22 H AT 200 RPM AND 37 °C IN TBLAC MEDIUM	51
FIGURE 22. PRODUCTION SCREENING OF SELP-59-A _{NRGD} IN <i>E. COLI</i> /ORIGAMI B (DE3) pET25:: <i>SELP-59-</i> <i>A_{CRGD}</i> TRANSFORMANTS AFTER 22 H AT 200 RPM AND 37 °C IN TBLAC MEDIUM	52

FIGURE 23. PRODUCTION SCREENING OF SELP-59-A_NRGD IN <i>E. COLI</i> /BL21 (DE3) pLYSE PET25:: <i>SELP-59-A_CRGD</i> TRANSFORMANTS AFTER 22 H AT 200 RPM AND 37 °C IN TBLAC MEDIUM	53
FIGURE 24. PURIFICATION OF THE SELP-59-A_CC3 POLYMER BY AMMONIUM SULPHATE PRECIPITATION	54
FIGURE 25. PURIFICATION OF THE SELP-59-A_CRGD POLYMER BY AMMONIUM SULPHATE PRECIPITATION	54
FIGURE 26. PURIFICATION OF THE SELP-59-A_NC3 POLYMER BY AMMONIUM SULPHATE PRECIPITATION	55
FIGURE 27. VISUAL ASPECT OF METHANOL-TREATED FILMS.	57
FIGURE 28. EXPERIMENTALLY DETERMINED AMIDE I REGION ATR-FTIR ABSORBANCE SPECTRA FOR THE NON-TREATED AND METHANOL SATURATED AIR-TREATED FILMS	58
FIGURE 29. BRIGHTFIELD AND FLUORESCENT MICROGRAPHS OF HACAT CELLS STAINED WITH HOECHST 34580 FOR DIFFERENT TIME POINTS, VISUALIZED WITH 100X AMPLIFICATION	60
FIGURE 30. BRIGHTFIELD AND FLUORESCENT MICROGRAPHS OF HACAT CELLS STAINED WITH DAPI FOR DIFFERENT CONCENTRATIONS AND TIME POINTS, VISUALIZED WITH 100X AMPLIFICATION.....	61
FIGURE 31. BRIGHTFIELD AND FLUORESCENT MICROGRAPHS OF SH-SY5Y CELLS STAINED WITH HOECHST 34580 FOR DIFFERENT TIME POINTS, VISUALIZED WITH 200X AMPLIFICATION.....	62
FIGURE 32. BRIGHTFIELD AND FLUORESCENT MICROGRAPHS OF SH-SY5Y CELLS STAINED WITH DAPI FOR DIFFERENT CONCENTRATIONS AND TIME POINTS, VISUALIZED WITH 200X AMPLIFICATION.....	63
FIGURE 33. FLUORESCENCE OVERLAY MICROGRAPHS OF SELP-59-A 100% FILMS TREATED AND NON-TREATED WITH THE REAGENTS USED FOR CELL FIXATION AND STAINING WITH HOECHST 34580 AND PHALLOIDIN, AFTER INCUBATION FOR 24 H WITH DMEM AT 37 °C, VISUALIZED WITH 100X AMPLIFICATION.....	64
FIGURE 34. FLUORESCENCE OVERLAY MICROGRAPHS OF SELP-59-A_CC3 FILMS TREATED AND NON-TREATED WITH THE REAGENTS USED FOR CELL FIXATION, AFTER INCUBATION FOR 24 H WITH DMEM AT 37 °C, VISUALIZED WITH 100X AMPLIFICATION.....	65
FIGURE 35. FLUORESCENCE OVERLAY MICROGRAPHS OF SELP-59-A_NC3 FILMS TREATED AND NON-TREATED WITH THE REAGENTS USED FOR CELL FIXATION, AFTER INCUBATION FOR 24 H WITH DMEM AT 37 °C, VISUALIZED WITH 100X AMPLIFICATION.....	66
FIGURE 36. FLUORESCENCE OVERLAY MICROGRAPHS OF SELP-59-A_CRGD FILMS TREATED AND NON-TREATED WITH THE REAGENTS USED FOR CELL FIXATION, AFTER INCUBATION FOR 24 H WITH DMEM AT 37 °C, VISUALIZED WITH 100X AMPLIFICATION.....	67
FIGURE 37. BRIGHTFIELD AND FLUORESCENCE MICROGRAPHS OF HACAT CELLS SEEDED AND CULTURED ON SURFACE SELP-59-A_CRGD FILMS FOR 24 H, STAINED WITH HOECHST 34580 AND PHALLOIDIN, VISUALIZED WITH 100X AMPLIFICATION	69

FIGURE 38. BRIGHTFIELD AND FLUORESCENCE MICROGRAPHS OF HACAT CELLS SEEDED AND CULTURED ON SURFACE SELP-59-A_NC3 FILMS FOR 24 H, STAINED WITH HOECHST 34580 AND PHALLOIDIN, VISUALIZED WITH 100X AMPLIFICATION	71
FIGURE 39. BRIGHTFIELD AND FLUORESCENCE MICROGRAPHS OF HACAT CELLS SEEDED AND CULTURED ON SURFACE SELP-59-A_CC3 FILMS FOR 24 H, STAINED WITH HOECHST 34580 AND PHALLOIDIN, VISUALIZED WITH 100X AMPLIFICATION	72
FIGURE 40. BRIGHTFIELD MICROGRAPHS OF SH-SY5Y CELLS SEEDED AND CULTURED ON SURFACE SELP-59-A_NC3 FILMS FOR 24 H, VISUALIZED WITH 200X AMPLIFICATION	73
FIGURE 41. BRIGHTFIELD MICROGRAPHS OF SH-SY5Y CELLS SEEDED AND CULTURED ON SURFACE SELP-59-A_CC3 FILMS FOR 24 H, VISUALIZED WITH 200X AMPLIFICATION	74
FIGURE 42. BRIGHTFIELD MICROGRAPHS OF SH-SY5Y CELLS SEEDED AND CULTURED ON SURFACE SELP-59-A_CRGD FILMS FOR 24 H, VISUALIZED WITH 200X AMPLIFICATION.....	75
FIGURE 43. SCHEMATIC REPRESENTATION OF PET25B(+) PLASMID	103
FIGURE 44. SCHEMATIC REPRESENTATION OF PCM13:: <i>SELP-59-A</i> PLASMID	104
FIGURE 45. SCHEMATIC REPRESENTATION OF PLYSE PLASMID	105
FIGURE 46. SCHEMATIC REPRESENTATION OF PRARE PLASMID	106
FIGURE 47. SCHEMATIC REPRESENTATION OF PDRIVE:: <i>SELP-59-A</i> PLASMID	107
FIGURE 48. SCHEMATIC REPRESENTATION OF PET25:: <i>ADAPTER</i> PLASMID.....	108
FIGURE 49. SCHEMATIC REPRESENTATION OF PET25:: <i>SELP-59-A</i> PLASMID	109
FIGURE 50. SCHEMATIC REPRESENTATION OF PET25:: <i>SELP-59-A+SELP-59-A</i> PLASMID.....	110
FIGURE 51. SCHEMATIC REPRESENTATION OF PET25:: <i>SELP-59-A_NC3</i> PLASMID	111
FIGURE 52. SCHEMATIC REPRESENTATION OF PET25:: <i>SELP-59-A_CC3</i> PLASMID	112
FIGURE 53. SCHEMATIC REPRESENTATION OF PET25:: <i>SELP-59-A_NRGD</i> PLASMID.....	113
FIGURE 54. SCHEMATIC REPRESENTATION OF PET25:: <i>SELP-59-A_CRGD</i> PLASMID.....	114
FIGURE 55. PET25:: <i>ADAPTER</i> SEQUENCING CHROMATOGRAM USING T7 PROMOTER PRIMER.....	119
FIGURE 56. PET25:: <i>SELP-59-A</i> SEQUENCING CHROMATOGRAM USING T7 PROMOTER PRIMER.....	120
FIGURE 57. PET25:: <i>SELP-59-A</i> SEQUENCING CHROMATOGRAM USING T7 TERMINATOR PRIMER	121
FIGURE 58. PET25:: <i>SELP-59-A+SELP-59-A</i> (DOUBLE INSERTION) SEQUENCING CHROMATOGRAM USING T7 PROMOTOR PRIMER.....	122
FIGURE 59. PET25:: <i>SELP-59-A+SELP-59-A</i> (DOUBLE INSERTION) SEQUENCING CHROMATOGRAM USING T7 TERMINATOR PRIMER.....	123
FIGURE 60. PET25:: <i>SELP-59-A_NC3</i> SEQUENCING CHROMATOGRAM USING T7 PROMOTOR PRIMER.....	124

FIGURE 61. pET25::*SELP-59-A_cC3* SEQUENCING CHROMATOGRAM USING T7 TERMINATOR PRIMER 125

FIGURE 62. pET25::*SELP-59-A_NRGD* SEQUENCING CHROMATOGRAM USING T7 PROMOTOR PRIMER 126

FIGURE 63. pET25::*SELP-59-A_cRGD* SEQUENCING CHROMATOGRAM USING T7 TERMINATOR PRIMER..... 127

FIGURE 64. EXPERIMENTALLY DETERMINED ATR-FTIR ABSORBANCE SPECTRA FOR AMIDE I REGION FOR THE NON-TREATED AND METHANOL SATURATED AIR-TREATED SELP-59-A_CAM 75%, SELP-59-A_CAM 25% FILMS. 128

LIST OF TABLES

TABLE 1. ADVANTAGES AND DISADVANTAGES OF EACH GROUP OF BIOMATERIALS	4
TABLE 2. EXAMPLES OF AMINO ACID REPEATING BLOCKS FOUND IN NATURAL STRUCTURAL PROTEINS.....	6
TABLE 3. INTEGRIN TYPES AND THEIR RESPECTIVE LIGANDS	11
TABLE 4. INTEGRINS AND PROTOTYPIC LIGANDS/CELL ADHESION SEQUENCES	13
TABLE 5. STRAINS USED FOR CLONING STEPS AND PROTEIN PRODUCTION AND ITS GENOTYPE.....	20
TABLE 6. PLASMIDS USED FOR GENE CLONING AND EXPRESSION	20
TABLE 7. PRIMERS USED TO OBTAIN THE ADAPTER AND ADHESION MOTIFS DNA SEQUENCES.....	22
TABLE 8. REAGENTS USED TO PERFORM PCR	22
TABLE 9. PCR CONDITIONS USED TO PERFORM PCR TO PRODUCE ADAPTER SEQUENCE	23
TABLE 10. PCR CONDITIONS TO OBTAIN NC3 ADHESION SEQUENCE	26
TABLE 11. PCR CONDITIONS TO OBTAIN <i>CC3</i> ADHESION SEQUENCE.....	26
TABLE 12. PCR CONDITIONS TO OBTAIN <i>NRGD</i> ADHESION SEQUENCE	27
TABLE 13. PCR CONDITIONS TO OBTAIN <i>cRGD</i> ADHESION SEQUENCE	27
TABLE 14. REAGENTS USED FOR THE ELABORATION OF ONE 10% SDS-PAGE GEL	28
TABLE 15. DIFFERENT FILMS PRODUCED BY COMBINATION OF SELP-59-A AND FUNCTIONALIZED POLYMERS	31
TABLE 16. ADHESION SEQUENCES CONTAINING RGD MOTIF USED TO FUNCTIONALIZE RECOMBINANT POLYMERS	37
TABLE 17. SEQUENCES INVOLVED IN CELL ADHESION SPECIFIC FOR CELLS OF THE NERVOUS SYSTEM	38

LIST OF COMMON ABBREVIATIONS

Amp	Ampicillin
Amp ^R	Ampicillin Resistance
ATCC	American Type Culture Collection
ATR-FTIR	Attenuated Total Reflectance – Fourier Transform Infrared
CAM	Cell Adhesion Molecule
d	days
Da	Dalton
DAPI	4',6-diamino-2-phenylindole
DMEM	Dulbecco's Minimal Essential Medium
DNA	Deoxyribonucleic Acid
EC	Human dermal microvascular endothelial cells
ECM	Extracellular Matrix
EGF	Epithelial Cell Growth Factor
ELPs	Elastin-like Protein
ELRs	Elastin-like Recombinamer
ESCs	Embryonic Stem Cells
FBS	Fetal Bovine Serum
FGF	Fibroblast Growth Factor
FGFR	Fibroblast Growth Factor Receptor
FS	Filtered Solution
HA	Hydroxyapatite
HSCs	Hematopoietic Stem Cells
HSPC	Heparan Sulphate Proteoglycan
ICAM	Intracellular Adhesion Molecules
IPTG	Isopropyl β -D-1-thiogalactopyranoside
ITT	Inverse Temperature Transition
Kan	Kanamycin
Kan ^R	Kanamycin Resistance
kb	kilobases
KC	Human dermal keratinocytes from adult skin

lac	α -lactose
LB	Lysogeny Broth
MadCAM	Addressin Cell Adhesion Molecules
MAP	Mussel Adhesion Protein
MIT	Massachusetts Institute of Technology
MSCs	Mesenchymal Stem Cells
MWM	Molecular Weight Marker
NCAM	Neural Cell Adhesion Molecule
NIH	American National Institute of Health
OD	Optical Density
PBPs	Protein-based Polymers
PBS	Phosphate-Buffered Saline Solution
PCR	Polymerase Chain Reaction
pDNA	plasmid Deoxyribonucleic Acid
PES	Polyethersulfone
rPBPs	Recombinant Protein-based Polymers
rpm	rotations per minute
SDS	Sodium Dodecyl Sulphate
SDS-PAGE	Sodium Dodecyl Sulphate - Polyacrylamide Gel Electrophoresis
SELP	Silk-elastin-like Protein
SLP	Silk-like Protein
T25	25 cm ² tissue culture flask
T75	75 cm ² tissue culture flask
TAE	Tris-Acetate-EDTA
TB	Terrific Broth
TCP	Tri-calcium Phosphate
TE	Tris-EDTA
T _i	Transition Temperature
v/v	volume per volume
VCAM	Vascular Cell Adhesion Molecule
VEGF	Vascular Endothelial Cell Growth Factor
w/v	weight per volume

wt%

weight percentage

1. Introduction

1. INTRODUCTION

Tissue Engineering is thought to be born more than 30 years ago at the Massachusetts Institute of Technology (MIT) when a group of scientists began researching in the area of living skin equivalents, driven by the lack of organ donors¹. Currently, tissue engineering is applied to the creation of functional constructs for tissue repair, to the study of stem cell behavior and provides models for studying numerous diseases². It makes use of what is known as the triad of tissue engineering: scaffold, cells and signaling molecules³. Tissue engineering combines principles from different areas including bioengineering, materials engineering and cell transplantation, integrating biological and artificial components to recreate the conditions present in the native body tissue⁴ (Figure 1). Using these principles it is possible to successfully regenerate several tissues including skin⁴⁻⁶, bone^{7,8}, cartilage^{9,10}, fatty tissues^{11,12}, nerve¹³, liver¹⁴ and cardiac tissue^{15,16}.

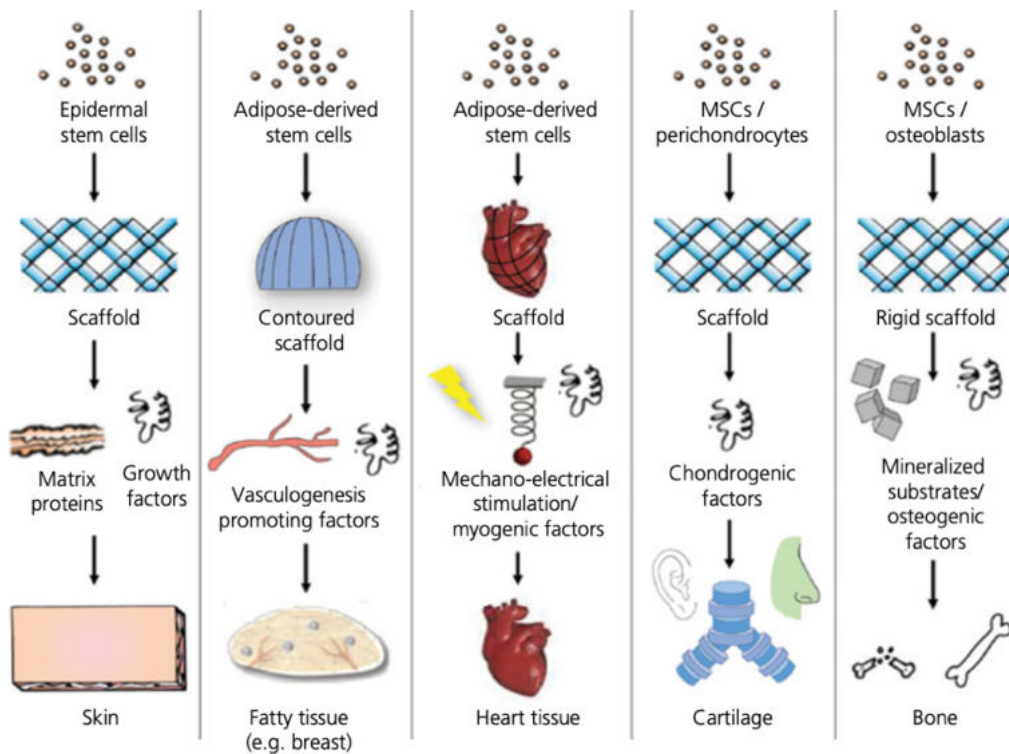


Figure 1. Engineering strategies in tissue regeneration for different tissue formation. MSCs: mesenchymal stem cells. Reproduced from ¹.

1.1. SCAFFOLDS

Some tissues and organs can be regenerated by cell injection to a target site. This is used in the case of diseases of the hematopoietic system, of capillary or small blood vessels like arterioles or even diseases related with cardiovascular system malfunction¹⁷. Nevertheless, these cases are relatively rare. The majority of large-sized tissues and organs with a defined three-dimensional structure require the existence of a support to sustain cell growth. This support is often termed as scaffold, template or artificial extracellular matrix¹⁷.

Scaffolds are engineered, preferable biodegradable, materials that provide a template for initial cell attachment and subsequent tissue ingrowth while (i) promote cell survival, proliferation and differentiation with minimum inflammation and toxicity to the host in its original and biodegraded forms; (ii) promote cell interaction, viability and extracellular matrix (ECM) deposition; (iii) allow the transport or delivery of gases, body liquids, nutrients and growth factors; and (iv) continue to offer structural support while being degradable at appropriate rates for tissue regeneration¹⁸⁻²⁰.

Although scaffolds are relatively successful at providing a structure for initial cell adherence, the lack of physical and chemical characteristics that are usually found in the ECM limits the capacity of the cells to regenerate or create a tissue¹⁷. In order to increase cell response to scaffolds, researchers began developing dynamic structures that do not only provide a mechanical support but also act on cells, actively stimulating and guiding tissue regeneration²¹ since they mimic the molecular environment of tissues, thus providing the ideal conditions for tissue regeneration¹. Currently, scaffolds are functional biomimetic structures with nanostructured surfaces incorporating bioactive agents that allow a finer control over cellular positioning, organization and interaction²².

Biomaterials play a central role in tissue engineering as base materials for the development of scaffolds²³. The most accepted definition of a biomaterial is the one employed by the American National Institute of Health (NIH) that describes a biomaterial as “any substance or combination of substances, other than drugs, synthetic or natural in origin, which can be used for any period of time, which augments or replaces partially or totally any tissue, organ or function of the body, in order to maintain or improve the quality of life of the individual”²⁴.

Usually, three groups of biomaterials are used in the fabrication of scaffolds: ceramics, synthetic polymers and natural polymers, each one with its own specific advantages and disadvantages²⁵ (Table 1).

Due to their mechanical properties, ceramics are mainly used in dental and orthopedic surgery. Their main application comprises the filling of bone defects and the coating of metallic implant surfaces to improve implant integration with the host bone²⁵. For bone regeneration applications, scaffolds composed

of ceramics such as hydroxyapatite (HA)²⁶ and tri-calcium phosphate (TCP)²⁷ are widely used. Ceramic scaffolds are characterized by high mechanical stiffness, very low elasticity and hard brittle surface²⁵. They display excellent biocompatibility and enhance bone regeneration, but their application for tissue engineering has been limited because of their brittleness, difficulty of shaping for implantation and low control in their degradation rate²⁵.

Table 1. Advantages and disadvantages of each group of biomaterials. Adapted from ^{25,28-31}.

Biomaterials	Advantages	Disadvantages
Ceramics	<ul style="list-style-type: none"> • High initial mechanical strength • Excellent biocompatibility to bone implantation • Enhance osteoblast differentiation and proliferation 	<ul style="list-style-type: none"> • Potential undesired inflammatory response • Significant reduction on their mechanical properties over time • Difficulty of shaping • Brittleness • Difficulty to control degradation rate
Synthetic polymers	<ul style="list-style-type: none"> • Easily tailored • Easily processable • Easily sterilizable • Surface modifiable • Controlled degradation rate • Low production costs 	<ul style="list-style-type: none"> • Risk of rejection due to reduced bioactivity • Mostly hydrophobic • Potential toxic degraded form • Potential immunological reaction
Natural polymers	<ul style="list-style-type: none"> • Biologically active • Usually promote excellent cell adhesion and growth • Biodegradability • Allow host cells to produce their own ECM and replace the degraded scaffold 	<ul style="list-style-type: none"> • Difficulty to obtain homogeneous and reproducible structures • High production costs • Inadequate mechanical properties • Risk of contamination

Numerous synthetic polymers have been used to produce scaffolds, including poly-L-lactic acid (PLLA)^{32,33}, polystyrene^{13,34-36}, polyethylene glycol (PEG)³⁷, polyglycolic acid (PGA)^{38,39} and poly-DL-lactic-co-glycolic acid (PLGA)⁴⁰. The success of these materials relies on the possibility of tailoring their architecture and controlling their degradation rate. However, they display reduced bioactivity and are mostly hydrophobic^{25,28}. Moreover, the degradation process by non-enzymatic hydrolysis of some synthetic polymers such as PLLA and PGA originates intermediate degradation products as lactic acid and/or glycolic acid, which reduces the local pH and induces an inflammatory reaction that can result in the acceleration of the polymer's degradation rate and cell and tissue necrosis^{25,41}.

Natural polymers are a third group of commonly used biomaterials. In nature, macromolecules such as polysaccharides and proteins are involved in tissue structural support, cell adhesion and migration, and chemokine storage and release²⁹. This makes them appealing to be used as materials for scaffolds, as they should provide similar functions for engineered tissues²⁹. Natural polymers such as collagen⁴², proteoglycans⁴³, alginate-based substrates⁴⁴ and chitosan^{13,45,46} have been used for the production of scaffolds directed for tissue engineering. Natural polymers are biologically active and typically promote excellent cell adhesion and growth^{47,48}. In most cases, they are biocompatible, biodegradable and allow host cells to produce their own ECM over time and replace the degraded scaffold²⁵. However, it is a challenge to produce scaffolds from biological materials with homogeneous and reproducible structures²⁵. Furthermore, extraction of these polymers from the natural sources is laborious, in some cases expensive, and results in low yields and ethical issues⁴⁹.

1.1.1. Protein-based polymers

In nature, structural materials are assembled from several classes of biological macromolecules such as nucleotides, polysaccharides and proteins. Among these molecules, structural proteins arise as a versatile and functional class.

The examination of the structure of natural structural fibrillar proteins and the elucidation of structure-property relationship disclosed the presence of short repeating amino acid sequences that form specific higher-order structures by intermolecular or intramolecular interactions, largely responsible for the unique physical properties of the natural proteins⁵⁰⁻⁵² (Table 2). These oligopeptide sequences encode a basic structural property that allows specific interactions to occur between similar oligopeptides. The repetition of the amino acid sequence propagates the structural property over the polypeptide chain⁵¹⁻⁵³. The assembly of similar structural chains creates a macromolecular polymeric material, in which the physical and mechanical properties are determined by the repeating amino acid sequence. As example, collagen triple-helix formation requires the repeating sequence -Gly-Xaa-Yaa (Xaa and Yaa can be any amino acid however, Xaa is often proline and Yaa hydroxyproline). The formation of hydrogen bonds between the backbone NH-group of glycine and the backbone CO of the residue in X-position of a neighboring chain is the major source of stability that results in mechanical properties such as stiffness^{54,55}. Silk fibroin repeating amino acid sequences form antiparallel β -sheet structures stabilized by hydrogen bonding, which results in a crystalline and mechanical strong material⁵⁶.

Table 2. Examples of amino acid repeating blocks found in natural structural proteins. Adapted from ^{50-52,57}.

Protein family	Repeat sequences/building block	Secondary Structure
Elastin	VPGVG, GVGVP, VPGG, APGVGV	β -spirals
Resilin	GGRPSDSYGAPGGGN, GYSGGRPGGQDLG	β -turns
Silk fibroin	GAGAGS	β -sheets
Dragline silk	polyalanine, GA / GGX / GPGXX	β -sheets / helices / β -turns
Collagen	GXaaYaa	Triple-helices
Keratin	MKQLEDK, VEELLSK, NYHLENE, VARKLKKL	Twisted-helices

Note: X, Xaa and Yaa can be any amino acid. The amino acids in the Xaa and Yaa positions of collagen are often proline and hydroxyproline, respectively.

Protein-based polymers (PBPs) are created by inspiration of these repetitive amino acidic sequences/building blocks found in fibrous proteins, offering an abundance of different mechanical properties that, together with its intrinsic biocompatibility, minimal cytotoxicity and controllable degradation, makes them potential materials for several uses⁵⁸⁻⁶¹. Consequently, PBPs have been intensively explored for biomedical applications and are expected to substitute synthetic polymers in many applications⁵⁶.

Through the years, materials scientists investigated the possibility of obtaining higher levels of control in polymer synthesis⁶². Advances in protein engineering and recombinant DNA technology allow the design and production of recombinant protein-based polymers (rPBPs) with absolute control of their molecular weight and stereochemistry, which allows the control of their properties^{63,64}. rPBPs are usually inspired by naturally occurring fibrous proteins such as silk⁶⁵⁻⁶⁸, elastin⁶⁹⁻⁷¹ and collagen⁷²⁻⁷⁴ and make use of the repetitive amino acid sequence motifs responsible for the physical and mechanical properties of the polymeric material^{56,75}.

1.1.1.1. Silk-elastin-like proteins

Silk-elastin-like proteins (SELPs) are a family of rPBPs composed of repetitive GAGAGS (G: glycine, A: L-alanine, S: L-serine) amino acid sequences found in silk fibroin and mammalian elastin conserved motif VPGVG (V: L-valine, P: L-proline)⁷⁶. The silk fibroin repetitive block is found in the silkworm *Bombyx mori* and spontaneously self-assembles into packed antiparallel β -sheet structures, stabilized by hydrogen bonding, providing crystallinity and mechanical strength^{56,64}. The elastin-like block is inspired by mammalian tropoelastin and consists of the pentapeptide VPGXG, where X, termed the guest residue, is any natural amino acid except proline⁶³. SELPs are designed to combine the crystallinity and mechanical strength of silk with the high resilience and water solubility of elastin in a single structure^{56,64}. The

macromolecular properties of the polymer are controlled by the proportions, number and sequence of these repeated motifs^{58,77}.

The elastin-based pentapeptide is a flexible component that has been reported to form β -turns, conferring elasticity⁷⁸. In the poly-pentapeptide, the β -turns are repeated regularly and act as spacers between the turns of the spiral, suspending chain segments in a relatively kinetically free state⁷⁹. The periodic introduction of elastin-like units in SELP sequence reduces the overall crystallinity of the system by disrupting the silk-like blocks and consequently increasing its flexibility and water solubility^{56,64}. The formulation of these copolymers is usually represented by the nomenclature [(S)x(E)y]_n, where S represents the silk block, x: the number of silk blocks; E represents the elastin-like block, y: the number of elastin-like blocks, and n is the number of repetitions of the overall copolymer^{50,56}.

SELP-59-A is a copolymer with formulation (S₅E₉)₉, consisting of nine tandem repetitions of five silk- and nine elastin-like blocks with sequences GAGAGS and VPAVG, respectively (Figure 2). The substitution of the central glycine (G) in the elastin sequence by L-alanine (A) demonstrated to significantly alter the mechanical properties and the thermoresponsive behavior of elastin-like polypeptides, resulting in unique properties. Elastin-like polypeptides (ELPs), also termed elastin-like recombinamers (ELRs), are composed of multiple repetitions of elastin-like blocks (typically with sequence VPGXG) and display a reversible inverse temperature transition (ITT) behavior in aqueous solutions, *i.e.* at temperatures above a specific threshold, the transition temperature (T_i), the polypeptide chain folds and self-assembles into a more ordered structure^{50,80}. This simple substitution showed to significantly alter the thermoresponsive behavior and the mechanical properties of poly(VPAVG) when compared with poly(VPGVG): while still displaying a reversible phase transition behavior (as do all other ELPs), poly(VPAVG) is characterized by an acute thermal hysteresis, self-assembling at temperatures above its T_i, but only resolubilizing when the temperature is strongly cooled down^{63,81}. The matrix resulting from the cross-linking of poly(VPAVG) exhibited similar properties to synthetic thermoplastic elastomers^{63,82}, with an Young's modulus two orders of magnitude higher than that for poly(VPGVG)⁸³, and has also demonstrated to be biocompatible both *in vitro* and *in vivo*⁸⁴.



Figure 2. Representation of SELP-59-A construct. The polymer contains 9 repeats of a monomeric unit with 5 repeats of the silk consensus sequence GAGAGS (S₅, green) and 9 repeats of the elastin-like sequence VPAVG (E₉, pink).

Due to the remarkable mechanical properties, biocompatibility and versatility of processing, SELPs have been used for biomedical applications such as in targeted drug delivery⁸⁵ and controlled gene release^{86,87}, scaffolds for tissue engineering⁸⁸, biodegradable plastics⁸⁹, wound dressings for skin regeneration⁵⁶ and ophthalmic applications⁹⁰. Among SELPs, SELP-59-A has been easily expressed and purified with high volumetric productivities^{91,92}, and processed into different types of materials such as fibers⁵⁶, transparent films⁶⁴, hydrogels and even multifunctional biocomposites^{69,93,94}.

1.2. SIGNALING MOLECULES

Animal cells do not survive without communication. They receive and respond to a variety of signaling molecules that are secreted or expressed on the surface of other cells⁹⁵. Structurally, the signaling molecules used by animals have a great range of complexity, from simple gases to proteins that can bind to intracellular receptors in the cytoplasm or nucleus, or to receptors expressed on the target cell surface⁹⁵. The binding between most signaling molecules and the receptor initiates signal transduction pathways that virtually regulate all cell functions including proliferation, survival, metabolism, movement, differentiation and adhesion^{95,96}.

1.2.1. Cell adhesion

From the signaling processes discussed above, cell adhesion regulation is of special interest for tissue engineering researchers. Cell adhesion is the ability of a single cell to stick to another cell or to the extracellular matrix (ECM)⁹⁷ through reversible interactions, such as hydrogen bonds, electrostatic interactions, van der Waals forces, and dipole-dipole interactions between two macromolecules⁹⁸. It is mediated by cell-surface proteins named cell adhesion molecules (CAMs)⁹⁹ that can be divided into four main classes comprising immunoglobulin super family CAMs, adhesins, mucin-like CAMs and integrins^{31,100}. Immunoglobulin super family CAMs, mucin-like CAMs and adhesins are involved in cell-to-cell adhesion, while integrins are essentially involved in cell-to-matrix adhesion⁹⁹. The crosstalk between cell-cell and cell-ECM adhesions plays an important role in tissue morphogenesis, being critical for the regulation of cell behavior¹⁰¹. Cells sense the mechanical stimuli such as force, stress, strain, substrate rigidity, topology and adhesiveness, and respond by converting them to biochemical signals which elicit specific cellular responses¹⁰² that regulate cell differentiation, cell cycle, migration, survival, and the development and maintenance of tissues^{96,97}.

In vitro, cell adhesion is a passive process that occurs in static culture conditions, usually in cell culture flasks⁹⁷. Cells undergo morphological changes due to passive deformation and active reorganization of the cytoskeleton that leads to cell-matrix attachment and spreading. The process of *in vitro* cell adhesion is defined by three stages (Figure 3): i) an initial stage, where the cell body attach to its substrate, ii) flattening and spreading of the cell body and, iii) organization of the actin skeleton with the formation of focal adhesions between the cell and its substrate⁹⁷.

In the initial stage, cells attach onto the substrate through interaction between CAMs and the matrix (phase I). Posteriorly, the number of interactions increases over time and cells continue flattening and spreading, resulting in the increment of contact area with the matrix (phase II)⁹⁷. In the last stage (phase III), cells completely spread over the surface and there is a reorganization and distribution of the actin skeleton around the cell's body edge. The strength of adhesion increases with the length of time a cell is allowed to adhere to the substrate⁹⁷.

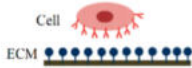
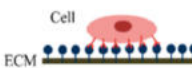
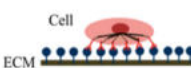
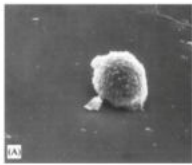
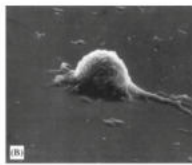
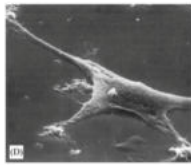
Cell adhesion phase	Phase I	Phase II	Phase III
Schematic diagram of cell adhesion			
Transformation of cell shape			
Cell adhesion intervention	Electrostatic interaction	Integrin bonding	Focal adhesion
Adhesion stages	Sedimentation	Cell attachment	Cell spreading and stable adhesion

Figure 3. *In vitro* cell adhesion stages. Adapted from ^{97,103}.

1.2.1.1. Cell-cell adhesion

Cell-cell adhesion can be temporary, such as the interactions between immune system cells⁹⁵, or stable cell-cell junctions that play a role in the formation and maintenance of tissues, as it allows cells in tissues to work in an integrated manner^{104,105}. Cell-cell adhesion is generally initiated by one or more CAMs such as immunoglobulin super family CAMs, mucin-like CAMs and adhesins⁹⁹. These CAMs cluster and form three major structures: tight junctions, adherens junctions and desmosomes¹⁰⁶. Tight junctions – a type of cell–cell adhesion in epithelial and endothelial cellular sheets – form a barrier impermeable to the

majority of soluble molecules between the two sides of the epithelium¹⁰⁷. Adherens junctions are cadherin-based adhesive structures formed from the association of cadherins on adjacent cells, associated with actin-binding/regulatory proteins¹⁰⁸. Finally, desmosomes are multiprotein complexes composed by proteins of the cadherin superfamily which recruit a variety of intracellular proteins that anchor intermediate filaments to the plasma membrane^{109,110}. Besides mediating cell adhesion, these specialized junctions provide mechanisms for rapid communication between cells⁹⁵.

1.2.1.2. Cell-ECM adhesion

The majority of animal cells is surrounded by an ECM, that fills the spaces between cells and binds cells and tissues together⁹⁵. It is a dynamic structure that acts as physical scaffold supporting cells, providing strength and elasticity, interacting with cell-surface receptors and controlling the availability of growth factors¹¹¹.

The ECM consists of a complex mixture of secreted proteins with both structural and functional roles³¹ embedded in a gel-like polysaccharide substance arranged in a unique, tissue-specific three-dimensional architecture^{31,95,111}. The main constituents of ECM are collagen, which represents about 90% of the dry weight of most tissues' ECM; elastin, which is an essential protein that provides resilience and elasticity to tissues and organs¹¹²; glycoproteins such as fibronectin, laminin, vitronectin, thrombospondin and tenascin, which play an important role in many cell surface interactions; glycosaminoglycans e.g. heparin and hyaluronic acid that promote water retention and contribute to the gel properties of the matrix; and growth factors such as vascular endothelial cell growth factor (VEGF), fibroblast growth factor (FGF), and epithelial cell growth factor (EGF) that, even though they represent a small portion of the ECM, play an important role as modulators of cell behavior^{31,113}.

Multiadhesive matrix proteins, such as glycoproteins, link components of the matrix both to one another and to attached cells⁹⁵. The continuous crosstalk between cells and molecules of the ECM mediated by membrane receptors leads to the development of patterns, morphogenesis, differentiation and maintenance of the differentiated phenotype¹¹⁴. Cell adhesion to the extracellular matrix is mainly mediated by integrins⁹⁵, heterodimers of non-covalently associated α and β subunits that can act as a bridge between surface adsorbed ECM proteins and interacting cells^{31,115}. Different types of α - and β -subunits and different combinations of them allow the existence of a large variety of integrins with the ability to bind to different types of ligands (Table 3)^{31,116}.

Table 3. Integrin types and their respective ligands. Adapted from ³¹.

Subunits	Ligands	
$\beta 1$	$\alpha 1$	Collagens, laminins
	$\alpha 2$	Collagens, laminins
	$\alpha 3$	Laminins, fibronectin, thrombospondin
	$\alpha 4$	Fibronectin, vascular cell adhesion molecule (VCAM)
	$\alpha 5$	Fibronectin
	$\alpha 6$	Laminins
	$\alpha 7$	Laminins
	$\alpha 8$	Fibronectin, tenascin
	$\alpha 9$	Tenascin
	$\alpha 10$	Collagens
	$\alpha 11$	Collagens
	αv	Fibronectin, vitronectin
	$\beta 2$	αL
αM		Fibrinogen, ICAMs
αX		Fibrinogen
αD		VCAM, ICAMs
$\beta 3$	αIIb	Collagens, fibronectin, vitronectin, fibrinogen, thrombospondin
	αv	Fibronectin, vitronectin, fibrinogen, thrombospondin, osteopontin, tenascin
$\beta 4$	$\alpha 6$	Laminins
$\beta 5$	αv	Vitronectin
$\beta 6$	αv	Fibronectin, tenascin
$\beta 7$	$\alpha 4$	Fibronectin, VCAM, Mucosal addressin cell adhesion molecule (MAdCAM)
	αE	E-cadherin
$\beta 8$	αv	Collagens, laminins, fibronectin

Both subunits contain a large extracellular domain, a transmembrane domain and a short cytoplasmic domain (Figure 4)^{31,116,117}. The extracellular domain of integrins binds to the extracellular matrix while the cytoplasmic domain interacts with components of cytoskeleton and with signaling molecules, responsible for the transduction of the signaling process^{31,116}. The matrix is linked to the cytoskeleton in a stable way by cell-matrix junctions – focal adhesions and hemidesmosomes – through the interaction of integrins with extracellular matrix molecules and with the cytoskeleton (Figure 4)^{95,118}. Focal adhesions attach a variety of cells to the extracellular matrix using integrins that mediate the attachment of actin fibers of the cytoskeleton to ECM molecules, such as fibronectin¹¹⁸. Hemidesmosomes mediate epithelial cells attachment to the basal laminae, using one specific integrin ($\alpha 6\beta 4$) that anchors laminin to intermediate filaments, instead of binding to actin⁹⁵.

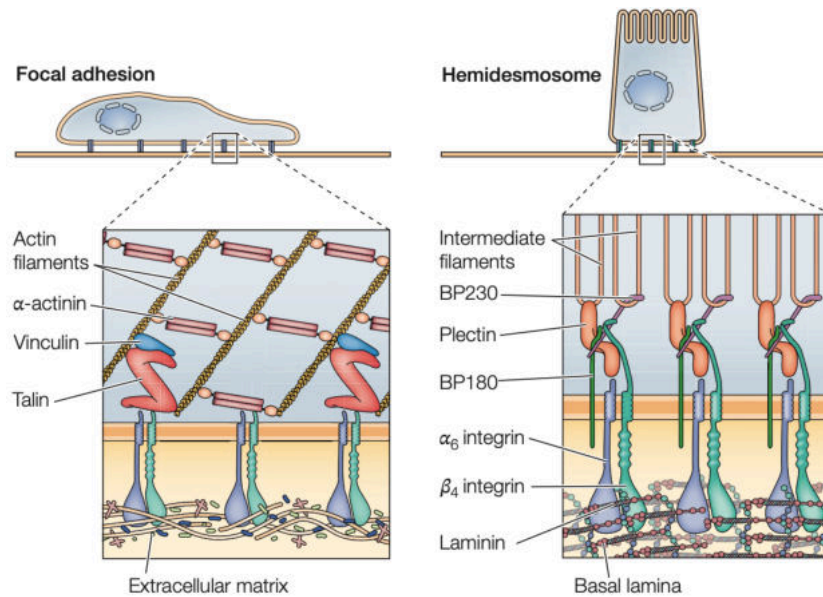


Figure 4. Cell-matrix junctions mediated by integrins. In focal adhesion, cytoplasmic domain of the subunit β binds to actin filaments by association with proteins such as α -actinin, vinculin and talin. In hemidesmosomes, $\alpha_6\beta_4$ integrin mediates anchorage of basal lamina layer to intermediate filaments via plectin. Reproduced from⁹⁵.

1.2.1.3. Adhesion sequences

The interaction between integrins and ECM (cell-ECM adhesion) occurs through the recognition, by integrins, of amino acid sequences present in ECM proteins termed cell adhesion sequences (Table 4), while the interaction between two CAMs (cell-cell adhesion) occurs through the recognition of sequences present in other CAMs.

Due to the role of CAM-mediated interactions on the subsequent cellular events of cellular recognition, these motifs are promising targets for manipulating cellular responses to biomaterials³¹. To date, several biomaterials have been engineered with adhesion sequences in order to improve cell interaction. Two main methods are used to include adhesion sequences in a biomaterial: chemical immobilization of whole ECM proteins^{119,120} or short peptide sequences (cell adhesion motifs) on the surface of a scaffold^{121,122}, or, in the case of recombinant proteins (typically rPBPs), by genetic manipulation of their structure¹²³⁻¹²⁵. The use of whole ECM proteins can result in their instability during the different modification processes and have the tendency to randomly fold, impairing the availability of CAMs to interact with cells²⁸. Due to these constraints, the use of short peptide sequences is preferable²⁸. Adhesion sequences are usually small but sufficient to promote cell adhesion with results often comparable to those obtained using entire proteins^{126,127}.

Table 4. Integrins and prototypic ligands/cell adhesion sequences. Adapted from ¹²⁸⁻¹³².

	Integrin	Prototypic ligands/cell adhesion sequences
RGD ligands	$\alpha 5\beta 1$	RGD; KQAGDV; LDV/IDS; IDA(PS); REDV
	$\alpha 8\beta 1$	RGD
	$\alpha v\beta 1$	RGD
	$\alpha v\beta 3$	RGD
	$\alpha v\beta 5$	RGD
	$\alpha v\beta 6$	RGD, DLXXL
	$\alpha v\beta 8$	RGD
	$\alpha IIb\beta 3$	RGD, KQAGDV, KGD, HHLGGAKQAGDV
Collagen ligands	$\alpha 1\beta 1$	GFOGER ^α ; GLOGER ^α ; GLQGER; GFKGER
	$\alpha 2\beta 1$	GFOGER ^α ; GROGER; GFKGER; DGEA; YGYGDALR; FYFDLR; RGD
	$\alpha 10\beta 1$	GFOGER ^α
	$\alpha 11\beta 1$	GFOGER ^α ; GLQGER; GFKGER
Laminin ligands	$\alpha 3\beta 1$	LN-511; LN-332; LN-211; RGD
	$\alpha 6\beta 1$	LN-511; LN-332; LN-111; LN-411
	$\alpha 6\beta 4$	LN-332; LN-511
	$\alpha 7\beta 1$	LN-111; LN-211; LN-411; LN-511; RGD
Leukocyte-specific receptors	$\alpha 4\beta 1$	RGD; LDV/IDS; QIDS; IDAPS; CS-1 peptide; CS-5 peptide
	$\alpha 4\beta 7$	LDV, LDT, CS-1 peptide
	$\alpha 9\beta 1$	AEIDGIEL; tenascin-c
	$\alpha E\beta 7$	HAV
	$\alpha L\beta 2$	L/IET; GPR
	$\alpha M\beta 2$	KRLDGS; P1 peptide; P2 peptide; GPR;
	$\alpha X\beta 2$	GPR
	$\alpha D\beta 2$	GPR

Note: sequences are given in single-letter amino acid code, where X is any amino acid. ^αO, hydroxyproline.

The prototypic adhesion signal sequence that is most commonly used to promote cell adhesion is the RGD (R: arginine, G: Glycine, D: aspartic-acid) tripeptide sequence^{103,133,142-145,134-141}, that was originally identified in fibronectin and binds to the fibronectin receptor, $\alpha 5\beta 1$ integrin. It is now known that numerous integrins recognize this sequence (Table 4)^{130,131}. RGD is present in a variety of adhesion proteins including fibronectin, vitronectin, fibrinogen, von Willebrand factor, thrombospondin, laminin, entactin,

tenascin, osteopontin, bone sialoprotein, and, upon denaturation or proteolytic cleavage, collagens^{128,131,132}. There are several variations of this adhesion motif, such as NGD, KGD and RHD, capable of binding to several RGD-directed integrins, although with lower affinity¹³¹.

While some adhesion sequences such as RGD are generic and promote the adhesion of almost all cell types, other sequences such as REDV (R: arginine, E: glutamic acid, D: aspartic acid, V: valine) have a more restrained activity. REDV is a sequence naturally present in the CS5 domain of fibronectin that have specific activity for endothelial cells^{146,147}. It was previously used to functionalize material surfaces¹⁴⁸ and rPBPs^{125,149–153} and it is appealing for small-diameter vascular grafts^{147,149}.

Not all sequences are unspecific and recognized by several different integrins: some sequences such as HHLGGAKQAGDV are recognized only by one integrin. Other integrins mediate cell-cell adhesion, binding to intercellular adhesion proteins such as ICAM, VCAM and MadCAM (Table 3). Some of these integrins, like $\alpha 4\beta 1$, have dual specificity and can bind to VCAM-1, but can also bind to fibronectin¹³¹.

The interaction between two CAMs in cell-cell adhesion events occurs through the recognition of sequences present in other CAMs, which have been identified mainly by structural analysis or by screening combinatorial libraries^{154,155}. Examples of these motifs are FGL (EYVVAENQQGKSKA), C3 (ASKKPKRNIKA), and NBP10 (AKKMWKKTW). These sequences are not frequently used for the functionalization of materials as they often compete with CAM-CAM interaction thus inhibiting cell-cell adhesion. Even so, there is one report on the use of C3 sequence for the functionalization of polymers to promote cell adhesion¹⁵⁶, demonstrating enhanced cell adhesion ability.

1.3. CELLS

The use of cells in tissue engineering targets the repopulation and repair of a damaged tissue¹⁵⁷. The ideal scenario would be the isolation of patient's cells by means of a small biopsy, expansion the cell number in the culture, seeding the cells onto a scaffold and implantation to the same patient¹⁷. However, for several reasons, this is not viable and a common procedure, and it is necessary the existence of alternative approaches.

The source of the cells to be used has a huge influence on the success of tissue engineering approaches and can be categorized based on their origin: autologous, when they belong to the patient; allogenic, when they have human origin but not belong to the patient; and xenogeneic, when they have a different animal origin¹⁷.

From an immunologic point-of-view, autologous cells are the most appropriate for tissue engineering due to the fact that they are not immunogenic and therefore immunosuppressive therapy is not required after implantation¹⁷. Although a preferred option, there are several limitations regarding this approach because of the invasive nature of cell collection and the potential for cells to be in a diseased state^{157,158}. Also, in many cases, a relatively low number of cells is available for harvesting and can result in some degree of donor-site morbidity whereas, cells from diseased or aged patients may not be appropriate for transplantation. In such cases, a common alternative is to use cells from different human or non-human donors¹⁵⁷. Allogenic cells are mostly used for skin regeneration¹⁵⁹, providing essential growth factors and cytokines for wound healing¹⁶⁰. However, there is the risk of transmission of viral infections (e.g., hepatitis B and C or HIV) between the donor and the receptor, besides the need of immunosuppressive therapies¹⁶¹. In the ongoing search for a reliable source of cells to replace lost cells, tissues and organs, research in the area of xenotransplantation has grown tremendously over the past four decades^{157,159}. During several years, the ability to genetically modify species, such as the pig, through transgenesis and nuclear transfer, to express human genes and to mutate detrimental genes expressed in pig cells, held a promise for engineered tissues¹⁵⁹. However, the publication of reports that revealed the presence of porcine endogenous retrovirus in pigs¹⁶² dramatically reduced the frequency of this animal's use as cell source due to the problem of cross-species pathogen infectivity, i.e. xenozoonosis^{17,159}. The transmission of infectious agents combined with the ethical, moral and social consequences, have reduced the enthusiasm for this approach¹⁵⁷.

The extent of cell differentiation also has influence on the success of tissue engineering¹⁷ as the presence of proliferative capacity to populate the scaffold and replace the damaged tissue is crucial. One option is the use human embryonic stem cells (ESCs)^{17,157,158}. ESCs can be derived from the blastocyst – a preimplantation stage embryo – or from primordial germ cells – cells of the early embryo that eventually differentiate into sperm and oocytes^{163,164}. ESCs are appealing as source for tissue engineering due to their virtual limitless expansion capacity and differentiation ability (capable to differentiate into potentially all body cells)^{157,158,165}. The use of these pluripotent stem cells have, however, some constrains: if ESCs are obtained from fertilized eggs that were not used after the infertile therapy of couples, these cells are allogenic to the patient who will receive them, which will trigger an immunologic response¹⁷. Although it is possible to overcome this problem by transferring the nuclear somatic cell to an enucleated egg, this technique raises ethical questions¹⁷. Some studies have shown that ESCs transplantation into immune-deficient mice elicits the formation of teratomas¹⁶⁶, tumor-like formations containing tissues belonging to

all three germ layers¹⁶⁷. Due to this, the complete differentiation and purification of the cells modified from ESCs is imperative for the clinical application in tissue engineering¹⁷.

Another promising possibility are multipotent stem cell populations, also known as adult stem cells, that are found mainly in the bone marrow and have the ability to differentiate into many lineages under appropriate conditions^{17,168}. The most extensively studied adult stem cell lines are hematopoietic stem cells (HSCs) and mesenchymal stem cells (MSCs)¹⁷. HSCs are able to differentiate into eosinophils, erythrocytes, megakaryocytes, osteoclasts and B and T cells. MSCs can differentiate into osteocytes, chondrocytes, adipocytes, tenocytes, myocytes and bone marrow stromal cells^{17,158,169}. The use of MSCs for tissue engineering purposes is considered safe when compared with ESCs, as no tumorigenesis has been reported¹⁷.

Several years ago it was reported the existence of additional tissue-resident adult stem cell populations that proliferate and differentiate to provide organ-specific cell types^{168,170-173}. The number of tissue-resident stem cells is variable among tissues. Some tissues are highly regenerative, as is the case of the skin – where it is possible to find proliferative keratinocytes, the liver – where hepatocytes respond to liver damage, and intestinal crypt that replenish the absorptive epithelium¹⁷, while the majority of the organs in a human body respond poorly to regenerative pressure (e.g., heart), possibly due to the low stem cell number¹⁶⁸. Even so, the application of adult stem cells in tissue engineering has limitations. In many cases, the number of cells collected from a patient is not sufficient for clinical application and it is necessary to multiply cells in *in vitro* cultures¹⁷. This process represents a challenge: when grown on a two-dimensional cell culture dish, the proliferative capacity of these cells is reasonably maintained, but eventually the de-differentiation occurs. When grown on three-dimensional substrates, the de-differentiation does not occur, but the rate of proliferation is drastically reduced¹⁷.

2. Aims

2. AIMS

The overall aim of this work is the development of functionalized genetically engineered SELP materials using SELP-59-A as the base protein polymer, via the inclusion of cell-binding motifs.

Interest in tissue engineering resulted in an increasing number of biomaterials available. However, many of these materials are non-bioactive and have none or little influence on cellular behavior as they fail to comply with the complex number of requisites such as cell adhesion, growth, differentiation, etc. Designing scaffolds that are favorable to cellular adhesion and growth is imperative to make advances in the reparation and regeneration of the functions of damaged tissues, as well as in the study of stem cell behavior and to provide models for the study of several diseases.

In order to provide a contribution towards such purpose, this work focused on the creation of novel materials with improved cell adhesion functions. The main objective was then divided in the following tasks:

- Creation of recombinant protein-based polymers based on silk and elastin integrating different cell binding motifs;
- Production and purification of the created materials;
- Evaluation of the cell and ECM-binding activity using mammalian cell cultures.

3. Materials and Methods

3. MATERIALS AND METHODS

3.1. BIOLOGICAL MATERIALS

3.1.1. Microorganisms

During this work, five strains of *Escherichia coli* were used, with genotypic characteristics described in Table 5. All bacterial strains were made competent (Annex I) and transformed with different variations of the plasmids shown in Table 6 and presented in Annex II. *E. coli* XL1-Blue (Stratagene) was used for the cloning steps and plasmid storage, whereas *E. coli* BL21(DE3) (Novagen), *E. coli* C43(DE3) and *E. coli* Origami B were used for protein production.

Table 5. Strains used for cloning steps and protein production and its genotype.

<i>E. coli</i> strain	Genotype
XL1-Blue	<i>recA1 endA1 gyrA96 thi-1 hsdR17 supE44 relA1 lac [F'proAB⁺ lac L⁺ΔM15 Tn10 (Tet^r)]</i>
BL21(DE3)	<i>F- ompT gal dcm lon hsdSb(r_s- m_s-) λ(DE3 [lacI lacUV5-T7 gene 1 ind1 Sam7 nin5])</i>
BL21(DE3) pLysE	<i>F- ompT gal dcm lon hsdSb(r_s- m_s-) λ(DE3 [lacI lacUV5-T7 gene 1 ind1 Sam7 nin5])pLysE (Carr^r)</i>
C43(DE3) pRARE	<i>F ompT hsdSB (r_s- mb-) gal dcm λ(DE3 [lacI lacUV5-T7 gene 1 ind1 Sam7 nin5]) pRARE (Carr^r)</i>
Origami B (DE3)	<i>F ompT hsdS_s(r_s m_s) gal dcm lacY1 ahpC λ(DE3 [lacI lacUV5-T7 gene 1 ind1 Sam7 nin5]) gor522::Tn10 trxB (Kan^r, Tet^r)</i>

Table 6. Plasmids used for gene cloning and expression.

Plasmids	Selective marker	Application
pDrive::SELP-59-A	Amp ^r , Kan ^r	Cloning vector
pCM13::SELP-59-A	Amp ^r	Expression vector
pET25b(+)	Amp ^r	Expression vector

Amp^r - ampicillin resistance; Kan^r - kanamycin resistance.

Cells were stored at -80 °C in glycerol 30% (v/v) until used. When needed, cells were inoculated in Lysogeny Broth (LB) (see Annex III) solid or liquid, supplemented with antibiotics as selective markers.

For protein production, cells were inoculated in Terrific Broth (TB) (see Annex III), using α -lactose (lac) or its synthetic analogous molecule Isopropyl β -D-1-thiogalactopyranoside (IPTG) as inducers of protein expression.

3.1.2. Mammalian cell lines

Evaluation of biomaterials cell adhesion was performed using mammalian cell cultures, namely the bone marrow cell line SH-SY5Y, a subline of the neuroblastoma parental line SK-N-SH derived from a metastatic bone tumor biopsy^{174,175}, and HaCaT, an immortalized human keratinocyte line¹⁷⁶.

SH-SY5Y cells were cultured according to American Type Culture Collection (ATCC) recommendations in a mixture (1:1) of Dulbecco's minimal essential medium (DMEM) and Ham's F12 nutrient Mixture, supplemented with 10% (v/v) fetal bovine serum (FBS), 1% (v/v) penicillin/streptomycin, 10 μ g/mL hygromycin B and 1% (v/v) L-glutamine. HaCaT were cultured in DMEM medium supplemented with 10% (v/v) FBS, 1% penicillin/streptomycin, 10 μ g/mL hygromycin B and 1% (v/v) L-glutamine.

Both cell lines were maintained in 25 cm² tissue culture flasks (T25) and 75 cm² tissue culture flasks (T75) in an incubator with 5% CO₂ at 37 °C.

3.2. CLONING STRATEGY

Genetic constructions were prepared by standard genetic engineering techniques using DNA sequences optimized for *E. coli* B codon usage. All DNA agarose gel electrophoresis were performed using 1% agarose gels and using Tris-acetate-EDTA (TAE) (see Annex III) as running buffer unless stated otherwise, and were stained using Midori Green Advance (NIPPON Genetics). GSR ladder 1kb (Grisp) was used as molecular weight marker (MWM).

3.2.1. pET25b(+) digestion

The pET25b(+) (Novagen) (see Annex II) expression plasmid was extracted from *E. coli* XL1-Blue using the GenElute™ Plasmid Miniprep Kit (Sigma-Aldrich) following the manufacturer's instructions. pDNA quantification was accessed by spectrophotometry with NanoDrop® ND-1000 UV-Vis Spectrophotometer (Thermo Fisher Scientific).

The plasmid was then digested using *Nde*I and *Hind*III Fast Digest restriction enzymes (Thermo Fisher Scientific) for 4 h at 37 °C. To avoid vector recircularization, dephosphorylation was performed using

Antarctic Phosphatase (New England BioLabs) for 30 min at 37 °C, followed by inactivation at 80 °C for 2 min. Accomplishment of full digestion reaction was confirmed by DNA agarose gel electrophoresis. The DNA band of the digested product was extracted from agarose gel and purified with NucleoSpin® Gel and PCR Clean-up (Macherey-Nagel) according to the manufacturer's instructions and quantified as described before. The digested plasmid was stored at -20 °C until further use.

3.2.2. Design and digestion of *adapter* sequence

A cloning adapter was designed to enable the cloning steps needed for this work in the pET25b(+). The *adapter* sequence was obtained by polymerase chain reaction (PCR) (LifeECO Thermal Cycler) using two primers that partially overlay (Table 7). The reaction was performed using the reagents depicted in Table 8 to a final volume of 50 µL, according to the conditions described in Table 9.

Table 7. Primers used to obtain the adapter and adhesion motifs DNA sequences. Primers overlay on highlighted nucleotides.

<i>adapter</i>	Forward	5' AAAACATATGGGTACCCACGTGACTAGTGAA 3'
	Reverse	5' GGGGAAGCTTTTAGAATTCAGTAGTCACGTG 3'
<i>nC3</i>	Forward	5' GGGGCATATGGCGAGCAAAAACCGAAACGCAATA 3'
	Reverse	5' GGGGGGTACCCGCTTTAATATTGCGTTTCGGTTT 3'
<i>cC3</i>	Forward	5' GGGGACTAGTGCAGCAAAAACCGAAACGCAATA 3'
	Reverse	5' GGGGGAATTCGCTTTAATATTGCGTTTCGGTTT 3'
<i>nRGD</i>	Forward	5' AAAACATATGTGCACCGCCGCGCGGATAGCCC 3'
	Reverse	5' AAAAGGTACCGCACGCCGGGCTATCGCCGCGGC 3'
<i>cRGD</i>	Forward	5' AAAAAGTGTGCACCGCCGCGCGGATAGCCC 3'
	Reverse	5' AAAAGAATTCGACGCCGGGCTATCGCCGCGGC 3'

Table 8. Reagents used to perform PCR.

Reagent	Volume (µL)
Accuzyme Mix 2X (Bioline)	25
Forward primer 10 µM	2
Reverse primer 10 µM	2
upH ₂ O	21

After PCR, the success of the reaction and band size were verified by DNA agarose gel electrophoresis and the remaining volume was purified using NucleoSpin® Gel and PCR Clean-up (Macherey-Nagel) according to the manufacturer's instructions. DNA quantification was performed as previously described.

Table 9. PCR conditions used to perform PCR to produce *adapter* sequence.

Step	Temperature (°C)	Time	Cycles
Initial denaturation	95	3 min	1
Denaturation	95	15 s	30
Annealing	47	15 s	
Extension	72	1.5 min	
Final extension	72	1 min	1

The purified PCR product was digested with *NdeI* and *HindIII* Fast Digest (Thermo Fisher Scientific) at 37 °C for 4 h. The digested DNA was then purified using NucleoSpin® Gel and PCR Clean-up (Macherey-Nagel) according to the manufacturer's instructions and quantified. The digested adapter sequence was stored at -20 °C until used.

3.2.3. Ligation of the *adapter* and pET25b(+)

Ligation of pET25b(+) and the *adapter* was performed overnight at room temperature using T4 DNA ligase (Thermo Fisher Scientific). The quantity of vector and insert to be used were calculated by the following formula, using the molar ratio of 5:1:

$$\frac{\text{ng of vector} \times \text{size of insert (kb)}}{\text{size of vector (kb)}} \times \frac{\text{molar ratio of insert}}{\text{molar ratio of vector}} = \text{ng of insert}$$

The resulting plasmid will be termed pET25::*adapter* from this point onwards.

Afterwards, 10 µL of the reaction were used for cell transformation using competent *E. coli* XL1-Blue (see Annex I), following the heat shock transformation method present in Annex IV. To confirm if the ligation

was successful, a screening protocol by DNA agarose gel electrophoresis was performed. The pDNA from 6 *E. coli* XL1-Blue transformants was extracted using GenElute™ Plasmid Miniprep Kit (Sigma-Aldrich) following the manufacturer's instructions and digested using *Ppu21I* (Thermo Fisher Scientific) for 4 h at 37 °C and analysed by electrophoresis. Positive results were also confirmed by DNA sequencing using cycle sequencing technology (dideoxy chain termination/cycle sequencing) (Eurofins Genomics).

3.2.4. Digestion of pET25::*adapter*

pET25::*adapter* was extracted from *E. coli* XL1-Blue using NZYMiniprep kit (NZYTech – Genes & Enzymes) and was digested with *Eco72I* (Thermo Fisher Scientific) for 5 h at 37 °C. Accomplishment of full digestion reaction was confirmed by DNA agarose gel electrophoresis. The DNA band of the digested product was extracted from agarose gel and purified with NucleoSpin® Gel and PCR Clean-up (Macherey-Nagel) according to the manufacturer's instructions.

To avoid recircularization, the digested plasmid was dephosphorylated by Antarctic Phosphatase (New England Biolabs), according to the manufacturer's instructions. Dephosphorylated sequence was purified using NucleoSpin® Gel and PCR Clean-up (Macherey-Nagel) according to the manufacturer's instructions and quantified.

3.2.5. SELP extraction from pDrive::*SELP-59-A* plasmid

pDrive::*SELP-59-A* plasmid (see Annex II) was extracted from *E. coli* XL1-Blue using NZYMiniprep kit (NZYTech – Genes & Enzymes) following the supplier's instructions and quantified. The *SELP-59-A* sequence was then extracted from the plasmid by restriction digestion with *Eam1104I* (Thermo Fisher Scientific) for 5 h at 37 °C.

Full digestion reaction and separation of the DNA bands were confirmed by DNA agarose gel electrophoresis. The DNA band with the molecular weight corresponding to SELP-59-A DNA coding sequence was extracted from agarose gel, purified with NucleoSpin® Gel and PCR Clean-up (Macherey-Nagel) according to the manufacturer's instructions and quantified.

3.2.6. SELP-59-A sequence extension

Since the excision of *SELP-59-A* with *Eam1104I* restriction enzyme produces sticky ends and the digestion of pET25::*adapter* with *Eco72I* restriction enzyme produces blunt ends, it was necessary to fill in the sticky ends of the *SELP-59-A* sequence to make the ligation compatible. This reaction was performed

using 23 μ L of Accuzyme Mix 2x (Bioline) and 23 μ L of *SELP-59-A* sequence, to a final volume of 46 μ L. The mixture was incubated at 72 °C for 45 min using a thermocycler (T100 Thermal Cycler, Bio-Rad). Extended *SELP-59-A* sequence was purified using NucleoSpin® Gel and PCR Clean-up (Macherey-Nagel) according to the manufacturer's instructions and quantified.

3.2.7. Ligation of pET25::*adapter* and *SELP-59-A*

The ligation of pET25::*adapter* and the *SELP-59-A* sequences was performed at room temperature for 1 h using T4 DNA ligase (Thermo Fisher Scientific) and transformed into *E. coli* XL1-Blue. The quantity of vector and insert to be used was calculated using the formula in section 3.2.3, using the molar ratio of 5:1. The resulting plasmid was named pET25::*SELP-59-A*.

Confirmation of gene insertion and right orientation was achieved by DNA extraction and digestion using *Pvu2*11 and *Hind*III of several transformants. Positive results were confirmed by DNA sequencing (Eurofins Genomics).

3.2.8. pET25::*SELP-59-A* digestion

pET25::*SELP-59-A* was extracted from *E. coli* XL1-Blue using NZYMiniprep kit (NZYTech – Genes & Enzymes) following the supplier's instructions and quantified using NanoDrop® ND-1000 UV-Vis Spectrophotometer (Thermo Fisher Scientific).

To posteriorly insert the adhesion sequences, pET25::*SELP-59-A* was digested at N- and C-terminus of the *SELP-59-A* sequence. N-terminus digestion was performed for 4 h at 37 °C using *Nde*I (Thermo Fisher Scientific) and *Kpn*I (Thermo Fisher Scientific). C-terminus digestion was performed in two steps, since the two restriction enzymes used have different optimal concentrations of enzyme reaction buffer. The first step was executed for 2 h at 37 °C, by mixing 20 μ L of pET25_SELP 101.3 ng/ μ L, 1 μ L of *Bcu*I (Thermo Fisher Scientific), 2.5 μ L of Tango Buffer (Thermo Fisher Scientific) and 1.5 μ L of upH₂O. When the first digestion was complete, 1 μ L of *Eco*R1 (Thermo Fisher Scientific) and 3.25 μ L of Tango Buffer (Thermo Fisher Scientific) were added to the reaction. The volume of Tango Buffer necessary to add was calculated according to the following formula: $V=A/8$, where V is the volume of buffer to be applied and A is the starting volume of the reaction mixture.

The optimal reaction conditions for the two double digest reactions were determined using the online tool DoubleDigest Calculator – Thermo Scientific

(<https://www.thermofisher.com/pt/en/home/brands/thermo-scientific/molecular-biology/thermo->

scientific-restriction-modifying-enzymes/restriction-enzymes-thermo-scientific/double-digest-calculator-thermo-scientific.html, Thermo Fisher Scientific).

3.2.9. Adhesion sequences design and insertion into pET25::SELP-59-A

The adhesion sequences were obtained by polymerase chain reaction (PCR) (T100 Thermal Cycler, Bio-Rad) using two primers that partially overlay (Table 7). The reaction was performed using the reagents present in Table 8 to a final volume of 50 μ L, according to the conditions described from Table 10 to Table 13.

After PCR, the success of the reactions and the size of the bands were verified by DNA agarose gel electrophoresis, the DNA purified and quantified. *nRDG* and *nC3* sequences were digested for 4 h at 37 $^{\circ}$ C using *NdeI* and *KpnI* (Thermo Fisher Scientific), whereas *cRGD* and *cC3* sequences were digested with *BclI* and *EcoRI* (Thermo Fisher Scientific).

Table 10. PCR conditions to obtain *nC3* adhesion sequence.

Step	Temperature ($^{\circ}$ C)	Time	Cycles
Initial denaturation	95	3 min	1
Denaturation	95	15 s	30
Annealing	50	15 s	
Extension	72	1.5 min	
Final extension	72	1 min	1

Table 11. PCR conditions to obtain *cC3* adhesion sequence.

Step	Temperature ($^{\circ}$ C)	Time	Cycles
Initial denaturation	95	3 min	1
Denaturation	95	15 s	30
Annealing	50.5	15 s	
Extension	72	1.5 min	
Final extension	72	1 min	1

Table 12. PCR conditions to obtain *nRGD* adhesion sequence.

Step	Temperature (°C)	Time	Cycles
Initial denaturation	95	3 min	1
Denaturation	95	15 s	30
Annealing	62	15 s	
Extension	72	1.5 min	
Final extension	72	1 min	1

Table 13. PCR conditions to obtain *cRGD* adhesion sequence.

Step	Temperature (°C)	Time	Cycles
Initial denaturation	95	3 min	1
Denaturation	95	15 s	30
Annealing	65	15 s	
Extension	72	1.5 min	
Final extension	72	1 min	1

Ligation occurred with the digested sequences and pre-digested and dephosphorylated pET25::*SELP-59-A* with the respective enzymes for N or C-terminal insertion for 1 h at room temperature. Ligation products were then used to transform *E. coli* XL1-Blue cells.

Successful insertion was confirmed by digestion of extracted pDNA from different transformants with the enzymes used before the ligation steps and verified by DNA agarose gel electrophoresis using SGTB (GRiSP Research Solutions) as running buffer. Positive results were sent for sequencing (Eurofins Genomics).

The resultant plasmids from the ligation between pET25::*SELP-59-A* and *nC3*, *cC3*, *nRGD* and *cRGD* will be named pET25::*SELP-59-A_nC3*, pET25::*SELP-59-A_cC3*, pET25::*SELP-59-A_nRGD* and pET25::*SELP-59-A_cRGD*, respectively, from this point onwards.

3.3. EVALUATION OF PROTEIN PRODUCING LEVELS

The confirmed constructions were transformed into *E. coli* BL21 (DE3) using the heat shock transformation protocol described in Annex IV. A production screening protocol was applied to 6 different transformants of each construction to evaluate each construction production levels and determine the

best producing colony. 10 ml of TBlac medium (see Annex III) supplemented with 100 µg/mL of ampicillin was inoculated with a single colony and grown for 20 h, at 37 °C, 200 rpm. As positive control it was used *E. coli* BL21(DE3) transformed with pCM13::*SELP-59-A* and as negative control it was used *E. coli* BL21(DE3) with no plasmid.

From each sample, 1 ml of cell culture was collected and centrifuged for 1 min at 14000 x g, resuspended in 100 µL of TE buffer (50 mM Tris, 1 mM EDTA at pH 8.0) and 25 µL of sample loading buffer (10% w/v SDS, 10 mM beta-mercapto-ethanol, 20% v/v glycerol, 0.2 M Tris-HCl pH 6.8, 0.05% w/v bromophenol blue) and centrifuged for 20 min at 16000 x g.

Production levels were analysed, comparing samples from crude extracts by sodium dodecyl sulphate polyacrylamide gel electrophoresis (SDS-PAGE) with a 10% SDS-PAGE gel (Table 14). To allow direct comparison between transformants, the OD_{600nm} of each culture was determined and samples were normalized for the same cell density (OD_{600nm} = 0.1) using the formula: OD_i x V_i = OD_f x V_f, where OD_i is the OD_{600nm} of the cell culture, V_i is the volume (µL) of supernatant to apply in each lane, OD_f is 0.1, and V_f is 125 (100 µL TE + 25 µL loading buffer). Protein marker II (NZYTech) was used as molecular weight marker.

Table 14. Reagents used for the elaboration of one 10% SDS-PAGE gel.

Reagent	Resolving gel	Stacking gel
30% Acrylamide/ 0.4% Bis	1565 µL	415 µL
1.875 M Tris pH 8.8	1875 µL	-
1.875 M Tris pH 6.8	-	630 µL
ddH ₂ O	1105 µL	1355 µL
10% SDS	47 µL	25 µL
10% APS	75 µL	25 µL
TEMED	7.5 µL	5 µL

Each SDS gel was run at a constant current flow of 15 mA (PowerPac™ Basic and Mini-PROTEAN® Tetra Cell, BioRad), for approximately 2 h. Gels were stained with 50 mL of fresh prepared aqueous copper chloride (CuCl₂) 0.3 M solution. Images were captured using ChemiDoc® XRS+ system and relative levels of protein expression were estimated using ImageJ® software (<https://imagej.net/Welcome>) to compare band intensity. The transformants with the highest expression levels were chosen to continue the work and stored frozen at -80 °C in glycerol 30% (v/v) until further use.

3.3.1. SELP-59-A_nRGD production optimization

In order to optimize the production of SELP-59-A_nRGD (pET25::*SELP-59-A_nRGD* expression product), pET25::*SELP-59-A_nRGD* was also transformed into *E. coli* BL21(DE3) pLysE, *E. coli* C43(DE3) pRARE and *E. coli* Origami B (DE3) for protein expression. All *E. coli* strains were transformed using the adapted TSS transformation protocol¹⁷⁷ (see Annex IV). Protein expression levels in *E. coli* C43(DE3) pRARE and *E. coli* Origami B (DE3) transformants were evaluated by a production screening protocol, as previous described. To evaluate the production levels on *E. coli* BL21(DE3) pLysE, 4 transformants were chosen for a production screening protocol using TB medium, induced at an $OD_{600nm}=0.8$, with IPTG to a final concentration of 1mM. Samples were taken 2 and 4 h after induction.

All samples were processed as mentioned in section 3.3. As positive and negative controls *E. coli* BL21(DE3) transformed with pET25::*SELP-59-A_nRGD* and *E. coli* BL21(DE3) were used, respectively.

3.4. PROTEIN PRODUCTION

E. coli BL21(DE3) cells containing the final constructions were grown in TBlac supplemented with 100 µg/mL for protein expression using the following conditions: 22 h of elapsed fermentation time; at 37 °C; 200 rpm of agitation, 250 mL in 1 L Erlenmeyer flasks sealed with cotton plugs (1:4 volume of medium to volume of flask ratio). After fermentation, cells were harvested by centrifugation at 10375 x g for 10 min, at 4°C and the pellets were frozen at -20 °C until purification.

3.5. PROTEIN PURIFICATION

Cells were resuspended in TE buffer (60 mL per liter of production) at 4 °C with agitation for 30 min and lysed by ultrasonic disruption (sonication) (750W, Vibra cell 75043, Fisher S. Bioblock Scientific). Sonication was performed with a probe of 25 mm diameter with 60% of amplitude, 3 s pulse on, 9 s pulse off, and a total active sonication time of 10 min.

In order to precipitate *E. coli* native proteins and to increase cell lysis, pH was adjusted to 3.5 with hydrochloric acid (HCl) 1.6 M, under agitation for 30 min, at 4 °C and centrifuged at 10695 x g, 20 min, 4 °C, for insoluble debris removal. The soluble polymers were then precipitated by the salting out technique using 25% of ammonium sulphate saturation (see section 3.6 for concentration optimization) by slowly adding ammonium sulphate to the supernatant under agitation at 4 °C. The resulting mixture was maintained on ice for 30 min followed by centrifugation at 10695 x g for 20 min at 4 °C. After

centrifugation, the precipitated polymer was resolubilized with upH₂O at 4 °C overnight and the resulting solution was dialyzed in a 10000-12000 Da membrane (Medicell Membranes, Ltd) against water at 4 °C. The dialyzed solution was centrifuged at 10695 x g, 20 min at 4 °C followed by filtration with a polyethersulfone (PES) 0.45 µm filter. The resulting solution was frozen at -80 °C and lyophilized (Christ Alpha 2-4 LD Plus, Bioblock Scientific) for water removal.

3.6. PROTEIN PURIFICATION OPTIMIZATION

To assess the optimal concentration of ammonium sulphate saturation for purification of each polymer, 10 mL supernatant of a production of 1 L were precipitated with 15, 20, 25, 30 and 35% ammonium sulphate saturation. Ammonium sulphate quantities were calculated using the online tool ammonium sulphate calculator (<http://www.encorbio.com/protocols/AM-SO4.htm>, Encor Biotechnology, Inc.).

Ammonium sulphate was slowly added to the supernatants under agitation at 4 °C and the mixture was incubated on ice for 30 min, followed by centrifugation at 10695 x g for 20 min at 4 °C. After centrifugation, the precipitated polymer was resolubilized in half of the initial volume with 4 °C upH₂O overnight.

Polymer precipitation was assessed by SDS-PAGE, by comparison of the quantity of protein present in the resuspended pellet and supernatant for each saturation. Samples of 100 µL from both the supernatant and the resuspended pellet were collected, and 25 µL of sample loading buffer were added. Gels were run and stained as stated in section 3.3.

The optimal concentration of ammonium sulphate to precipitate each polymer was the lowest saturation that led to total polymer precipitation. This saturation is the one in which it is no longer possible to observe a band in the sample of the supernatant in SDS-PAGE gels.

3.7. SOLVENT CASTING AND POST-PROCESSING TREATMENT OF FILMS

SELP-59-A and SELP-59-A_CAMs films were prepared by solvent casting using formic acid as solvent by dissolution of the pure lyophilized protein to a final concentration of 3% (w/v). Different films were produced by combining SELP-59-A with different percentages of functionalized polymer (0, 25, 50 75 and 100 wt%) (Table 15). Then, 130 µL of each protein solution was cast into a 10 mm (diameter) polytetrafluoroethylene (PTFE, Teflon®) mold and allowed to dry at room temperature until complete solvent evaporation (Figure 5).

Since SELP films are water soluble and the application involves contact with aqueous solutions, insolubility was induced by treatment with methanol-saturated air at room temperature for 48 h in a desiccator.

Table 15. Different films produced by combination of SELP-59-A and functionalized polymers.

Film	SELP-59-A_CAM (wt%)	SELP-59-A (wt%)
SELP-59-A_CAM 25%	25	75
SELP-59-A_CAM 50%	50	50
SELP-59-A_CAM 75%	75	25
SELP-59-A_CAM 100%	100	0

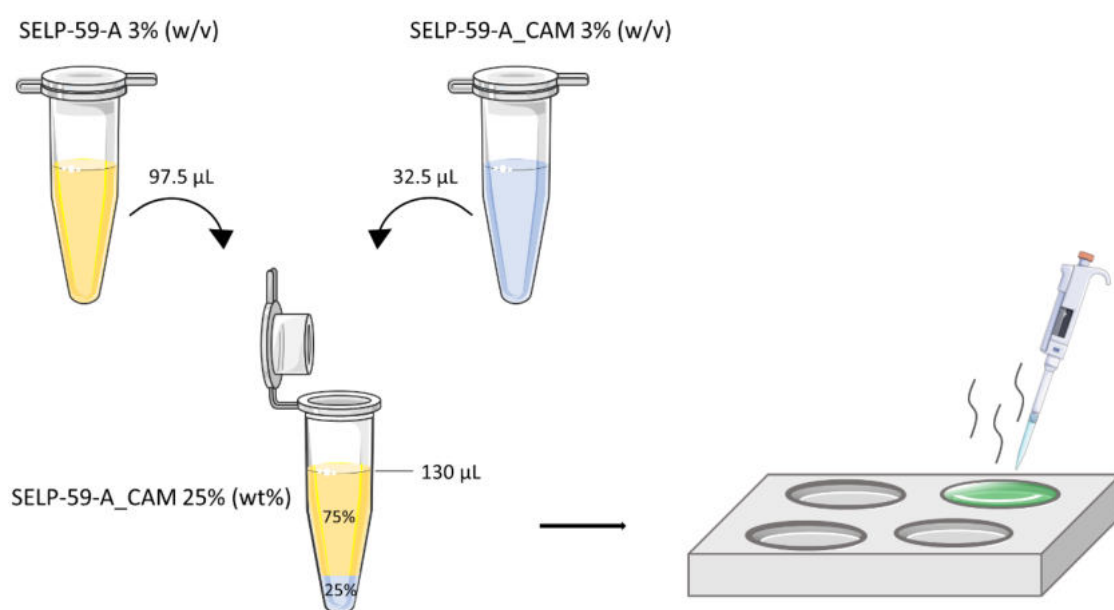


Figure 5. Schematic representation of film preparation process.

3.8. FILM CHARACTERIZATION

Treated and untreated films were characterized using attenuated total reflectance-Fourier transform infrared (ATR-FTIR) spectroscopy. Spectra were acquired from 4000 cm^{-1} to 400 cm^{-1} at room temperature with a Spectrum Two spectrometer (Perkin Elmer) coupled with an UATR (single reflection

diamond, Perkin Elmer) accessory. Spectra were collected after 64 scans with a resolution of 4 cm^{-1} with automatic correction of atmospheric $\text{CO}_2/\text{H}_2\text{O}$.

3.9. MAMMALIAN CELL LINES STAINING OPTIMIZATION

300 μL of a suspension of HaCaT cells at a density of 2.0×10^5 cells/mL were seeded per well into a surface treated sterile 24-well plate (TPP®) and incubated for 24 h at $37\text{ }^\circ\text{C}$ with 5% CO_2 in a humidified environment. Following incubation, cells were washed with sterile phosphate-buffered saline solution (PBS) 1x (see Annex III) at $37\text{ }^\circ\text{C}$ and incubated with Hoechst 34580 (Sigma-Aldrich) $5\text{ }\mu\text{M}$ for 15, 30 and 40 min or 4',6-diamidino-2-phenylindole (DAPI) (Invitrogen) $5\text{ }\mu\text{M}$ for 15 min, DAPI $2.5\text{ }\mu\text{M}$ for 30 min and DAPI $0.5\text{ }\mu\text{M}$ for 60 min (Figure 6). One well without probe was used as negative control. After the stipulated incubation time for each probe, cells were washed with 200 μL of sterile PBS 1x at $37\text{ }^\circ\text{C}$. Afterwards, PSB was replaced by 200 μL of sterile PBS 1x at $37\text{ }^\circ\text{C}$.

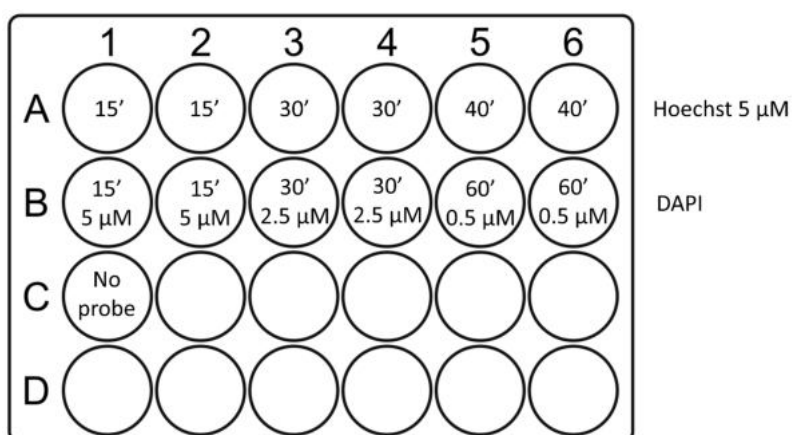


Figure 6. 24-well plate scheme used for cell staining optimization.

SH-SY5Y cells were seeded using 500 μL of cell suspension per well at a density of 2×10^5 cells/mL into a sterile surface treated 24-well plate (TPP®) and incubated for 24 h at $37\text{ }^\circ\text{C}$ with 5% CO_2 in a humidified environment. Following incubation, cells were washed with sterile PBS 1x at $37\text{ }^\circ\text{C}$ and incubated with the same probes as mentioned above to HaCaT cell line. For both cell lines, fluorescence was observed using a fluorescence microscope (Olympus IX71 inverted microscope) with micrographs from random locations being recorded and compared.

3.10. EVALUATION OF THE EFFECT OF THE CELL'S FIXATION PROCESS ON FILM STRUCTURE AND STAINING.

Films were washed with 300 μ l of sterile PBS 1x and incubated for 24 h with 300 μ l of DMEM + 10% FBS medium using an untreated sterile 24-well plate (Sarstedt).

The films subjected to the fixation process had the culture medium aspirated and were washed with 300 μ l of PBS 1x. Then, 300 μ l of formaldehyde 3.7% were added and incubated for 10 min at room temperature. Films were washed 2 times with 300 μ l of PBS 1x. PBS was replaced by 300 μ l of 0.1% TritonX-100, which was allowed to incubate 5 min at room temperature. Films were washed 2 times with 300 μ l of PBS 1x. The staining was only performed on SELP-59-A 100%, SELP-59-A_nC3 100% and SELP-59-A_cRGD films, by incubation with 100 μ l of Rhodamine Phalloidin (Abcam) in each well at 37 ° C in the dark for 20 min. The wells were washed 2 times with PBS 1x and 100 μ L of Hoechst 34580 (Sigma-Aldrich) 5 μ M were placed in each well and allowed to incubate at 37 ° C for 15 min followed by observation under a microscope (Olympus IX71 inverted microscope).

In the films not subjected to the fixation process, the culture medium was aspirated, and films were washed with 300 μ l of PBS 1x. 100 μ l of Rhodamine Phalloidin were placed in in each well and incubated at 37 ° C in the dark for 20 min. The films were washed 2 times with PBS 1x and posteriorly incubated at 37 ° C for 15 min with 100 μ L of Hoechst 34580 (Sigma-Aldrich) 5 μ M. The wells were then washed with 300 μ l of PBS 1x and observed under a microscope (Olympus IX71 inverted microscope).

3.11. CELL ADHESION ASSAYS

Films were washed with 300 μ L of sterile PBS 1x and incubated at room temperature for 30 min with complete culture medium for hydration and sterilization. 50 μ L of HaCaT and SH-SY5Y cell suspension were seeded on top of each film at a density of 5.4×10^6 and 2.0×10^6 , respectively, using an untreated sterile 24-well plate (Sarstedt) and incubated for 2 h at 37 °C with 5% CO₂ in a humidified environment. After incubation, 250 μ L of culture medium were added to each well and the plate incubated for 24 h at 37 °C with 5% CO₂. As viability control, 50 μ L of cell suspension at the same densities mentioned above were incubated into a sterile surface treated 24-well plate (TPP®) for 2 h at 37 °C with 5% CO₂ in a humidified environment. After incubation, 250 μ L of culture medium were added to each well and the plate incubated for 24 h at 37 °C with 5% CO₂. In order to maintain moisture inside the plates and prevent the loss of culture medium volume, 300 μ l of sterile PBS 1x were added in unused wells.

After the incubation period, the culture medium was aspirated and films washed with 300 μ l of PBS 1x. Then, 300 μ l of formaldehyde 3.7% were added in each well and incubated for 10 min at room temperature. Films were washed 2 times with 300 μ l of PBS 1x. Afterwards, PBS was replaced by 300 μ l of 0.1% TritonX-100, which was allowed to incubate 5 min at room temperature. Films were washed 2 times with 300 μ l of PBS 1x. 100 μ l of Rhodamine Phalloidin were added and incubated in each well at 37 ° C in the dark for 20 min. The films were washed 2 times with PBS 1x and 100 μ L of Hoechst 34580 (Sigma-Aldrich) 5 μ M were incubated in each well at 37 °C for 15 min followed by observation under a microscope (Olympus IX71 inverted microscope).

4. Results and Discussion

4. RESULTS AND DISCUSSION

4.1 CREATION OF RECOMBINANT PROTEIN-BASED POLYMERS BASED ON SILK AND ELASTIN INTEGRATING DIFFERENT CELL BINDING MOTIFS

4.1.1 Adhesion sequences selection

With the objective to produce SELP-59-A polymers that promote cell adhesion, it was necessary to select adhesion sequences in order to functionalize the polymer. The chosen strategy includes the selection of a sequence that has activity in a broad spectrum of cell lines, and another sequence that was specific to a limited number of cell lines.

The RGD sequence was chosen as the sequence that promote the adhesion of a large number of cell lines, due to its well-studied behavior in numerous cell lines and it is recognized by several integrins. Since the integrin-ligand specificity and affinity depends not only on the adhesion sequence itself but also on the adjacent amino acids¹⁷⁸ and the stereochemical conformation of the peptide chain^{144,179}, research was made to select the sequence of amino acids that promotes higher cell adhesion (Table 16).

Previous studies have reported that cyclic RGD peptides increase cell adhesion and spreading up to 100 times when compared to linear analogues^{180,181}. However, cyclic RGD was not considered to be applied in the functionalization of SELP-59-A due to the fact that the circularization of the RGD sequence involves chemical processes that could potentially lead to the modification of the structure of the SELP-59-A and the loss of its desirable physical, mechanical and biological properties.

The RGD sequence chosen to functionalize SELP-59-A was the one studied by Widhe and collaborators¹⁴⁴ (CTGRGDSPAC), in which two amino acids flanking the original fibronectin sequence (VTGRGDSPAS) were substituted for cysteines. This modification leads to the formation of a disulfide bridge, which exposes the RGD sequence steadily. The authors were inspired by the natural position of the RGD sequence in the fibronectin molecule at the edge of a hairpin turn loop, which exposes the sequence and allows the recognition by integrins¹⁸². Recombinant spider silk functionalized with this sequence obtained significantly better results than recombinant spider silk not functionalized with adhesion sequences (P <0.01 for human dermal microvascular endothelial cells (EC), P <0.05 for human MSC and P <0.0001 for normal human epidermal keratinocytes from adult skin (KC)).

Table 16. Adhesion sequences containing RGD motif used to functionalize recombinant polymers. Highlighted sequence was the amino acid sequence chosen to functionalize SELP-59-A. Approximated efficiency values compared with non-functionalized polymer. (*) median value, since the mean it was not available. MAP: mussel adhesion protein; SLP: silk-like polymer; HeLa: human epithelioid cervix carcinoma cells; HEK293T: human embryonic kidney cells mutated in SV40 large T antigen; CHO: Chinese hamster ovary cells; BALB/3T3: mouse embryonic fibroblasts; Saos-2: human osteosarcoma cells.

Sequence	Polymer	Position	Cell line	Incubation period	Efficiency	Reference
GRGDSP	MAP (fp-151)	C-terminus	HeLa	18 h	+12.5%	Hwang, D. S. <i>et al.</i> , (2007) ¹³⁵
			HEK293T		+10.8%	
			CHO		+20%	
GRGDSPG	SLP (eADF4(C16))	C-terminus	BALB/3T3	1.5 h	+67.1%	Wohlrab, S. <i>et al.</i> , (2012) ¹⁴⁵
CTGRGDSPAC	SLP (4RepCT)	N-terminus	EC	1 h	+280%*	Widhe, M. <i>et al.</i> ,(2016) ¹⁴⁴
			MSC		+700%*	
			KC		+2350%*	
VTGRGDSPAS	SLP (4RepCT)	N-terminus	KC	1 h	+1300%*	Widhe, M. <i>et al.</i> ,(2016) ¹⁴⁴
STGRGDSPAS	SLP (4RepCT)	N-terminus	KC	1 h	+1100%*	Widhe, M. <i>et al.</i> ,(2016) ¹⁴⁴
RGD	SLP (4RepCT)	N-terminus	EC	1 h	+65%*	Widhe, M. <i>et al.</i> ,(2016) ¹⁴⁴
			MSC		+200%*	
			KC		+500%*	
AVTGRGDSPASS	ELP	(ELP-RGD-ELP) ₅	Saos-2	24 h	+42.6%	Costa, R. R. <i>et al.</i> , (2009) ¹³⁴
				4 d	+36.7%	
				7 d	+168.8%	

Note: sequences are given in single-letter amino acid code.

The adhesion sequence that promote the adhesion of a limited number of cell lines was chosen after target cells/tissue were selected.

Nervous system injuries, particularly on the nerves, caused by contusion, stretch or laceration usually lead to total or partial loss of function due to the loss of axonal continuity, which causes nerve degeneration¹⁸³. While nerves can regenerate on their own and recover total or partial function when injuries are small, larger injuries must be surgically treated to promote coaptation, i.e. the joining or adjustment of the truncated axonal extremities to one another^{184,185}. When coaptation is not possible, the most common method of treatment is the use of autografts to promote the reinnervation¹⁸⁵⁻¹⁸⁷. However, drawbacks such as the requirement of two surgeries and the removal of tissue from the patient fuel the search for better alternatives^{187,188}.

An alternative to the nerve graft is to use a scaffold, providing structural support for neural cell growth and guiding nerve regeneration¹⁸⁶. Several scaffolds have already been used for this purpose, using mainly aligned electrospun fibers of synthetic biomaterials^{185,189-191} and composite fibers containing whole proteins or peptides sequences^{186,187,192} to guide both developing and regenerating neurons *in vitro* and *in vivo*¹⁹³.

To stimulate nerve tissue regeneration, the adhesion sequence chosen to functionalize SELP-59-A should promote cell adhesion, as well as neuritogenesis (the formation of new neurites, which develop into axons

and dendrites)¹⁹⁴ and synaptogenesis (the process of synapse formation, synapse maintenance and activity-dependent synapse refinement and elimination)^{195,196}. Several sequences were considered for this purpose (Table 17).

Table 17. Sequences involved in cell adhesion specific for cells of the nervous system. The highlighted sequence corresponds to selected amino acid sequence to functionalize SELP-59-A. NCAM: neural cell adhesion molecule; FGFR: fibroblast growth factor receptor; HSPG: heparan sulfate proteoglycan.

Peptide name/sequence	Identity/localization	Receptor/module	Effects
NBP10/AKKMWKKTW	Artificial peptide	NCAM/IgI	Induction of neurite outgrowth ¹⁹⁷ Inhibition of NCAM-mediated cell adhesion ¹⁹⁷
C3/ASKKPKRNIKA	Artificial peptide	NCAM/IgI FGFR/IgII–IgIII	Induction of neurite outgrowth ^{198,199} Enhancement of presynaptic function at low concentration ¹⁹⁹ Inhibition of NCAM-mediated adhesion ²⁰⁰ Neuroprotection against apoptosis ²⁰¹ Promotion of synapse formation ¹⁹⁹ Protection against teratogen-induced embryotoxicity ²⁰² Promotion of phenotypic neuronal differentiation ^{200,203}
HBP/KGRDVLKDKVRFI	NCAM/IgII	Heparin/HSPG	Induction of neurite outgrowth ²⁰⁴
FGL/EVYWAENQQGSKA	NCAM/FN3,II	FGFR/IgII–IgIII	Induction of neurite outgrowth ²⁰⁵ Neuroprotection against apoptosis ²⁰⁵ Promotion of phenotypic neuronal differentiation ²⁰³ Modulation of synaptic plasticity ^{206–208} Anti-neuroinflammation ²⁰⁹
ENFIN2/AFYRTIQWTME ENFIN11/ARWSKGFQWMM	Artificial peptides	NCAM/FN3,1-2	Induction of neurite outgrowth ²¹⁰
P2/ GRILARGEINFK	NCAM/IgII	NCAM/IgI	Induction of neurite outgrowth ²¹¹ Neuroprotection against apoptosis ²¹¹ Inhibition of NCAM-mediated adhesion ²¹²
Plannexin/DVRRGIKKT	NCAM/IgII	NCAM/IgIII	Induction of neurite outgrowth ²¹³ Neuroprotection against apoptosis ²¹³ Promotion of phenotypic neuronal differentiation ²⁰³ Modulation of synaptic plasticity ²¹⁴
BCL/NLIKQDDGGSPIRHY	NCAM/FN3,II	FGFR/IgII–IgIII	Induction of neurite outgrowth ²¹⁵
EncaminA/SIDRVEPYSSTAQVQFD	NCAM/FN3,I	FGFR/IgII–IgIII	Induction of neurite outgrowth ²¹⁶
EncaminC/KAEWKSLGEEAWHSK EncaminE/TIMGLKPETRYAVR	NCAM/FN3,I	FGFR/IgII–IgIII	Induction of neurite outgrowth ²¹⁶ Promotion of neuronal survival ²¹⁶ Enhancement of presynaptic function ²¹⁶

Note: sequences are given in single-letter amino acid code.

Although these sequences are not often used to promote cell adhesion to materials, they have potential to be used to stimulate nerve tissue regeneration, considering that the majority of them were identified in a molecule involved in cell-cell adhesion (NCAM), which is abundantly expressed in the nervous system²⁰¹. NCAM plays a crucial role in neuronal development, regeneration and synaptic plasticity, by functioning as signaling receptor, initiating a complex network of signaling transduction cascades^{154,155,217}. All these functions are triggered by the homophilic interaction between NCAMs of adjacent cells, or by the heterophilic bond of NCAM molecules to different molecules, such as ECM molecules like heparin, or membrane receptors such as FGFR^{217,218}.

Considering the effects of each of the sequences, C3 was chosen as it fulfills all the requirements mentioned above and should promote neuron adhesion and survival.

4.1.2 Design of genetic constructions

Studies show that the initial codons of a DNA sequence are directly related to the transcription and translation rates of a gene²¹⁹⁻²²⁴ as well as the solubility²²⁵ and the half-life time of a protein^{226,227}. Furthermore, the biological activity of functionalized polymers depends on the contact of adhesion sequences with cells. Since it is not possible to predict the conformation of the adhesion sequence on the functionalized polymer, each of the chosen sequences was placed at the N- and C-terminal of the SELP-59-A sequence (Figure 7) to increase the probability of success.

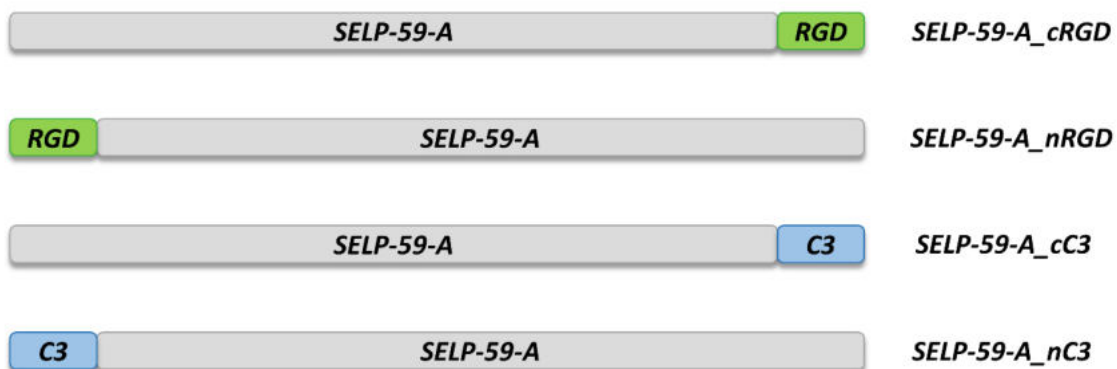


Figure 7. Schematic representation of the constructions designed.

pET25b(+) plasmid was chosen to design the genetic constructs, since the SELP-59-A polymer was previously produced with high productivity (500 mg/L)⁹² using the pET system⁷⁶, through a modified pET25b(+) plasmid (pCM13::*SELP-59-A*).

Since pET25b(+) plasmid does not have the appropriate restriction sites to design the desired sequences, an adapter with the characteristics described in Figure 8 was designed. For this, two primers that partially overlap were used (Table 7), which is able to form the complete sequence through PCR, as described in the section 3.2.2. The success of the PCR and the size of the band were confirmed by DNA agarose gel electrophoresis (Figure 9).

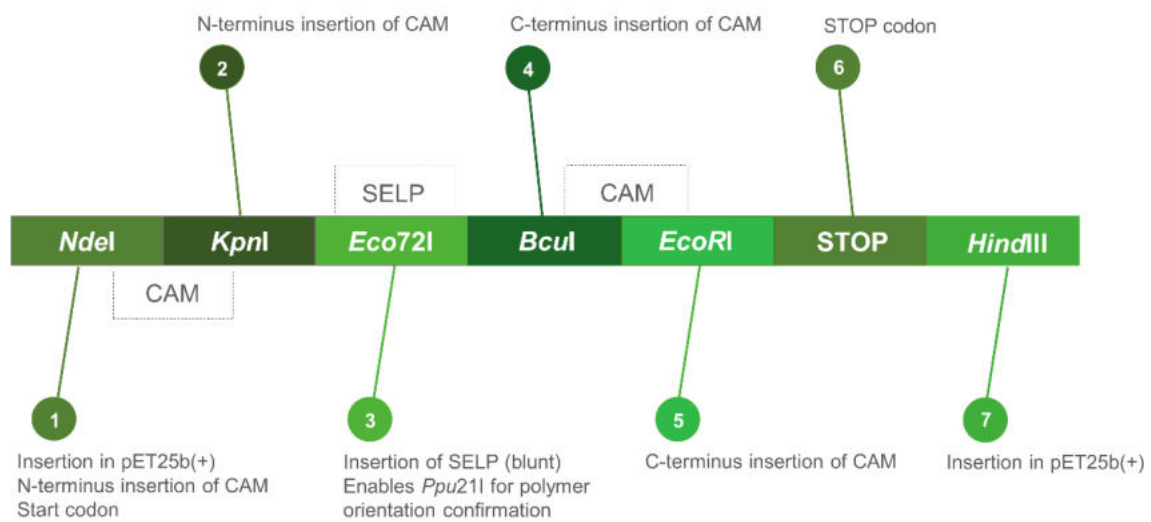


Figure 8. Schematic representation of the adapter designed, depicting recognition sequences for restriction enzymes.

The *adapter* sequence was digested with *NdeI* and *HindIII* and ligated to linearized pET25b(+), previously digested with the same enzymes. The ligation was confirmed by digestion with *Ppu21I* (Figure 10), showing the expected molecular weight DNA bands, and further confirmed by DNA sequencing (see Annex V, Figure 55). The resulting plasmid was named pET25::*adapter*.

The DNA sample present in lane 2 of Figure 10B was chosen due to the amount of DNA extracted and to the absorption graph obtained in the NanoDrop®, which indicated a solution with DNA at a higher purity.

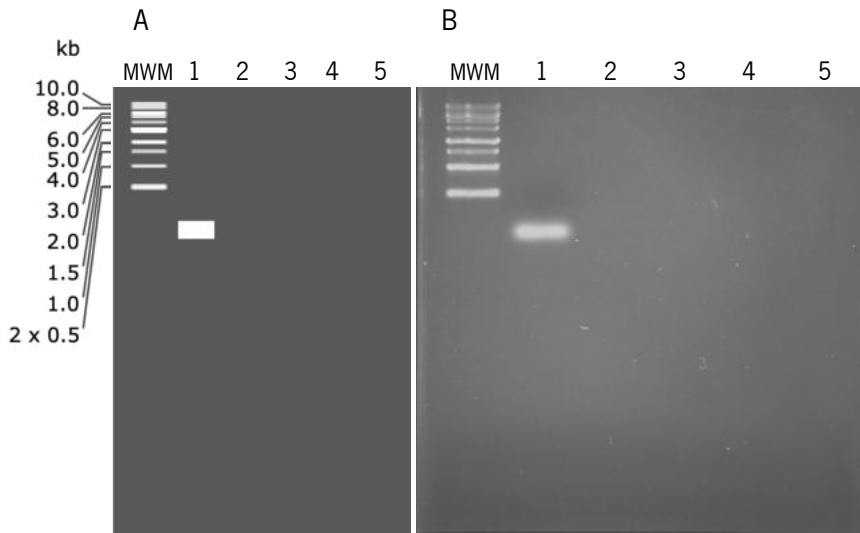


Figure 9. Adapter sequence in a 1% agarose gel. A – *In silico* simulation (SnapGene®). B – Electrophoretic analysis showing the PCR product, in a 1% agarose gel stained with Midori Green Advance. MWM corresponds to the molecular weight marker (GSR ladder 1kb - Grisp). No modifications other than cropping, resizing and contrast adjustment were applied to the images.

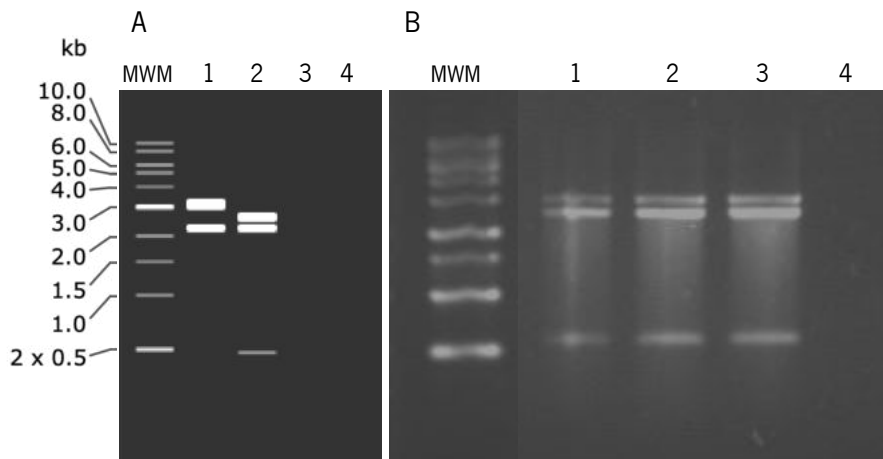


Figure 10. pET25::adapter digested with *Ppu21I*. A – *In silico* simulation (SnapGene®) of the digestion of pET25b(+) vector (lane 1), used as negative control, and pET25::adapter (lane 2) in a 1% agarose gel stained with Midori Green Advance. B – Electrophoretic analysis showing the digestion product of DNA from different transformants after restriction digestion, in a 1% agarose gel stained with Midori Green Advance. MWM corresponds to the molecular weight marker (GSR ladder 1kb - Grisp). No modifications other than cropping, resizing and contrast adjustment were applied to the images.

To insert the *SELP-59-A* sequence, pET25::adapter was digested with *Eco72I*. The success of full digestion reaction was confirmed by DNA agarose gel electrophoresis (Figure 11).

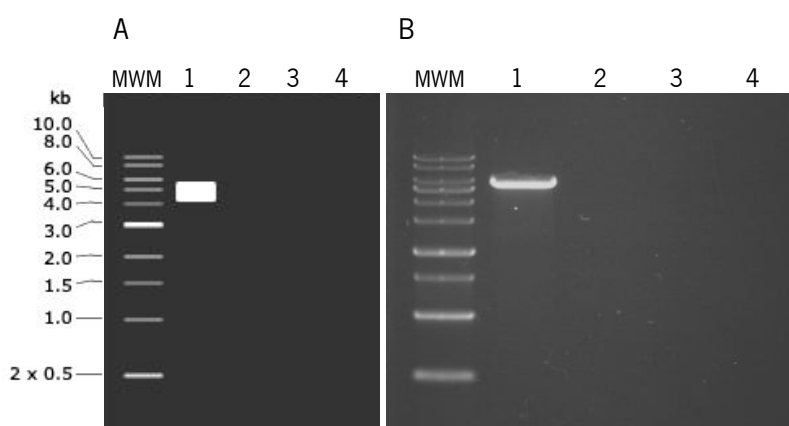


Figure 11. pET25::*adapter* plasmid digested with *Eco72I*. A – *In silico* simulation (SnapGene®). B – Electrophoretic analysis showing the PCR product, in a 1% agarose gel stained with Midori Green Advance. MWM corresponds to the molecular weight marker (GSR ladder 1kb - Grisp). No modifications other than cropping, resizing and contrast adjustment were applied to the images.

SELP-59-A was extracted from pDrive::*SELP-59-A* by digestion using *Eam1104I* (not shown). Since this restriction enzyme produces sticky ends, and the digestion of pET25::*adapter* with *Eco72I* produces blunt ends, it was necessary to fill in the sticky ends of the *SELP-59-A* to make the ligation compatible. The ligation and the orientation of the *SELP-59-A* sequence was initially evaluated by digestion with *Ppu21I* and *HindIII* restriction enzymes as depicted in Figure 12. None of the band profiles exactly matched the one predicted (lane 2 of Figure 12A), although the profile of lanes 2 and 5 of Figure 12B resembled the expected profile. Thus, the DNA of the transformants 2 and 5 was digested with *NdeI* for plasmid linearization and insertion confirmation (Figure 13B), followed by DNA sequencing of the DNA from the transformant corresponding to lane 5 of Figure 13B (see Annex V, Figure 56-57). The plasmid resultant from the ligation was named pET25::*SELP-59-A*.

In the lane 6 of Figure 12B it was verified a double insertion of *SELP-59-A*. As this construct may be interesting for future applications, the insertion and correct orientation of both *SELP-59-A* sequences was confirmed by sequencing (see Annex V, Figure 58-59). Since none of the other transformants presented a positive or interesting result for possible future applications, these were not considered to proceed.

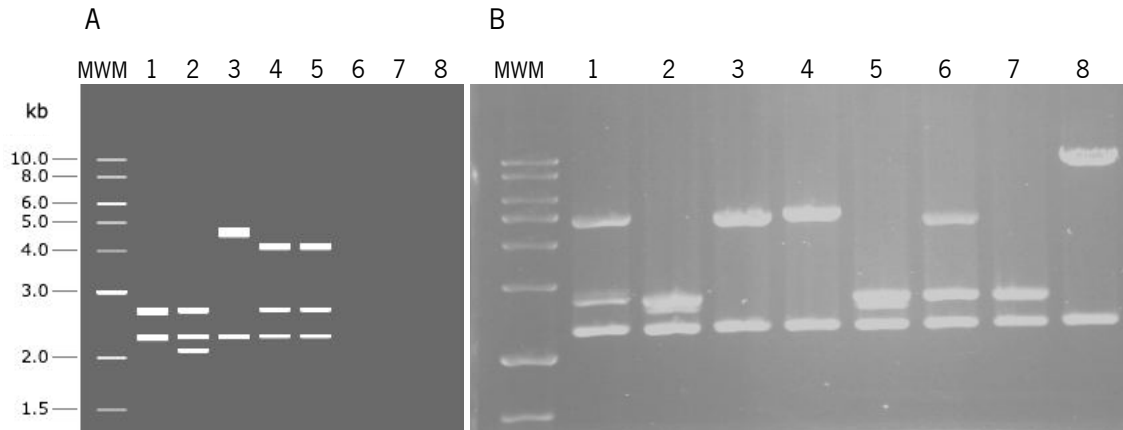


Figure 12. pET25::SELP-59-A digested with *Ppu21* and *HindIII*. A – *In silico* simulation (SnapGene®) of the digestion of pET25::adapter (lane 1); pET25::SELP-59-A vector (lane 2); pET25::SELP59-A with *SELP-59-A* inserted in the reverse orientation (lane 3); pET25::SELP-59-A+SELP-59-A (lane 4); pET25::SELP-59-A+SELP-59-A inserted in the reverse orientation (lane 5); B – Electrophoretic analysis showing the digestion product of DNA from different transformants after restriction digestion, in a 1% agarose gel stained with Midori Green Advance. MWM corresponds to the molecular weight marker (GSR ladder 1kb - Grisp). No modifications other than cropping, resizing and contrast adjustment were applied to the images.

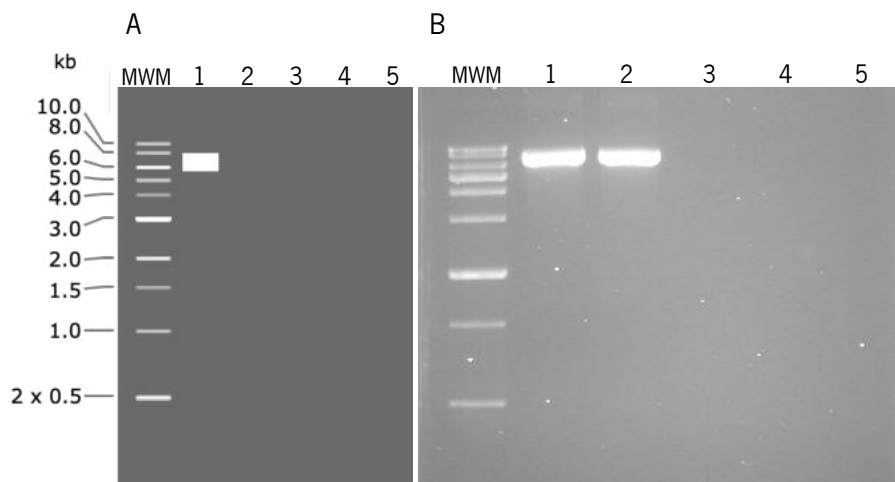


Figure 13. pET25::SELP-59-A plasmid digested with *NdeI*. A- *In silico* simulation (SnapGene®). B –Electrophoretic analysis showing the digestion product of DNA from transformant 2 (lane 1) and 5 (lane 2) after restriction digestion, in a 1% agarose gel stained with Midori Green Advance. MWM corresponds to the molecular weight marker (GSR ladder 1kb - Grisp). No modifications other than cropping, resizing and contrast adjustment were applied to the images.

As for the adapter sequence cloning, the adhesion sequences were designed using two primers that partially overlap, which formed the complete sequence by PCR. The success of the PCR and the size of the band were confirmed by DNA agarose gel electrophoresis (Figure 14).

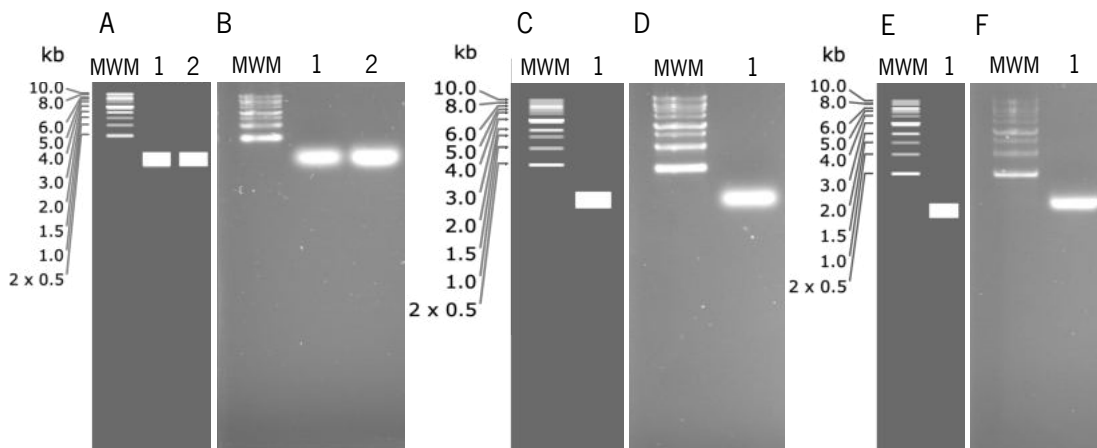


Figure 14. Adhesion sequences in a 1% agarose gel. A – *In silico* simulation (SnapGene®) of *nC3* (lane 1) and *nRGD* (lane 2) adhesion sequences in a 1% agarose gel. B – Electrophoretic analysis showing the PCR product of *nC3* and *nRGD* (lane 1 and 2, respectively) in a 1% agarose gel stained with Midori Green Advance. C – *In silico* simulation (SnapGene®) of *cRGD* sequence in a 1% agarose gel. D – Electrophoretic analysis showing the PCR product of *cRGD* sequence in a 1% agarose gel stained with Midori Green Advance. E – *In silico* simulation (SnapGene®) of *cC3* sequence in a 1% agarose gel. F – Electrophoretic analysis showing the PCR product of *cC3* sequence in a 1% agarose gel stained with Midori Green Advance. MWM corresponds to the molecular weight marker (GSR ladder 1kb - Grisp). No modifications other than cropping, resizing and contrast adjustment were applied to the images.

nC3 and *nRGD* were digested with *NdeI* and *KpnI*, and *cC3* and *cRGD* were digested with *BclI* *EcoRI*. Each adhesion sequence was ligated to linearized pET25::*SELP-59-A*, previously digested with the same enzymes. The ligation was verified by digestion with the enzymes used to insert the adhesion sequences. The electrophoretic analysis did not show the expected molecular weight DNA band profile (Figure 15), as the DNA bands corresponding to the excised adhesion sequences and to the digested plasmid appears to have higher molecular weight than expected. In the case of construction resulting from the ligation between pET25::*SELP-59-A* and *nRGD*, the amount of DNA used for the screening was below the probe detection limit, and therefore it was not possible to observe a band corresponding to the excised adhesion sequence (not shown).

All the ligations were later confirmed by DNA sequencing. The resulting plasmids were named pET25::*SELP-59-A_nC3*, pET25::*SELP-59-A_cC3*, pET25::*SELP-59-A_nRGD* and pET25::*SELP-59-A_cRGD* (see Annex V, Figure 60-64 for DNA sequencing results).

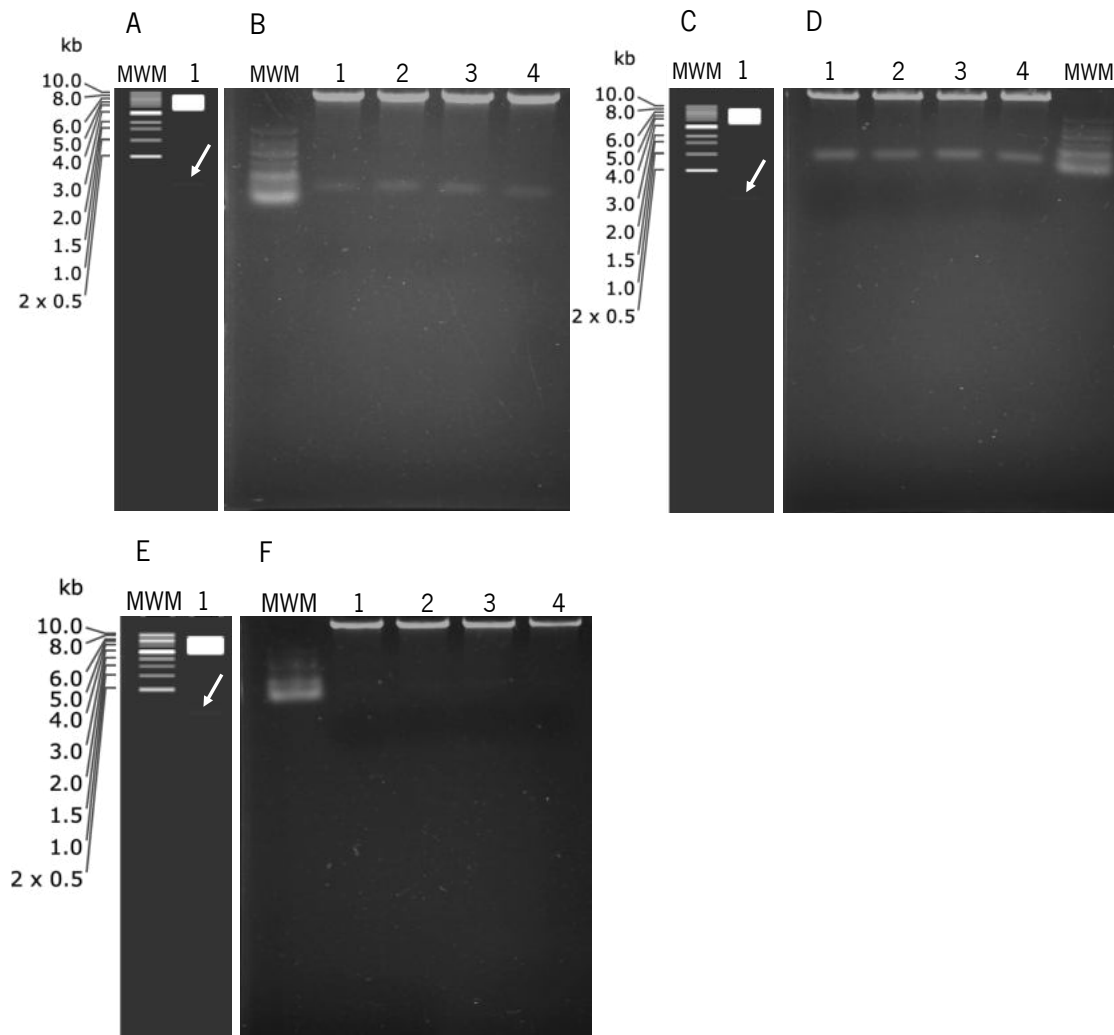


Figure 15. Ligation confirmation of the adhesion sequences. A – *In silico* simulation (SnapGene®) of pET25::*SELP-59-A_nC3* digested with *NdeI* and *KpnI*. B – Electrophoretic analysis showing the digestion products of DNA from different pET25::*SELP-59-A_nC3* transformants after digestion with *NdeI* and *KpnI* in a 1% agarose gel stained with Midori Green Advance. C – *In silico* simulation (SnapGene®) of pET25::*SELP-59-A_cC3* digested with *BclI* and *EcoRI*. D – Electrophoretic analysis showing the digestion products of DNA from different pET25::*SELP-59-A_cC3* transformants after digestion with *BclI* and *EcoRI* in a 1% agarose gel stained with Midori Green Advance. E – *In silico* simulation (SnapGene®) of pET25::*SELP-59-A_cRGD* digested with *BclI* and *EcoRI*. F – Electrophoretic analysis showing the digestion products of DNA from different pET25::*SELP-59-A_cRGD* transformants after digestion with *BclI* and *EcoRI* in a 1% agarose gel stained with Midori Green Advance. White arrows point to the band corresponding to the excised adhesion sequence. MWM corresponds to the molecular weight marker (GSR ladder 1kb - Grisp). No modifications other than cropping, resizing and contrast adjustment were applied to the images.

4.2 PRODUCTION AND PURIFICATION OF THE CREATED MATERIALS

4.2.1 Production of recombinant polymers

All confirmed constructions were transformed into *E. coli* BL21 (DE3). Previous experience with SELP-59-A production using both the pET system⁷⁶ and this strain resulted in high productivities, being the first choice for this work.

To evaluate the production levels of SELP-59-A by BL21 (DE3) transformed with pET25::*SELP-59-A*, pCM13::*SELP-59-A* and pET25::*adapter* were used as positive and negative control, respectively (Figure 16). The SDS-PAGE analysis did not show the expected molecular weight bands as SELP-59-A have an expected molecular weight of 55 kDa, but the bands of interest, pointed by the arrows, seem to have a molecular weight of approximately 75 kDa. This abnormal gel mobility that is believed to be due to the high hydrophobicity of the polymer⁷⁶ was verified throughout all the SDS-PAGE analysis and was previously reported by several authors^{76,156,228-231}. For a precise determination of the molecular weight of polymers a qualitative method such as mass spectrometry should be used.

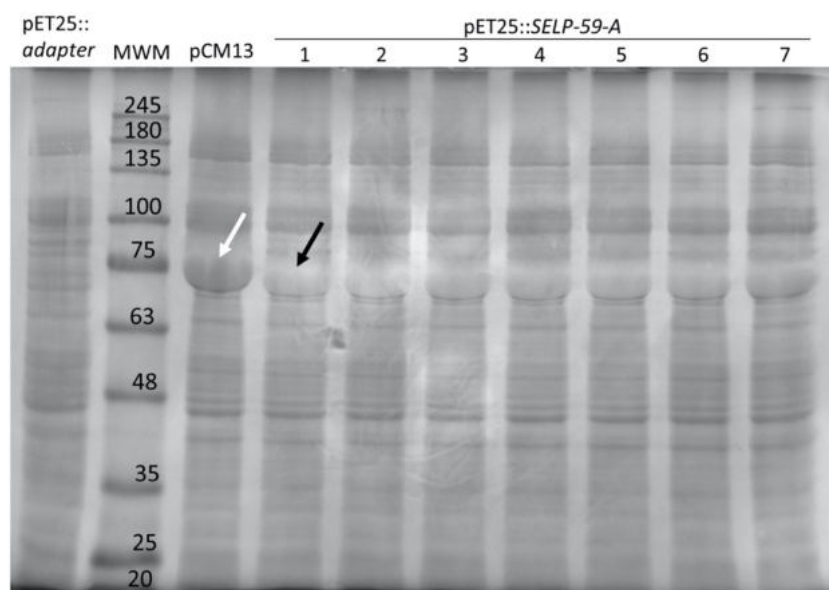


Figure 16. SDS-PAGE analysis of SELP-59-A production in *E. coli* BL21 (DE3) pET25::*SELP-59-A* transformants after 22 h at 200 rpm and 37 °C in TBlac medium. pET25::*adapter* and pCM13, used as negative and positive controls, correspond to *E. coli* BL21 (DE3) transformed with pET25::*adapter* and pCM13::*SELP-59-A*, respectively. Arrows point to the bands of interest; black arrow indicates SELP-59-A polymer band of the chosen transformant. Loaded samples were normalized to the same cell density ($OD_{600nm} = 0.1$). Gel was stained with $CuCl_2$ 0.3 M. MWM corresponds to the molecular weight marker (Protein marker II, NZYTech). No modifications other than cropping and resizing were applied to the image.

The production level of SELP-59-A of all pET25::*SELP-59-A* transformants was lower than the one observed on the pCM13::*SELP-59-A* transformants (Figure 16). The pET25::*SELP-59-A* transformant pointed by the black arrow was chosen to be used as control in future production screenings.

A production screening was performed to evaluate the expression levels of the functionalized polymers, with an expected molecular weight of 56.06 kDa in case of SELP-59-A_cC3 and SELP-59-A_nC3, and 55.79 kDa in case of SELP-59-A_cRGD and SELP-59-A_nRGD. Relative levels of protein expression were estimated comparing band intensity, aiming to the determination of the best producing colony. As observed in Figure 17, the production levels of SELP-59-A_cC3 were lower than SELP-59-A production using pCM13::*SELP-59-A* plasmid and very similar to SELP-59-A production using pET25::*SELP-59-A* plasmid. Based on the SDS-PAGE analysis, the transformant number 5 (black arrow) was chosen to proceed.

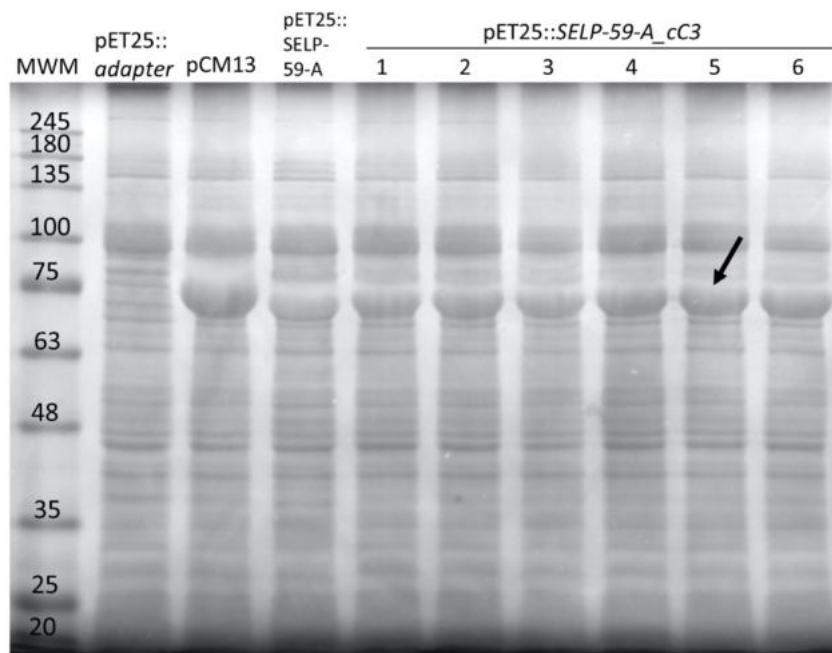


Figure 17. SDS-PAGE analysis of SELP-59-A_cC3 production in *E. coli* BL21 (DE3) pET25::*SELP-59-A_cC3* transformants after 22 h at 200 rpm and 37 °C in TBlac medium. pET25::adapter and pCM13, used as negative and positive controls, correspond to *E. coli* BL21 (DE3) transformed with pET25::adapter and pCM13::*SELP-59-A*, respectively. Arrow points to the band corresponding to SELP-59-A_cC3 polymer of the chosen transformant. Loaded samples were normalized to the same cell density ($OD_{600nm}=0.1$). Gel was stained with $CuCl_2$ 0.3 M. MWM corresponds to the molecular weight marker (Protein marker II, NZYTech). No modifications other than cropping and resizing were applied to the image.

The production levels of SELP-59-A_nC3 were similar to SELP-59-A production using pCM13::*SELP-59-A* plasmid, and higher than SELP-59-A production using pET25::*SELP-59-A* plasmid (Figure 18). Based on the results, the transformant number 4 (black arrow) was chosen to proceed.

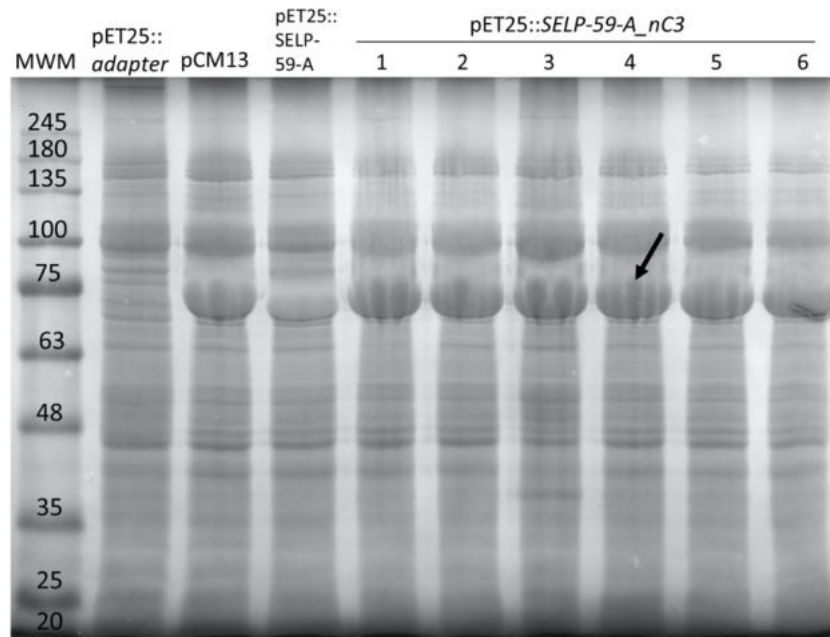


Figure 18. Screening of SELP-59-A_nC3 production in several colonies of *E. coli* BL21 (DE3) after 22 h at 200 rpm and 37 °C in TBlac medium. pET25::adapter and pCM13, used as negative and positive controls, correspond to *E. coli* BL21 (DE3) transformed with pET25::adapter and pCM13::*SELP-59-A*, respectively. Arrow points to the band corresponding to SELP-59-A_nC3 polymer of the chosen transformant. Loaded samples were normalized to the same cell density ($OD_{600nm}=0.1$). Gel was stained with $CuCl_2$ 0.3 M. MWM corresponds to the molecular weight marker (Protein marker II, NZYTech). No modifications other than cropping and resizing were applied to the image.

As observed in Figure 19, the production levels of SELP-59-A_cRGD were lower than SELP-59-A production using pCM13::*SELP-59-A* plasmid and comparable to SELP-59-A production using pET25::*SELP-59-A* plasmid. The BL21 (DE3) pET25::*SELP-59-A_cRGD* transformant 3 produced a truncated polymer. The truncation is possibly caused by a nonsense mutation that results in the introduction of a premature stop codon in the DNA sequence that leads to the production of an incomplete protein²³². Based on the SDS-PAGE results, the transformant number 5 (black arrow) was chosen to proceed.

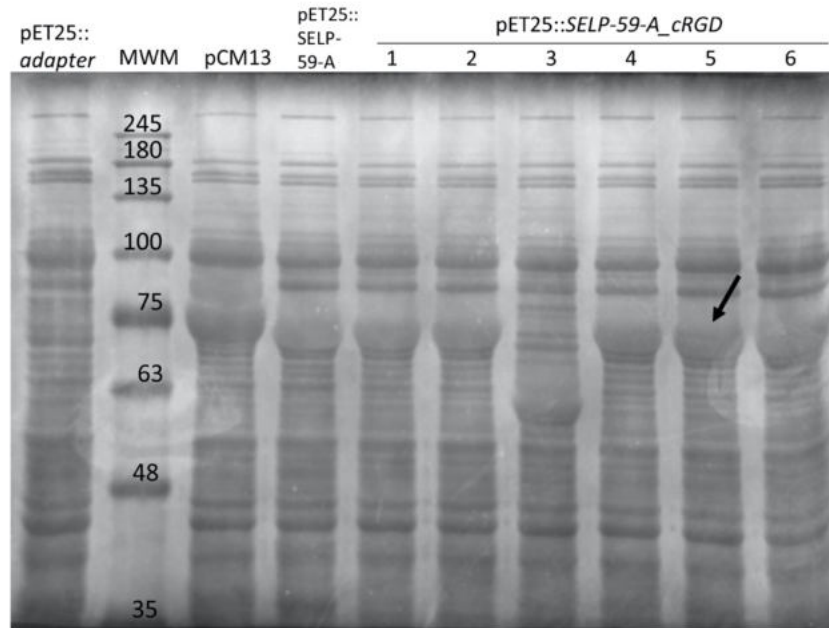


Figure 19. Production screening of SELP-59-A_cRGD in *E. coli* BL21 (DE3) pET25::*SELP-59-A_cRGD* transformants after 22 h at 200 rpm and 37 °C in TBlac medium. pET25::adapter and pCM13, used as negative and positive controls, correspond to *E. coli* BL21 (DE3) transformed with pET25::adapter and pCM13::*SELP-59-A*, respectively. Arrow points to the band corresponding to SELP-59-A_cRGD polymer of the chosen transformant. Loaded samples were normalized to the same cell density ($OD_{600nm}=0.1$). Gel was stained with $CuCl_2$ 0.3 M. MWM corresponds to the molecular weight marker (Protein marker II, NZYTech). No modifications other than cropping and resizing were applied to the image.

A production screening was also performed to evaluate the production levels of SELP-59-A_nRGD. As observed in Figure 20, the levels of SELP-59-A_nRGD production were undetectable.

The expression of pET25::*SELP-59-A_nRGD* was also performed in *E. coli* C43 (DE3) pRARE (Figure 21), *E. coli* Origami B (DE3) (Figure 22) and *E. coli* BL21 (DE3) pLysE (Figure 23).

E. coli C43 (DE3) strain generally overcomes the toxicity associated with recombinant proteins overexpression using the bacteriophage T7 RNA polymerase expression system²³³, transformed with pRARE plasmid, that carry genes of tRNA which are rare in *E. coli*²³⁴.

To overcome the possible insolubility of the protein caused by the existence of cysteines in the RGD sequence, the *E. coli* Origami B (DE3) strain was used to enable disulfide bond formation, which improves protein solubility²³⁵.

BL21(DE3) has the T7 RNA polymerase gene under the control of lacUV5 promoter inducible by IPTG²³⁶. The gene of interest can, however, be expressed without induction, which might be toxic to the cells²³⁷, when the produced protein is toxic. *E. coli* BL21 (DE3) pLysE is transformed with a plasmid which encodes

T7 lysozyme that is expressed at high level, that inhibits the transcriptional activity of T7 RNA polymerase through direct complex formation^{238,239}.

The expression of SELP-59-A_nRGD in these strains revealed no improvement over the BL21(DE3) strain (Figure 20).

Due to the extremely low production levels of SELP-59-A_nRGD, the remaining work was continued with the other three functionalized polymers.

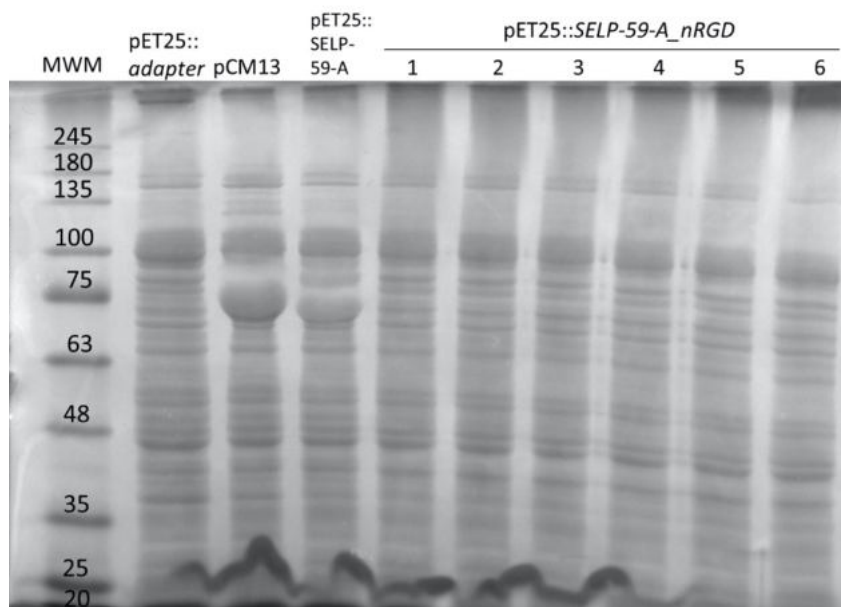


Figure 20. SDS-PAGE analysis of SELP-59-A_nRGD production in *E. coli* BL21 (DE3) pET25::SELP-59-A_nRGD transformants after 22 h at 200 rpm and 37 °C in TBlac medium. pET25::adapter and pCM13, used as negative and positive controls, correspond to *E. coli* BL21 (DE3) transformed with pET25::adapter and pCM13::SELP-59-A, respectively. Loaded samples were normalized to the same cell density ($OD_{600nm}=0.1$). Gel was stained with $CuCl_2$ 0.3 M. MWM corresponds to the molecular weight marker (Protein marker II, NZYTech). No modifications other than cropping and resizing were applied to the image.

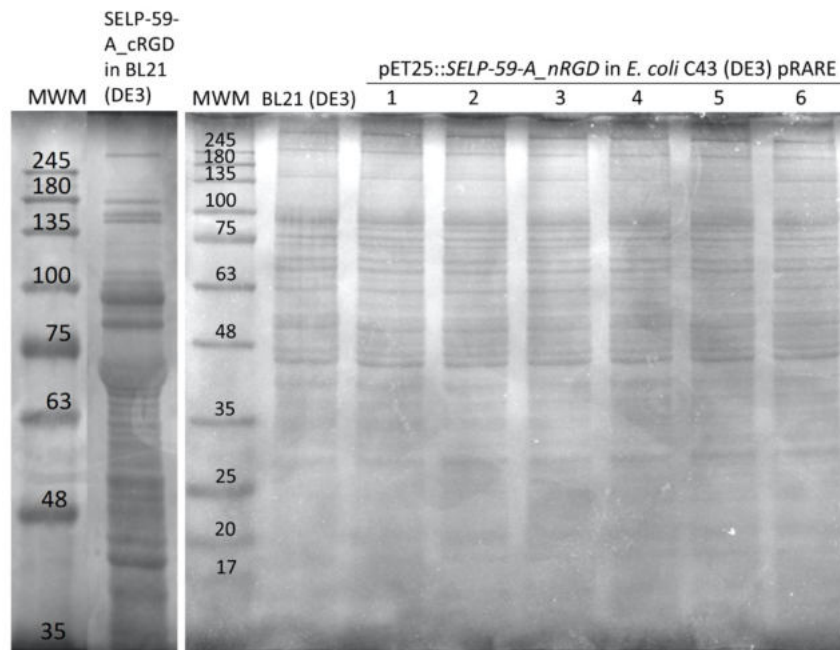


Figure 21. Production screening of SELP-59-A_nRGD in *E. coli* C43 (DE3) pRARE pET25::SELP-59-A_cRGD transformants after 22 h at 200 rpm and 37 °C in TBlac medium. *E. coli* BL21 (DE3) transformed with pET25::SELP-59-A_cRGD was used as control (BL21 (DE3) lane). The production screening result of the chosen BL21 (DE3) SELP-59-A_cRGD producer is presented for demonstration of expected band size (lane SELP-59-A_cRGD in BL21 (DE3)). Loaded samples were normalized to the same cell density ($OD_{600nm}=0.1$). Gels were stained with $CuCl_2$ 0.3 M. MWM corresponds to the molecular weight marker (Protein marker II, NZYTech). No modifications other than cropping and resizing were applied to the images.

The difference in production levels of the different polymers can be a consequence of the amino acids upstream of the SELP-59-A sequence, since as previously stated, the initial codons are directly related to the transcription and translation rates of a gene and the half-life time of a protein.

Previously results obtained by the group (unpublished) show that the presence of lysines at the N-terminal of the SELP polymer increases the production of the polymer, while the presence of cysteines at the N-terminal inhibits its production.

The results obtained suggest that the amino acids of the adapter sequence that are located upstream of the SELP-59-A sequence decrease the yield of the polymer, since the production of SELP-59-A by pET25::SELP-59-A is considerably lower than the production of the same polymer by pCM13::SELP-59-A (Figure 16), but is very similar to SELP-59-A_cC3 polymer production (Figure 17).

When the C3 sequence is inserted in the N-terminal of SELP-59-A, the yield of the polymer production is higher. This increase may be due not only to the loss of the adapter's initial amino acid sequence, but also to the fact that it is a lysine-rich sequence.

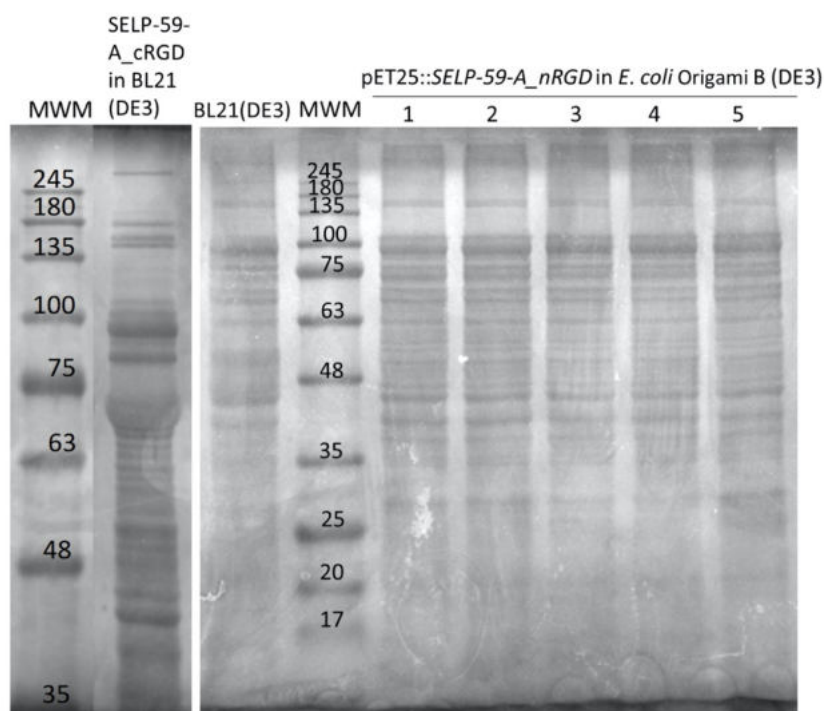


Figure 22. Production screening of SELP-59-A_nRGD in *E. coli* Origami B (DE3) pET25::SELP-59-A_cRGD transformants after 22 h at 200 rpm and 37 °C in TBlac medium. *E. coli* BL21 (DE3) transformed with pET25::SELP-59-A_cRGD was used as control (BL21 (DE3) lane). The production screening result of the chosen BL21 (DE3) SELP-59-A_cRGD producer is presented for demonstration of expected band size (lane SELP-59-A_cRGD in BL21 (DE3)). Loaded samples were normalized to the same cell density ($OD_{600nm}=0.1$). Gels were stained with $CuCl_2$ 0.3 M. MWM corresponds to the molecular weight marker (Protein marker II, NZYTech). No modifications other than cropping and resizing were applied to the images.

However, inexplicably, when the RGD sequence is inserted in the C-terminal, the production of polymer increases when compared to the production of SELP-59-A with pET25::SELP-59-A, being still lower than the production of SELP-59-A_nC3 and the production of SELP-59-A by pCM13::SELP-59-A.

The production of SELP-59-A_nRGD was not achieved, possibly due to the presence of cysteines at the polymer N-terminus, since cysteine is one of the referenced amino acids that exerts a major influence on the transcription and translation rates of a DNA sequence as well as on the solubility of a protein^{219-223,225-227}. Even though efforts have been made to solve a possible insolubility of the SELP-59-A_nRGD polymer through transformation into *E. coli* Origami B, it is still possible that the protein is insoluble and therefore has not been detected in the analysis, since it only analyzes the soluble fraction of the cell lysate. In the future, a production screening of the insoluble fraction of the cells could potentially reveal the existence of polymer production.

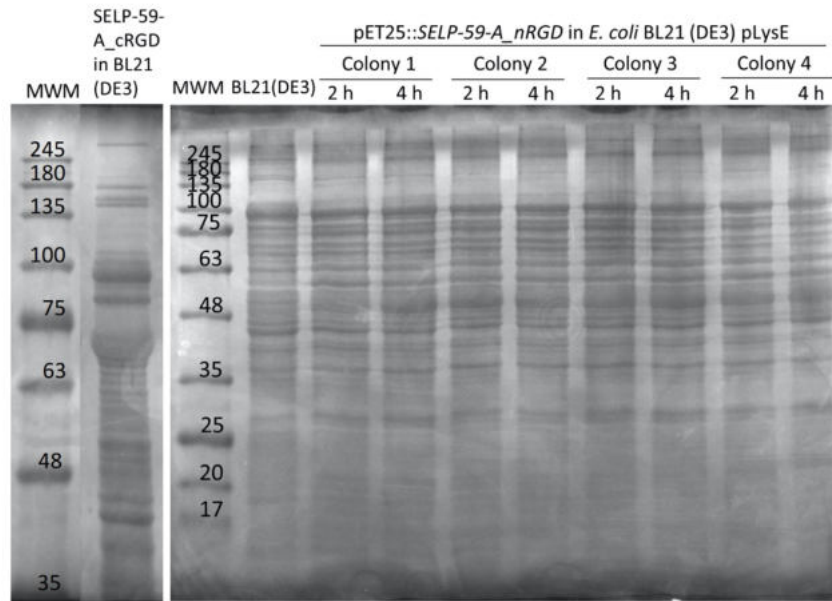


Figure 23. Production screening of SELP-59-A_nRGD in *E. coli* BL21 (DE3) pLysE pET25::SELP-59-A_cRGD transformants after 22 h at 200 rpm and 37 °C in TBlac medium. *E. coli* BL21 (DE3) transformed with pET25::SELP-59-A_cRGD was used as control (BL21 (DE3) lane). The production screening result of the chosen BL21 (DE3) SELP-59-A_cRGD producer is presented for demonstration of expected band size (lane SELP-59-A_cRGD in BL21 (DE3)). Loaded samples were normalized to the same cell density ($OD_{600nm}=0.1$). Gels were stained with $CuCl_2$ 0.3 M. MWM corresponds to the molecular weight marker (Protein marker II, NZYTech). No modifications other than cropping, copy, paste and resizing were applied to the images.

Although theoretically better SELP-59-A_nRGD production could be achieved using *E. coli* BL21 (DE3) pLysE instead of *E. coli* BL21 (DE3) pLysS, since it expresses more T7 lysozyme than pLysS, it has been verified by several authors that some proteins that are expressed at low level/not expressed with pLysE can achieve protein expression using pLysS^{237,239}. It could be interesting in the future to transform pET25::SELP-59-A_nRGD into BL21 (DE3) pLysS as it could potentially lead to the production of SELP-59-A_nRGD in the soluble fraction.

4.2.2. Polymer purification

The purification of the polymers was achieved using a protocol optimized by our group. Sonication was performed to disrupt *E. coli* cells and release the cytoplasmic content, followed by pH adjustment to 3.5 for *E. coli* native proteins precipitation and help in unaccomplished cell lysis. The soluble polymers were then precipitated by salting out, using different ammonium sulphate saturations to assess the optimal concentration for each polymer (Figure 24 - Figure 26).

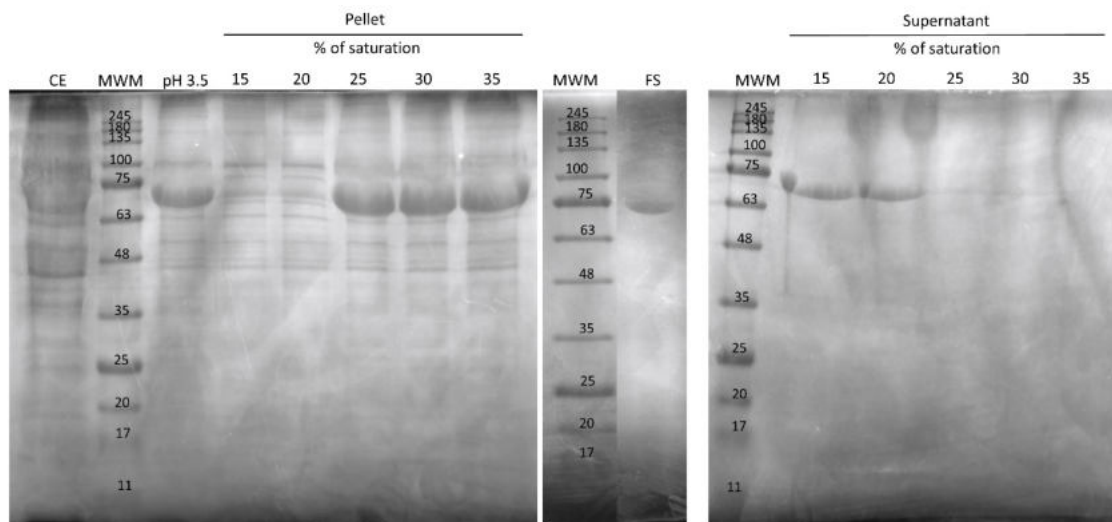


Figure 24. Purification of the SELP-59-A_cC3 polymer by ammonium sulphate precipitation. The cell crude extract (CE lane) was subjected to a pH decrease for precipitation of endogenous proteins. The soluble acid-treated lysate (pH 3.5 lane) was saturated with increasing concentrations of ammonium sulphate (indicated above each lane). Depending on the concentration used, the polymer either precipitated or stayed in the supernatant. Increased purity was obtained by dissolving the precipitated polymer in upH₂O and let overnight at 4 °C, followed by dialysis, centrifugation and filtration (filtered solution (FS) lane). Gels were stained with CuCl₂ 0.3 M. MWM corresponds to the molecular weight marker (Protein marker II, NZYTech). No modifications other than cropping, copy, paste and resizing were applied to the images.

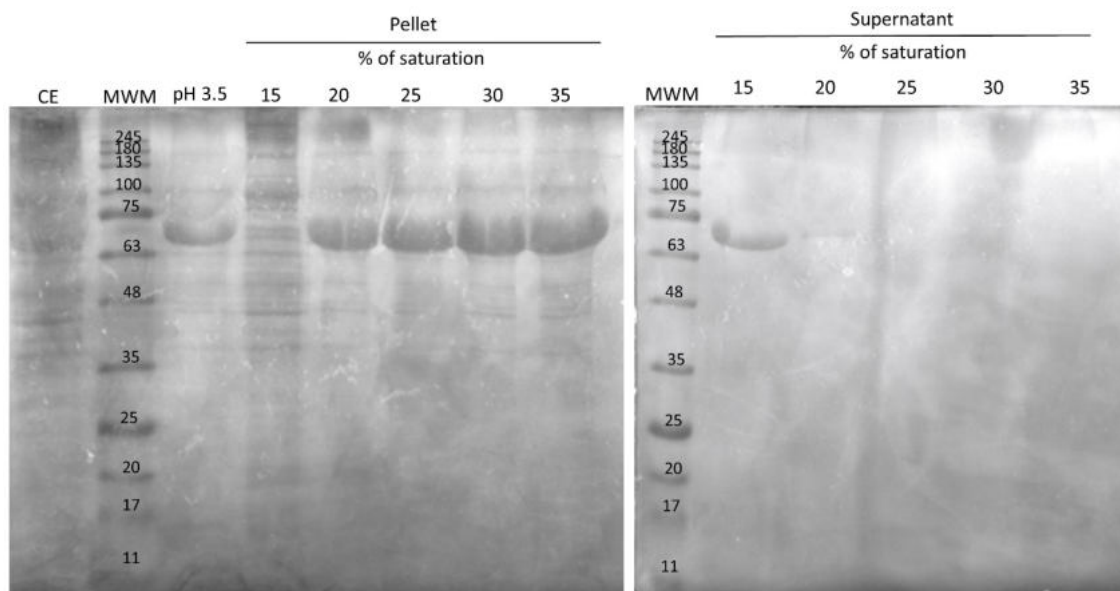


Figure 25. Purification of the SELP-59-A_cRGD polymer by ammonium sulphate precipitation. The cell crude extract (CE lane) was subjected to a pH decrease for precipitation of endogenous proteins. The soluble acid-treated lysate (pH 3.5 lane) was saturated with increasing concentrations of ammonium sulphate (indicated above each lane). Depending on the concentration used, the polymer either precipitated or stayed in the supernatant. Gels were stained with CuCl₂ 0.3 M. MWM corresponds to the molecular weight marker (Protein marker II, NZYTech). No modifications other than cropping, copy, paste and resizing were applied to the images.

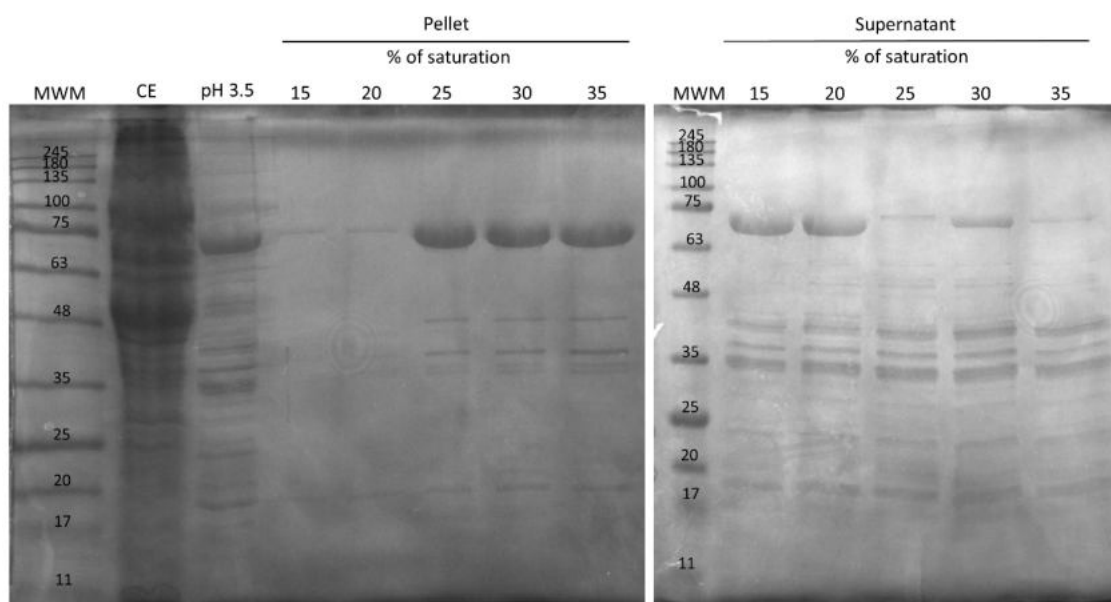


Figure 26. Purification of the SELP-59-A_nC3 polymer by ammonium sulphate precipitation. The cell crude extract (CE lane) was subjected to a pH decrease for precipitation of endogenous proteins. The soluble acid-treated lysate (pH 3.5 lane) was saturated with increasing concentrations of ammonium sulphate (indicated above each lane). Depending on the concentration used, the polymer either precipitated or stayed in the supernatant. Gels were stained with CuCl_2 0.3 M. MWM corresponds to the molecular weight marker (Protein marker II, NZYTech). No modifications other than cropping, copy, paste and resizing were applied to the images.

The optimal concentration of ammonium sulphate to precipitate each polymer was the lowest saturation that led to total polymer precipitation, in which it is no longer possible to observe a band in the sample of the supernatant in SDS-PAGE gels. For all polymers the optimal concentration of ammonium sulphate to precipitate the polymers was 25%.

The protein band on the supernatant of 30% ammonium sulphate saturation (Figure 26) can be explained by lower agitation of the sample or by a possible error in the quantity of ammonium sulfate added to the sample, which led to the non-precipitation of the polymer.

After centrifugation, the precipitated polymer was resolubilized with upH_2O and dialyzed against water. The dialysis membrane allows the flow of proteins with a molecular weight lower than 10000-12000 Da, which eliminate small contaminant proteins. The dialyzed solution was centrifuged to remove the remaining contaminant proteins and was finally filtered to increase purity (FS lane from Figure 24).

4.2.3. Processing of the polymers

SELP-59-A and SELP-59-A_CAMs polymers were processed into films, prepared by solvent casting using formic acid as solvent to fully dissolve the lyophilized protein. Different films were produced by combining SELP-59-A with different percentages of the functionalized polymers (0, 25, 50, 75 and 100 wt%) (Table 15). Then, each protein solution was cast into a PTFE mold and allowed to dry until complete solvent evaporation. An overnight evaporation was sufficient to have completely dry films for all samples made. Since SELP films are water soluble⁶⁴ and the application involves contact with aqueous solutions, film insolubility was induced by treatment with methanol-saturated air (see visual aspect of the produced films in Figure 27). This process was previously adopted by several authors to promote structural stability with an induced physical cross-linking process by dehydration that results in an increase of the β -sheet content^{56,64,94,240}.

To assess the secondary structural changes, treated and untreated films were characterized by ATR-FTIR spectroscopy. ATR-FTIR spectra results from the energy absorption by vibrating chemical bonds²⁴¹. Two bands are mainly used to study protein structure: amide I (C=O stretch vibration, N-H bending and C-N stretching) and amide II (mainly N-H bend and C-N stretch vibrations)²⁴¹. The amide I vibration, absorbing near 1650 cm^{-1} , is most commonly used for secondary structure analysis²⁴², since C=O stretching vibrations of the peptide bonds are modulated by the secondary structure²⁴³.

Before methanol treatment, the absorption spectra of the amide I display a broad band centered at 1626 cm^{-1} (Figure 28A-G). The broadness of the band indicates the existence of numerous secondary structures, while the center of the peak suggests that the secondary structure is dominated by β -sheets^{64,69,94,240,244}. The pronounced shoulder centered at 1650 cm^{-1} is usually associated to random coil formations²⁴⁴. After methanol treatment, the amide I peak shifts to lower wavenumbers and the band becomes more narrowed, reflecting a conversion from a more unordered, random coil structure to an ordered, β -sheet conformation^{69,245} (See Appendix I, Figure 64 for the absorbance spectra of the remaining films). The β -sheet structures are stabilized by hydrogen bonding, which cause more robust physical cross-links, providing crystallinity to the material, which ultimately results in water insolubility^{64,69,90}.

The analysis of the amide I bands of Figure 28H allows the identification of differences between SELP-59-A 100% and SELP-59-A_CAM 100% films. The peak centered at 1650 cm^{-1} in SELP-59-A_CAM 100% films spectra can be explained by the increase of random coils content, due to the modification, by the adhesion sequences, of the conditions that allow the formation of beta-sheets by SELP-59-A polymer.

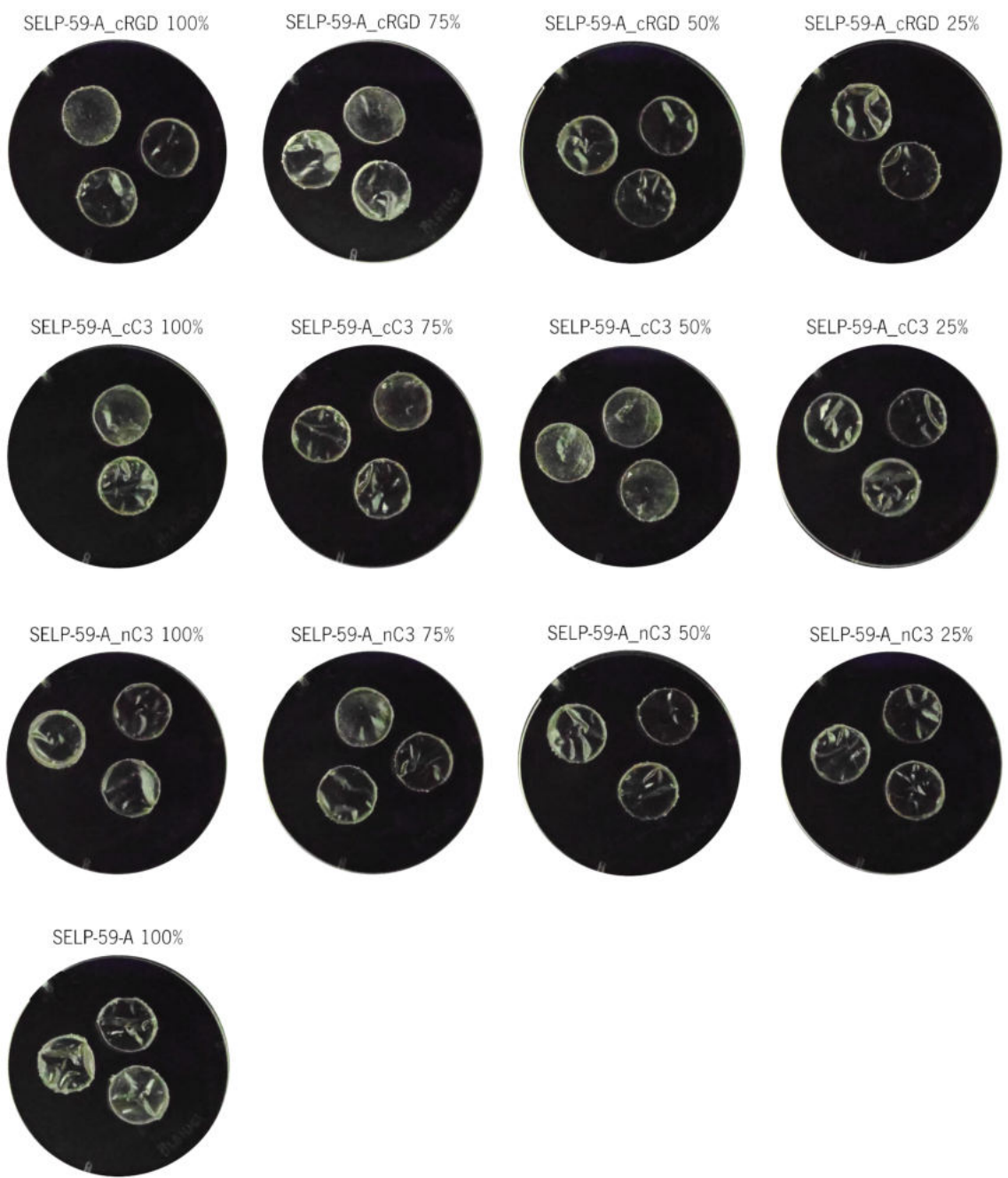


Figure 27. Visual aspect of methanol-treated films.

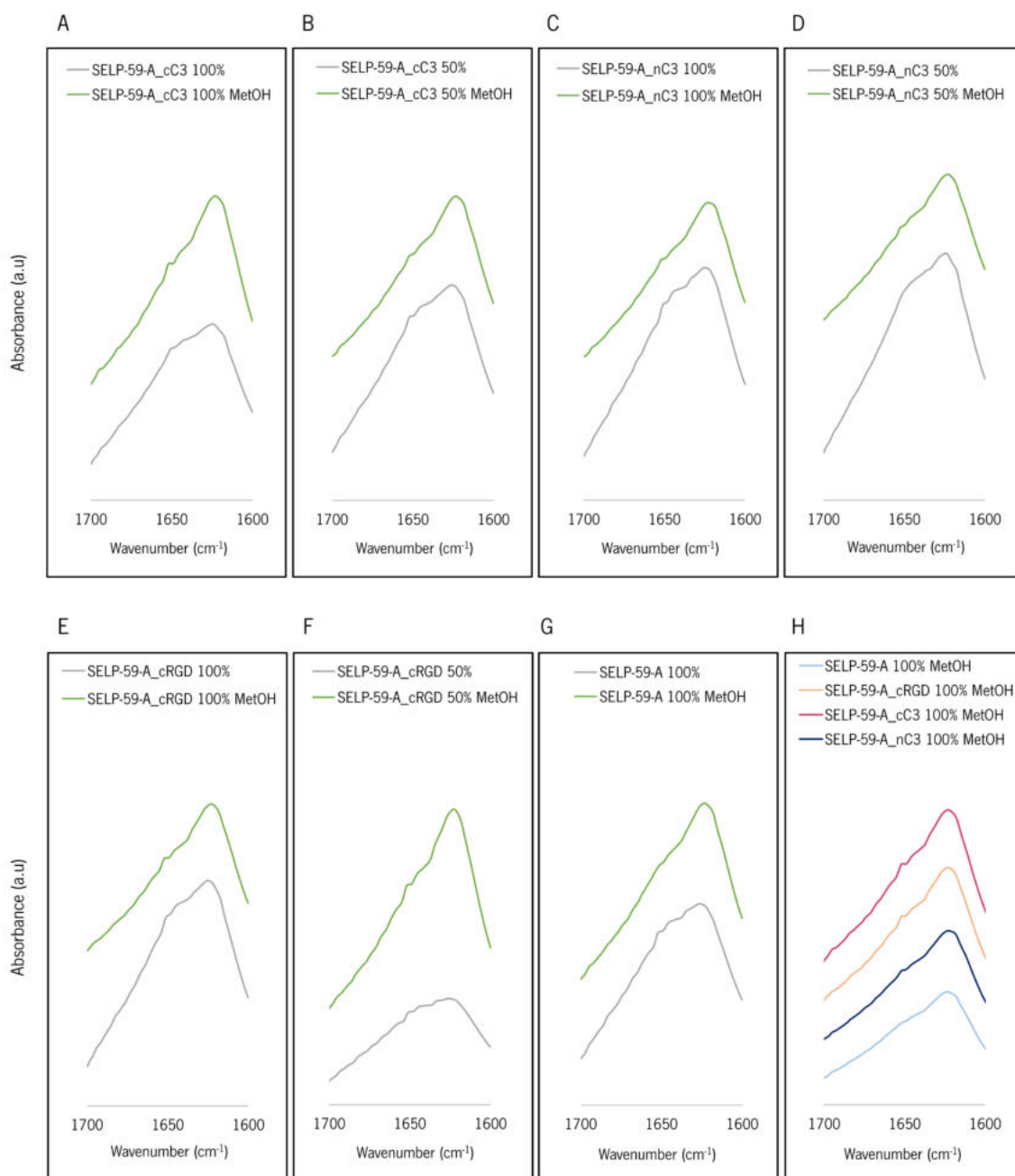


Figure 28. Experimentally determined amide I region ATR-FTIR absorbance spectra for the non-treated and methanol saturated air-treated films. (A-G) – SELP-59-A_CAM 100%, SELP-59-A_CAM 50% and SELP-59-A 100% films; H – Amide I region ATR-FTIR absorbance spectra for the SELP-59-A 100% and SELP-59-A_CAM 100% methanol air-treated films.

4.3 EVALUATION OF CELL AND ECM-BINDING ACTIVITY OF SELP-59-A_CAM FILMS USING MAMMALIAN CELL CULTURES

The evaluation of films ability to promote cell adhesion was performed using two cell lines: HaCaT and SH-SY5Y. The choice of the SH-SY5Y cell line is due to the fact that it expresses NCAM²⁴⁶, which will interact with the C3 adhesion sequence and promote cell adhesion to films. HaCaT cell line was selected since the chosen RGD sequence promoted better adhesion on keratinocytes (Table 16).

4.3.1 Mammalian cell lines staining optimization

Due to the disparity of values found in the literature for concentration and incubation time for nuclear-specific dyes, an optimization of these parameters was performed for each of the cell lines. HaCaT and SH-SY5Y cells were seeded into surface treated wells and incubated for 24 h, followed by incubation with Hoechst 34580, from now on designated as Hoechst, or DAPI (Figure 6), as mentioned in Section 3.9. As observed in Figure 29, 15 min of incubation time using Hoechst was sufficient for HaCaT nuclear staining. Longer incubations times resulted in similar results. Furthermore, DAPI (Figure 30) showed very similar nuclear staining ability when compared to Hoechst (Figure 29), especially when comparing the results of cell staining with DAPI 5 μ M 15 min to those obtained using Hoechst 5 μ M 15 min. However, DAPI appeared to be forming clusters (yellow spots) that are visible in brightfield micrographs.

In Figure 31 it is possible to verify that, for SH-SY5Y cell line, 15 min of incubation time with Hoechst is sufficient to stain the cell population uniformly. Longer incubation times lead to the loss of uniformity in cell staining and signal saturation. DAPI did not stain the population evenly, (Figure 32) and formed visible clusters. Both dyes appear to have some selectivity. The staining selectivity observed using SH-SY5Y could be explained by the yeast contamination or by the morphology of the cell line, as the cells grow as a mixture of floating and adherent cells, which can lead to a dirtier profile.

Due to a yeast contamination in SH-SY5Y cells, this optimization assay will be repeated for validation of the results in future experiments.

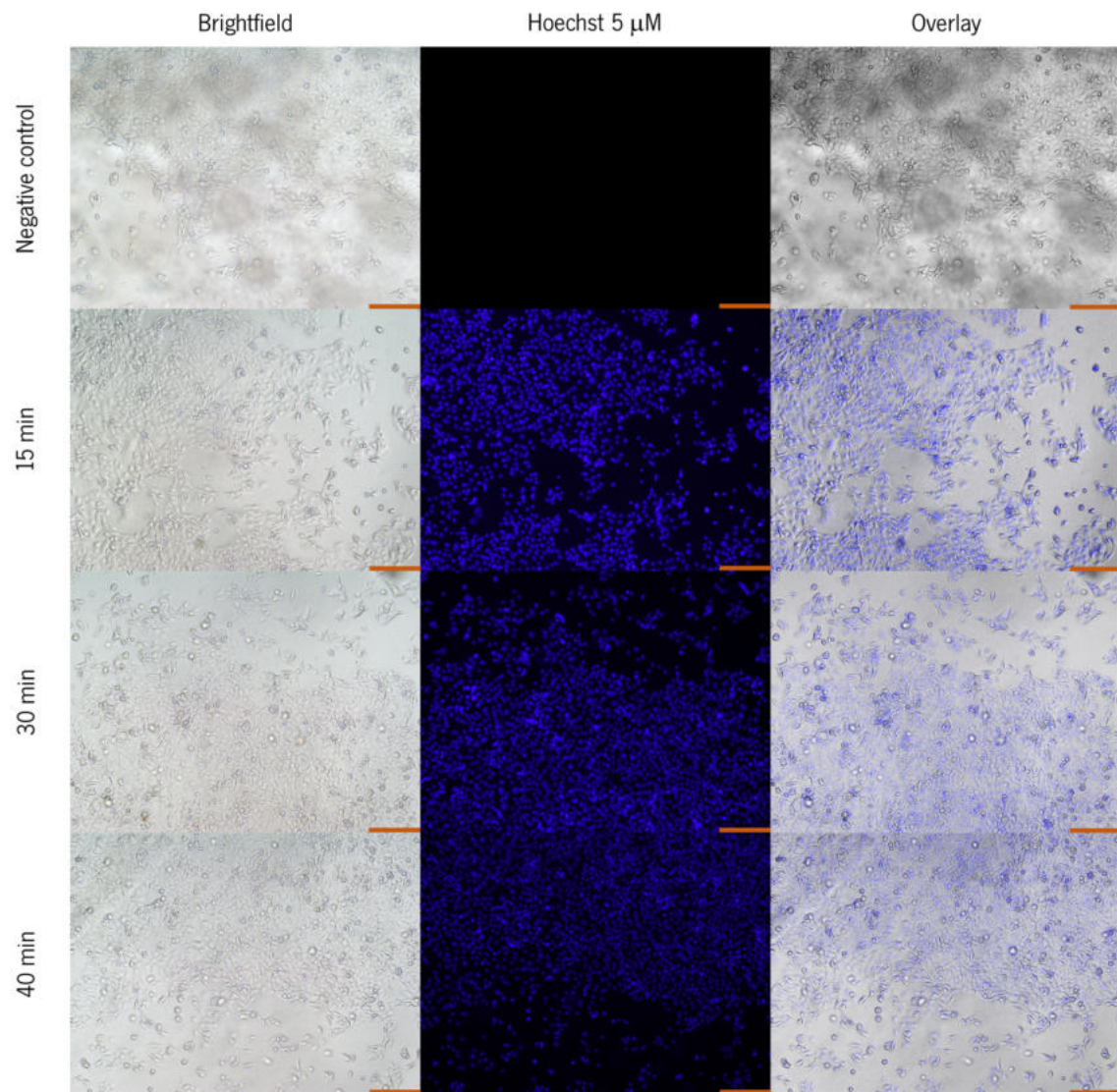


Figure 29. Brightfield and fluorescent micrographs of HaCaT cells stained with Hoechst 34580 for different time points, visualized with 100x amplification. Scale bar represents 200 μm.

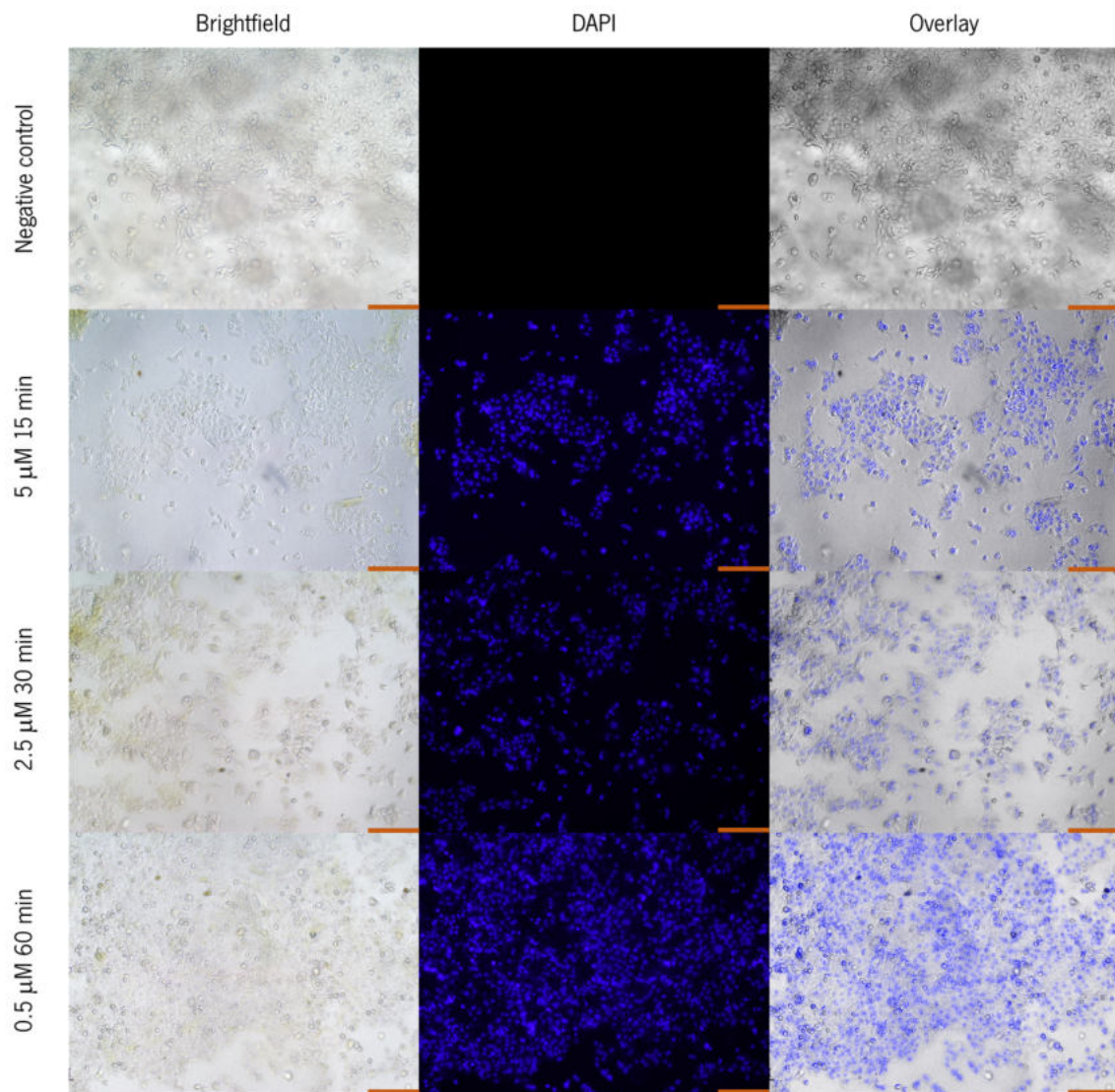


Figure 30. Brightfield and fluorescent micrographs of HaCaT cells stained with DAPI for different concentrations and time points, visualized with 100x amplification. Scale bar represents 200 μm.

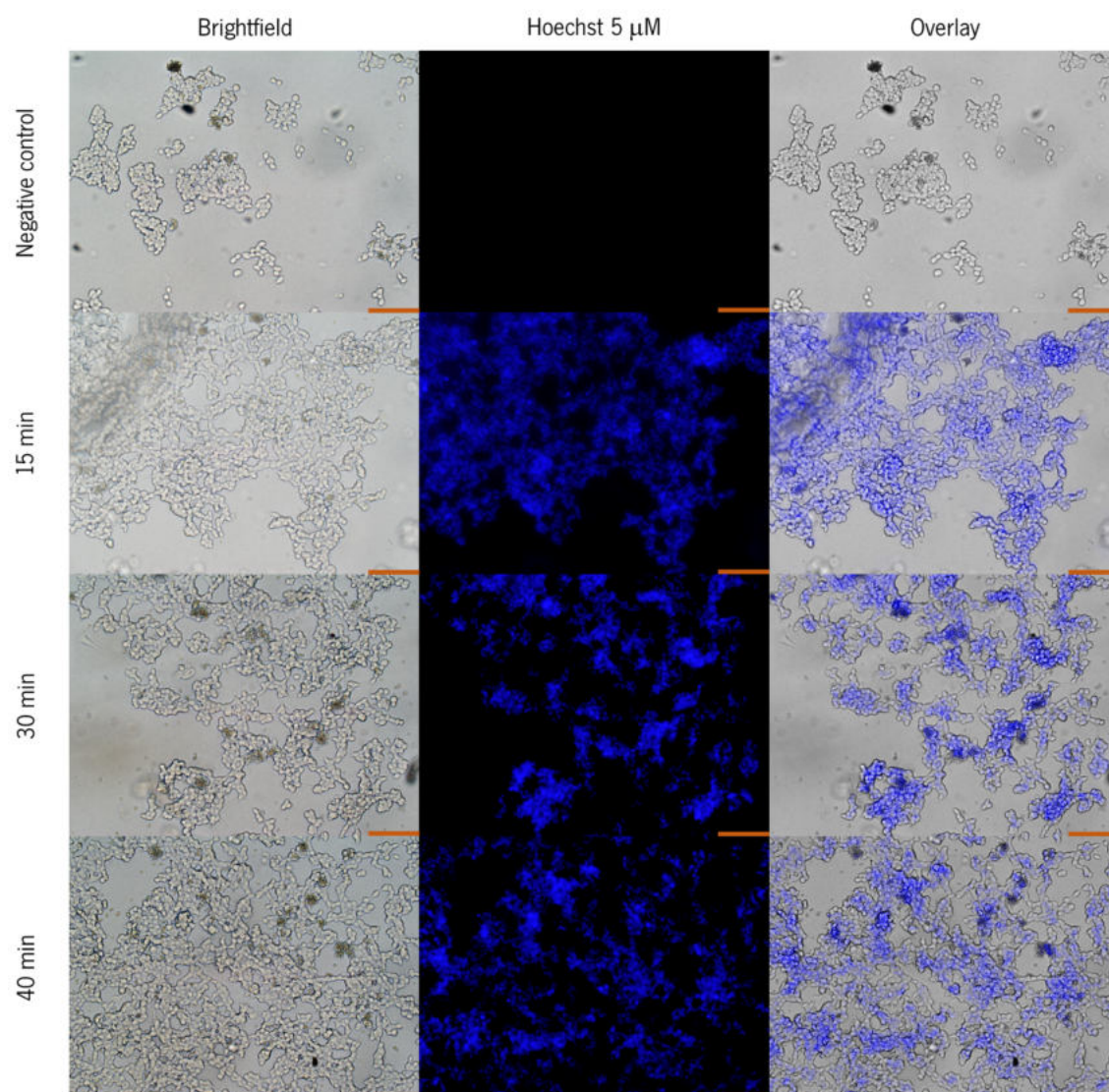


Figure 31. Brightfield and fluorescent micrographs of SH-SY5Y cells stained with Hoechst 34580 for different time points, visualized with 200x amplification. Scale bar represents 100 μm.

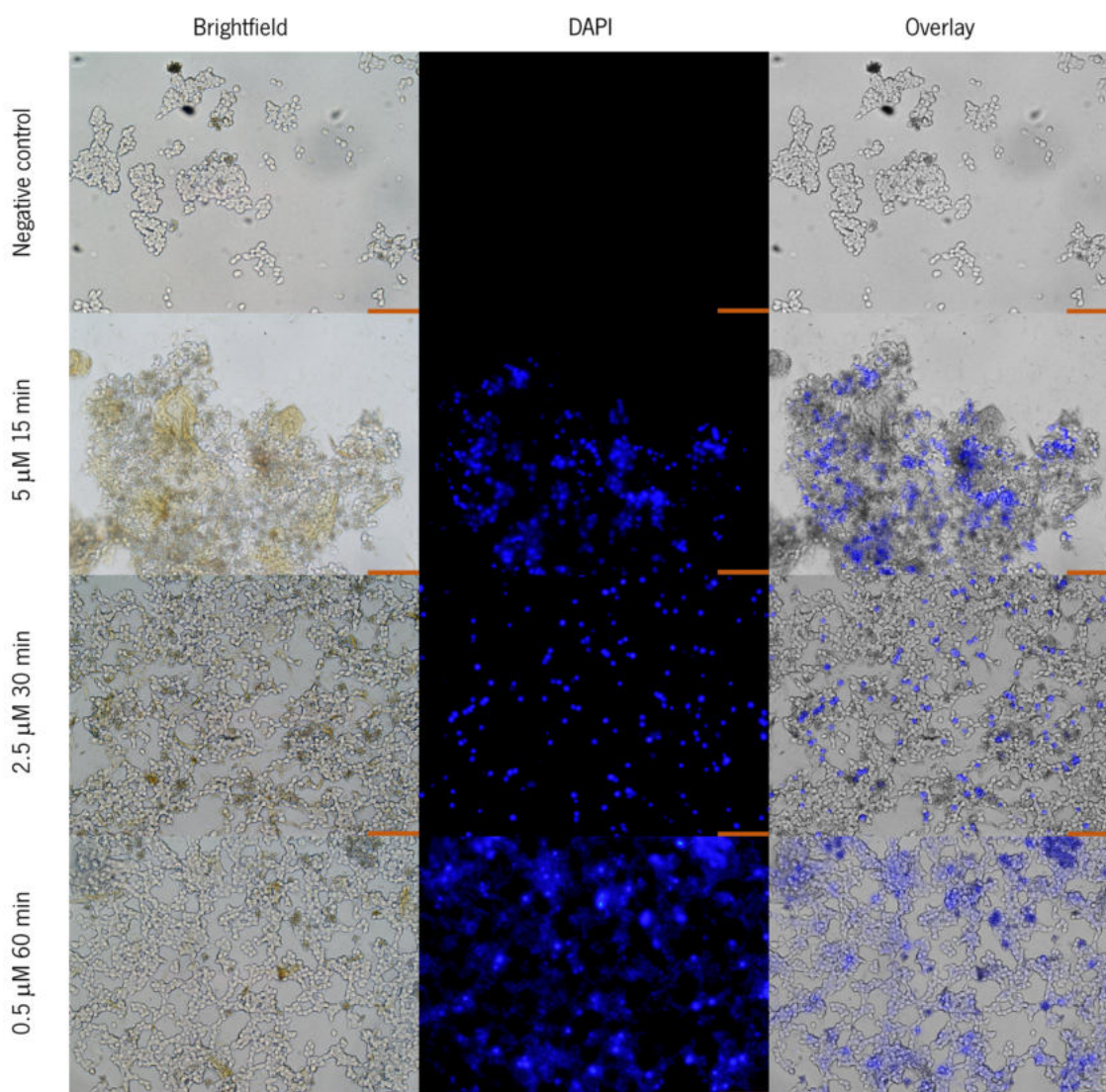


Figure 32. Brightfield and fluorescent micrographs of SH-SY5Y cells stained with DAPI for different concentrations and time points, visualized with 200x amplification. Scale bar represents 100 μm .

4.3.2 Assessment of the effect of the cell's fixation process on film structure and staining

Since the cell membrane is not permeable to Rhodamine Phalloidin, from now on designated as Phalloidin, which is necessary for the observation of the cell's cytoskeleton, it is necessary the fixation and permeabilization of cells. The fixation process requires the use of a fixative agent – formaldehyde was chosen for this assay – that reacts with groups on amino acids such as lysine, arginine, threonine, cysteine, tyrosine, serine and glutamine, and forms methylene bridges (cross-links) between them²⁴⁷. Since the produced films are composed of protein, it is important to evaluate any significant visual changes in their structure, which may hinder the observation of cells, when exposed to the fixative agent.

The exposure of the films to the fixation process (Figure 33 – Figure 36) does not cause significant visible changes in the morphology of the films. The morphological variation observed among the films is not necessarily caused by exposure to the reagents in the fixation process. As can be seen in Figure 27, there is inherent morphological variability in films.

The staining of the cells with fluorescent dyes involves the direct contact between the dyes and the films. To evaluate a possible affinity between the films and the dyes, the SELP-59-A 100% (Figure 33), SELP-59-A_nC3 100% (Figure 35) and SELP-59-A_cRGD 100% (Figure 36) films were incubated with the fluorescent dyes.

Although the micrographs show the staining by Hoechst in some samples, these results were not consistent throughout the assays. Hoechst is a nuclear-specific dye, and this unspecific staining could be related to a DNA contamination; residues that were not removed during the film washing steps; microscope illumination, since the fluorescence is visible only in the left corner of the images; or even a problem in the image acquisition software, since in addition to the non-consistent results, all films had initial fluorescence in the 3 channels – blue, red and green – (not shown), even with films that were not incubated with any probe.

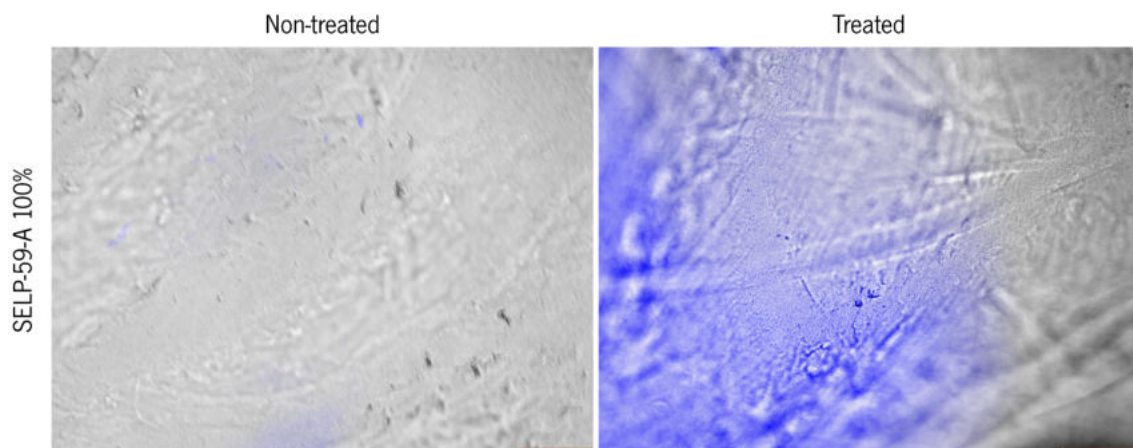


Figure 33. Fluorescence overlay micrographs of SELP-59-A 100% films treated and non-treated with the reagents used for cell fixation and staining with Hoechst 34580 and Phalloidin, after incubation for 24 h with DMEM at 37 °C, visualized with 100x amplification. Scale bar represents 200 μm .

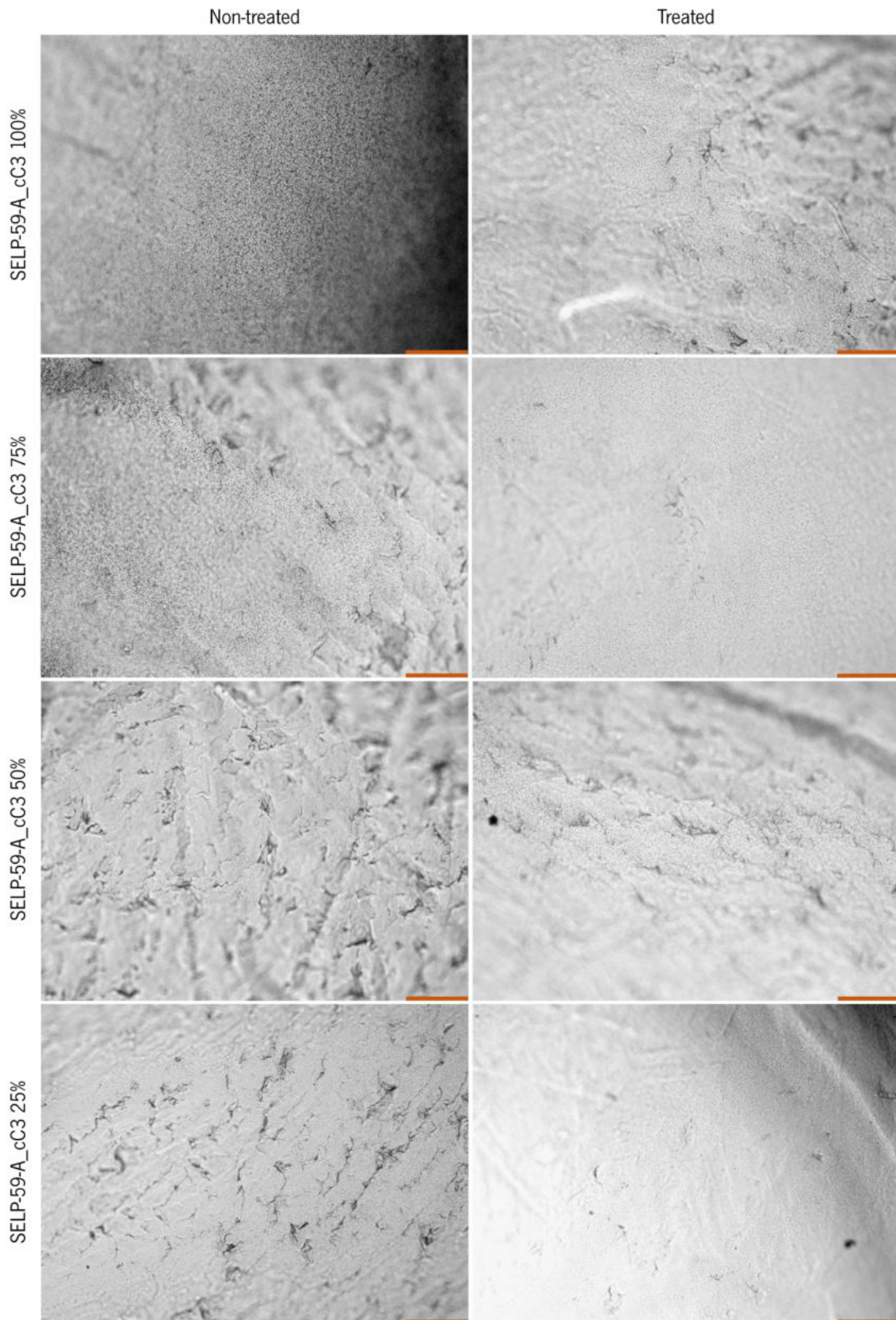


Figure 34. Fluorescence overlay micrographs of SELP-59-A_cC3 films treated and non-treated with the reagents used for cell fixation, after incubation for 24 h with DMEM at 37 °C, visualized with 100x amplification. Scale bar represents 200 μ m.

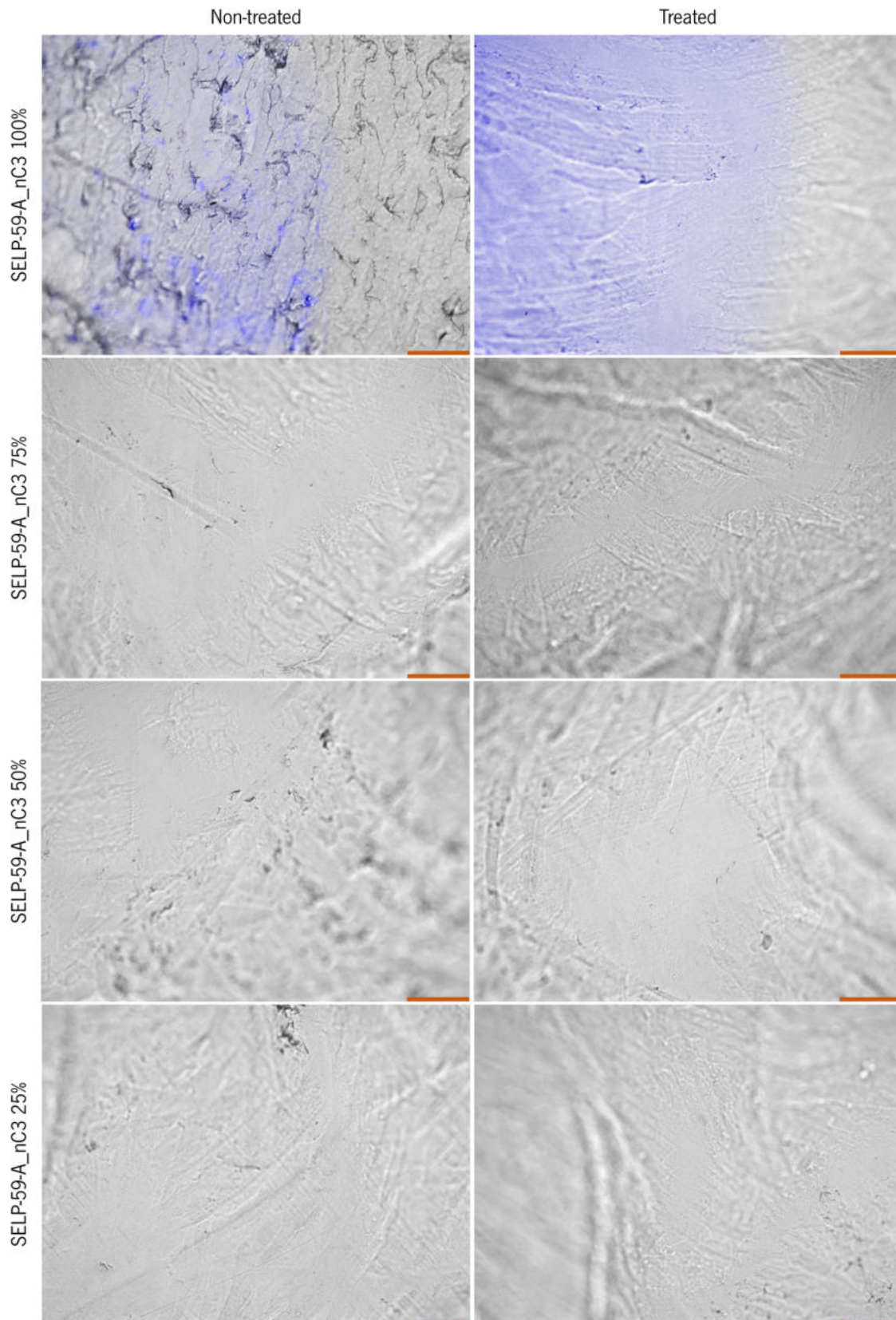


Figure 35. Fluorescence overlay micrographs of SELP-59-A_nC3 films treated and non-treated with the reagents used for cell fixation, after incubation for 24 h with DMEM at 37 °C, visualized with 100x amplification. SELP-59-A_nC3 100% films were stained with Hoechst 34580 and Phalloidin. Scale bar represents 200 μm .

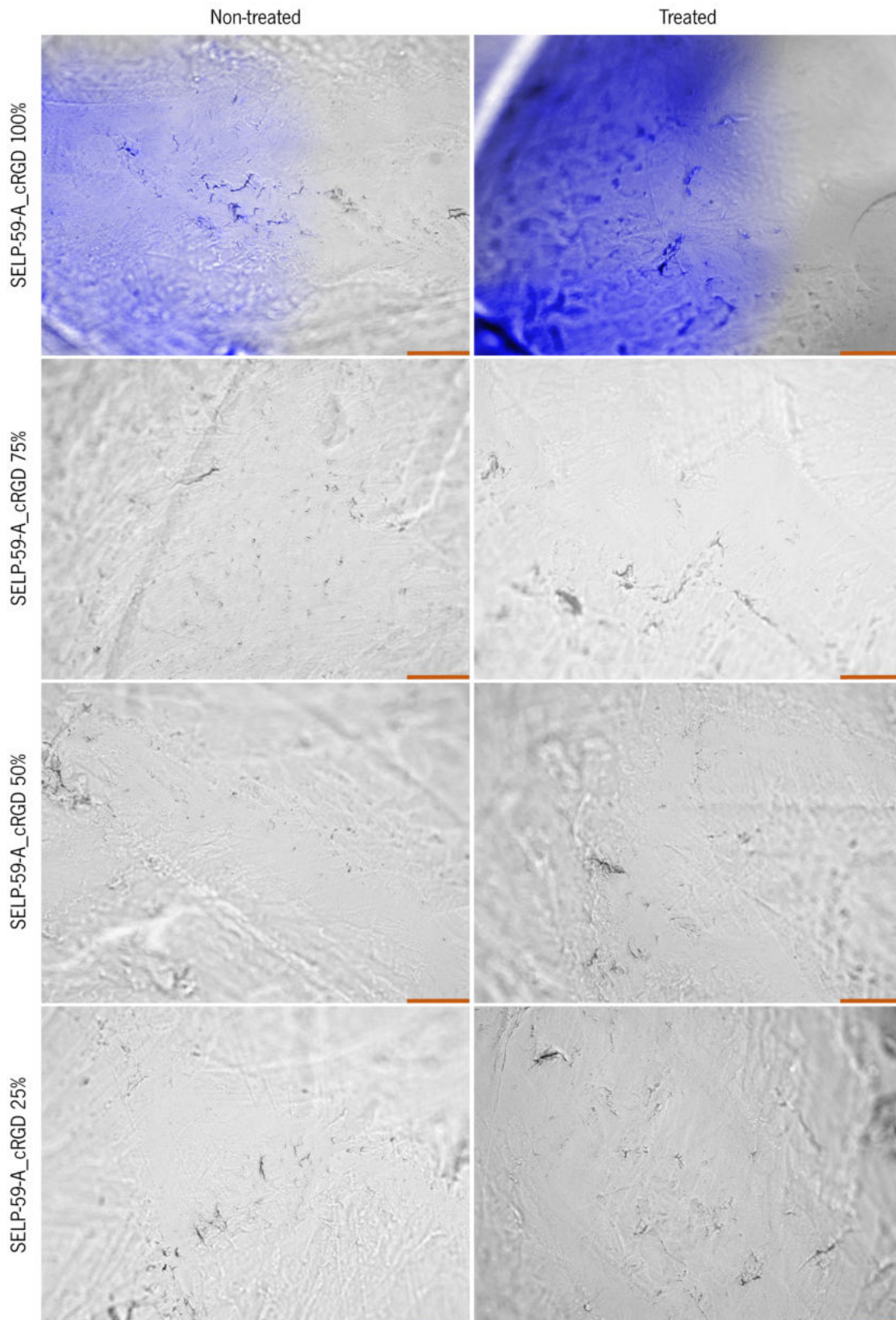


Figure 36. Fluorescence overlay micrographs of SELP-59-A_cRGD films treated and non-treated with the reagents used for cell fixation, after incubation for 24 h with DMEM at 37 °C, visualized with 100x amplification. SELP-59-A_cRGD 100% films were stained with Hoechst 34580 and Phalloidin. Scale bar represents 200 μ m.

4.3.3 Cell adhesion assays

To evaluate the ability of the films to promote cell adhesion, HaCaT and SH-SY5Y cells were cultured on the surface of the methanol-treated films for 24 h, as mentioned in Section 3.11. As viability control, cells were cultured on surface treated wells. Following the incubation, cells were fixated and incubated with Hoechst and Phalloidin and observed under a fluorescence microscope. Micrographs of representative locations were recorded.

The cultured HaCaT cells from the viability control had the expected confluence and morphology (Figure 37).

When compared to the remaining SELP-59-A_cRGD films, SELP-59-A_cRGD 25% led to the adhesion of less HaCaT cells, which appear to be in an early stage of spreading (Figure 37). The small spreading area and the increasing of cell circularity are already described in the literature as a consequence of low concentration of RGD adhesion motif^{103,248,249}.

There is an increment in cellular adhesion of HaCaT cells to SELP-59-A_cRGD films from the films made of SELP-59-A_cRGD 25% to SELP-59-A_cRGD 50%, remaining constant in the films with higher percentage of the functionalized polymer. SELP-59-A_cRGD 100%, SELP-59-A_cRGD 75% and SELP-59-A_cRGD 50% films have similar number of adhered cells and cell morphology, which appear to be in an intermediate stage of adhesion, as the cells seem more spread over the film surface, when compared to SELP-59-A_cRGD 25% films. Several authors have already reported this phenomenon, in which cell adhesion and spreading increase until a certain concentration of adhesion motif is reached, a value from which these parameters remain stable^{250,251}. Previous assays also report another type of cell response using polymers functionalized with the RGD sequence, in which there is an increase in the number of cells adhered to the films until a determined sequence concentration is reached. However, contrary to what was observed in this work, from that concentration value, the number of adhered cells decreases⁶⁹.

Based on the literature, there is a critical RGD density (interligand spacing of <70 nm) that is crucial for the establishment of stable integrin-mediated adhesion^{252,253}, whereas cells adhere poorly when adhesion motifs are spaced farther apart^{251,252}. It is possible that the spacing <70 nm between RGD motifs is reached somewhere between the concentration 25% and 50% of functionalized polymer. This hypothesis could be tested in future experiments using immunofluorescence, not only to assess the distance between the adhesion motifs, but also to evaluate the homogeneity of their distribution on the surface of the films, since it is believed that not only the concentration but also the distribution of the adhesion domains affect cell adhesion^{248,250-252,254}.

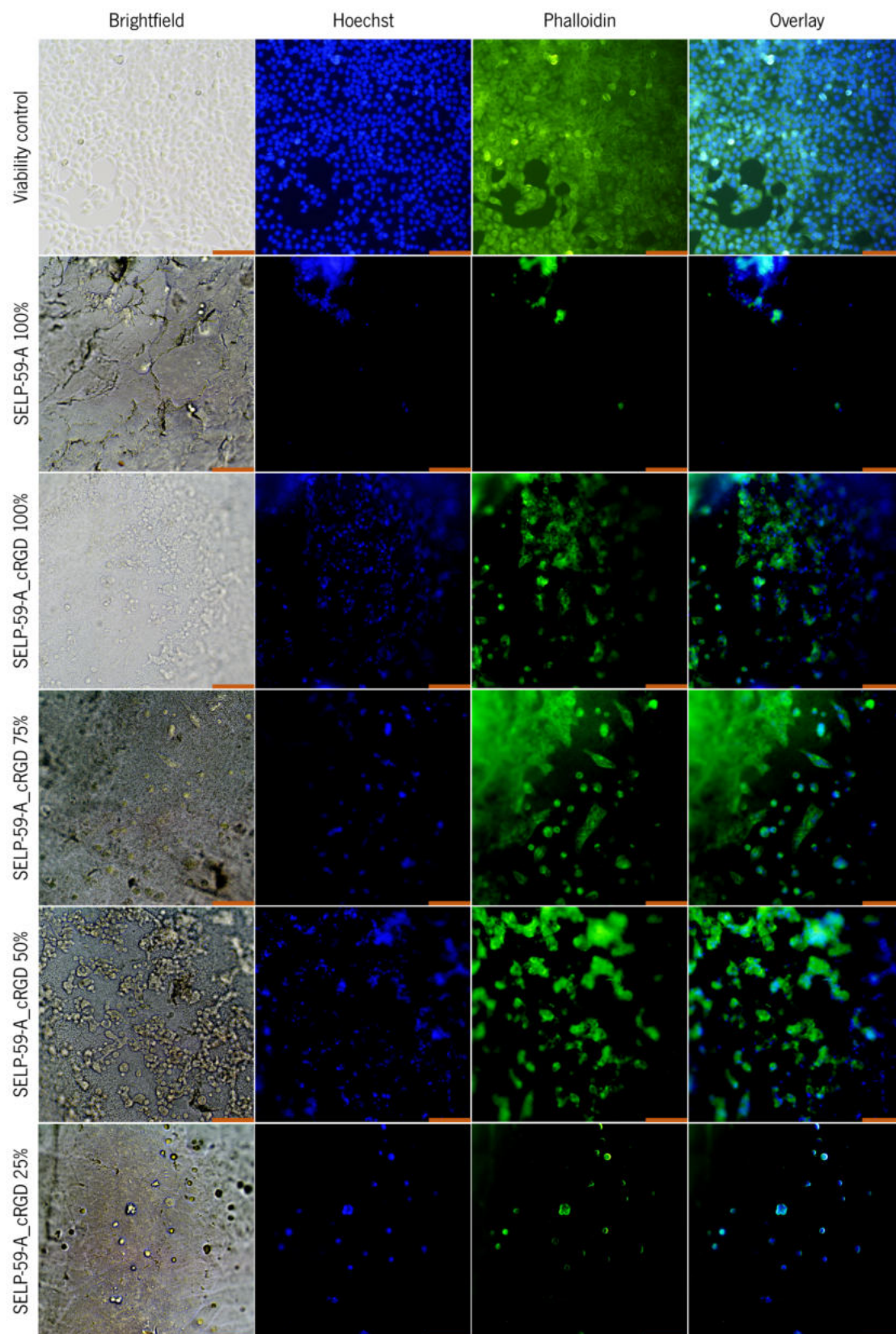


Figure 37. Brightfield and fluorescence micrographs of HaCaT cells seeded and cultured on surface SELP-59-A_cRGD films for 24 h, stained with Hoechst 34580 and Phalloidin, visualized with 100x amplification. Cells seeded and cultured on surface SELP-59-A 100% films and on surface of a surface treated well for 24 h stained with Hoechst 34580 and Phalloidin were used as controls. Scale bar represents 200 μm .

There is a limiting factor restraining cell adhesion to the SELP-59-A_cRGD films. Contrary to what is reported by other authors²⁵⁰, in this work the limiting factor is not the surface crowding, considering that there is still free surface area in all films. It is possible that the cell adhesion is limited by the insufficient number of RGD motifs. It could be interesting to functionalize the SELP-59-A in the N- and C-terminal with the RGD sequence to increase the concentration of adhesion sequence in the films, in order to promote a possible increase in cell adhesion. Another factor that possibly could be limiting the adhesion of cells is the availability of CAMs on the surface of the film. It is possible that not all adhesion motifs are arranged on the surface of the film and available to interact with the cells. This hypothesis could be tested in the future, using immunofluorescence to assess the presence of adhesion motifs on the surface of the films. When incubated on SELP-59-A_nC3 films, the number of HaCaT cells adhered to the films increases with increasing concentrations of adhesion sequence in the films (Figure 38). The cells on SELP-59-A_nC3 75% and 100% films appear to be in an advanced state of adhesion, as the cells seem completely spread over the film surface. The use of fluorescent dyes was particularly useful in these films, in which the confluence of cells is higher, in order to get a better sense of the number of cells adhered to the films. The cell adhesion obtained using HaCaT cells and the C3 adhesion sequence was unexpected. Although the association between NCAM and FGFR has been reported in several non-neuronal cell types^{218,255-257}, the level of response obtained was not predictable, since the biological significance of FGFR activation by NCAM remains elusive in non-neuronal cell types²⁵⁸.

As seen on Figure 39, the HaCaT cells incubated on SELP-59-A_cC3 films appear to behave similarly to those incubated in SELP-59-A_nC3 films, as they adhere more to the films with higher concentrations of adhesion sequence. The films functionalized with C3 sequence, both on N- and C-terminal, promoted cell adhesion of a higher number of HaCaT cells which are in a more advanced state of adhesion than the cells of the positive control.

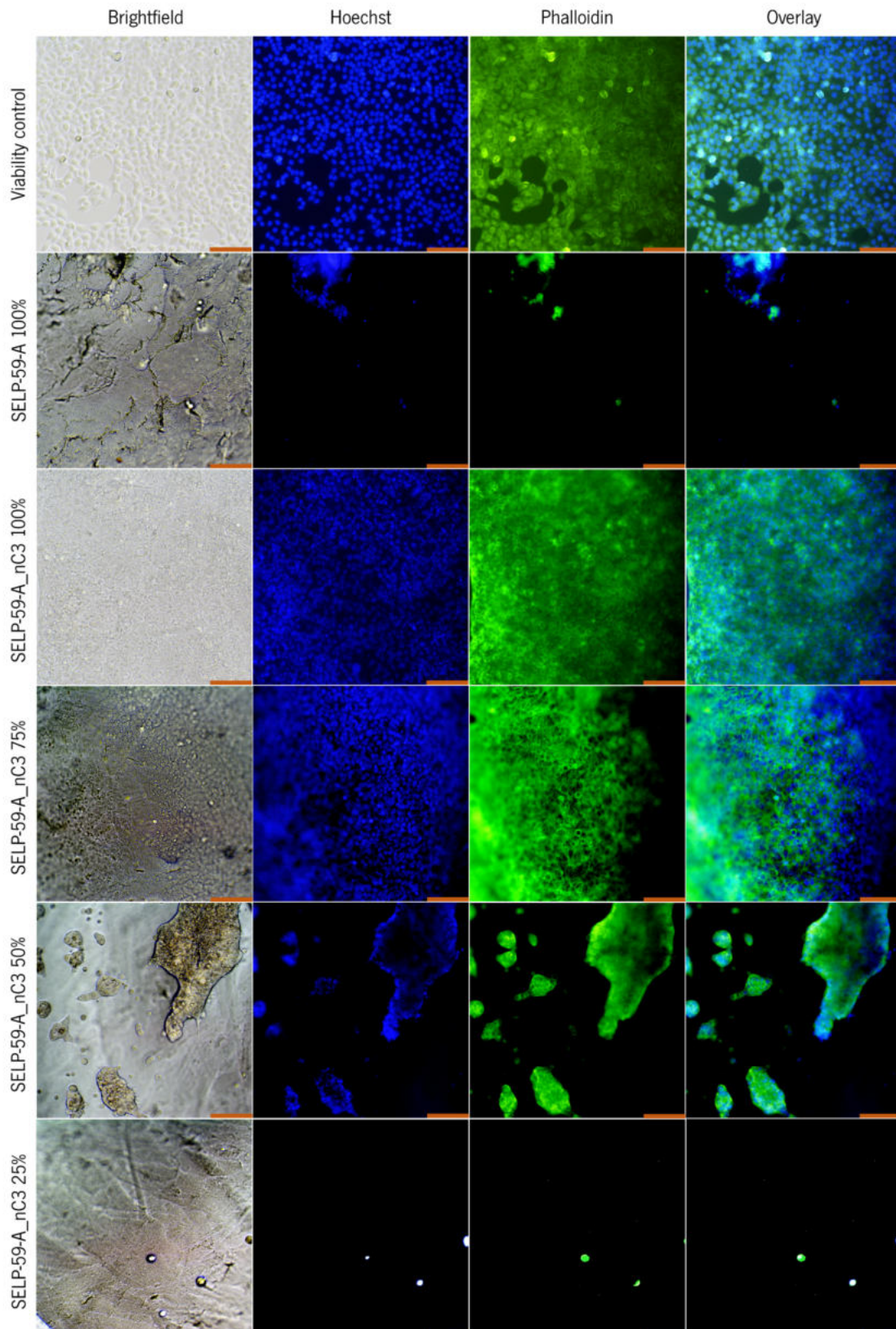


Figure 38. Brightfield and fluorescence micrographs of HaCaT cells seeded and cultured on surface SELP-59-A_nC3 films for 24 h, stained with Hoechst 34580 and Phalloidin, visualized with 100x amplification. Cells seeded and cultured on surface SELP-59-A 100% films and on surface of a surface treated well for 24 h stained with Hoechst 34580 and Phalloidin were used as controls. Scale bar represents 200 μm .

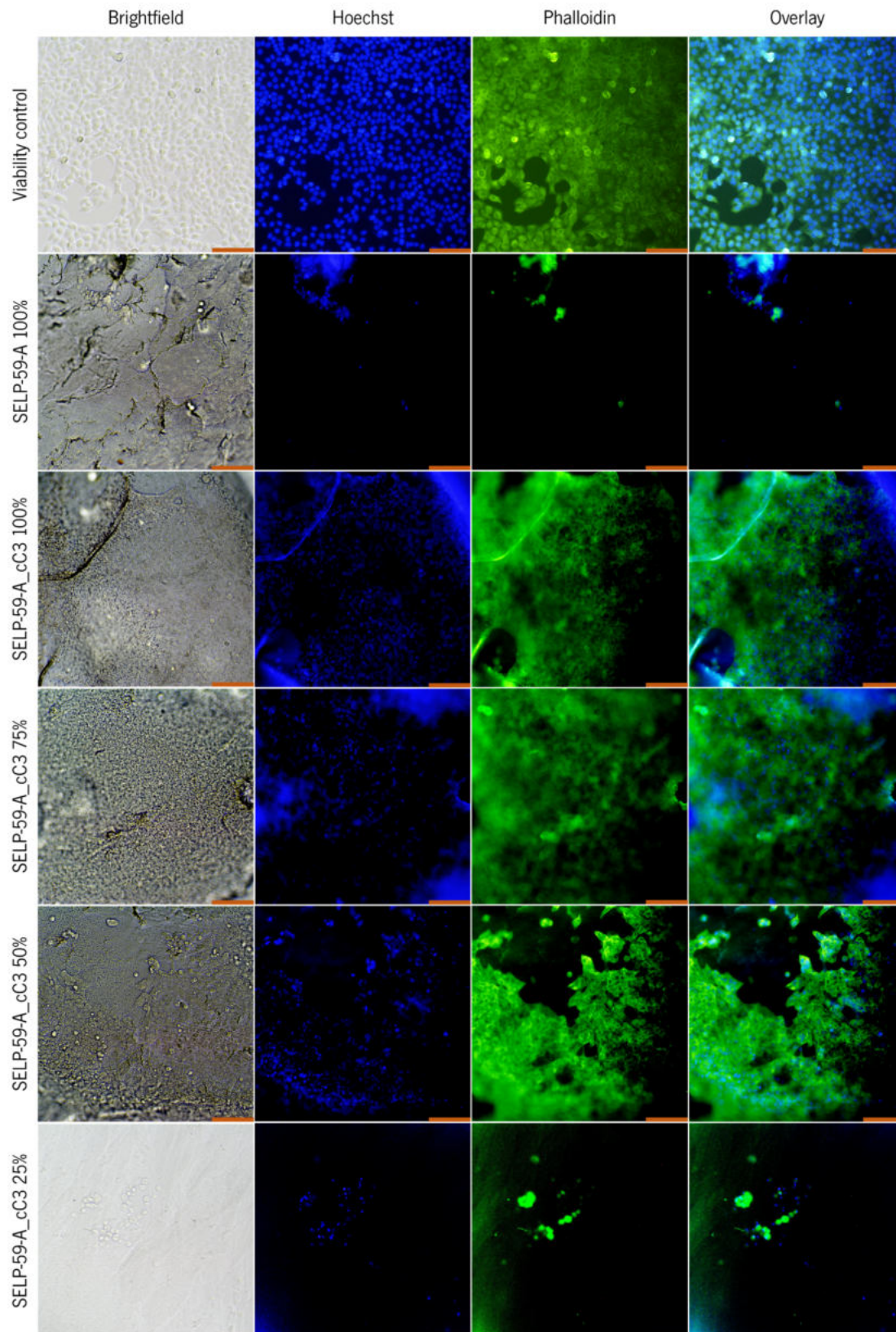


Figure 39. Brightfield and fluorescence micrographs of HaCaT cells seeded and cultured on surface SELP-59-A_cC3 films for 24 h, stained with Hoechst 34580 and Phalloidin, visualized with 100x amplification. Cells seeded and cultured on surface SELP-59-A 100% films and on surface of a surface treated well for 24 h stained with Hoechst 34580 and Phalloidin were used as controls. Scale bar represents 200 μm .

There were complications with fluorescence observation using SH-SY5Y cells, although SHSY5Y cells were fixed and stained with Hoechst and Phalloidin.

When incubated on SELP-59-A_nC3 films, the number of SH-SY5Y cells adhered to the films increases with increasing concentrations of adhesion sequence (Figure 40). SELP-59-A_nC3 100%, 75% and 50% films promoted greater cell adhesion than the viability control (Figure 40). However, contrary to what was observed with HaCaT cells (Figure 38), SH-SY5Y appear to be in an early stage of cell adhesion, as the cells have circular morphology.

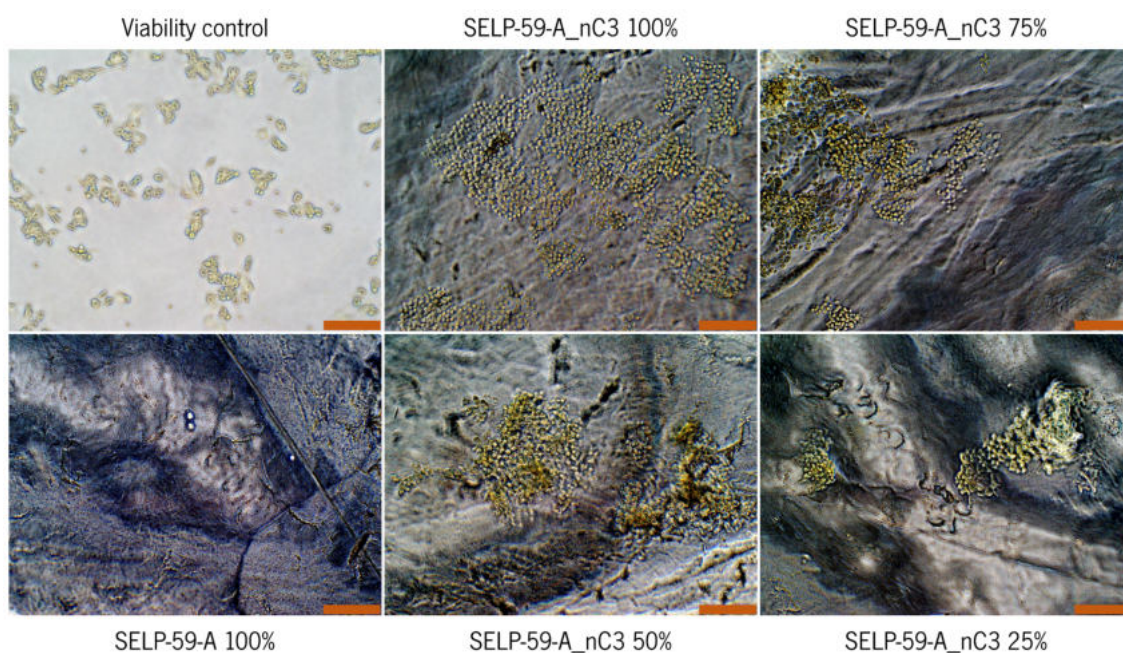


Figure 40. Brightfield micrographs of SH-SY5Y cells seeded and cultured on surface SELP-59-A_nC3 films for 24 h, visualized with 200x amplification. Cells seeded and cultured on surface SELP-59-A 100% films and on surface of a surface treated well for 24 h were used as controls. Scale bar represents 100 μ m.

When compared to the remaining SELP-59-A_cC3 films, SELP-59-A_cC3 75% seem to promote the adhesion of more cells (Figure 41). However, there does not appear to exist a correlation between the amount of adhesion sequence and the number of cells adhered to the films.

There was an increased difficulty in the observation of the cells, as the surface morphology of some films was modified throughout the assays, which became more irregular. This phenomenon was frequently verified in SELP-59-A_cC3 films incubated with HaCaT (Figure 39), but was also observed in SELP-59-A_cC3 and SELP-59-A_cRGD films using SH-SY5Y cells, as seen in Figure 41 and Figure 42, respectively.

This alteration appears to be caused by the cells, since it was not verified in the control assays after incubation of the films for 24 h with culture medium at 37 °C (Figure 33 – Figure 36).

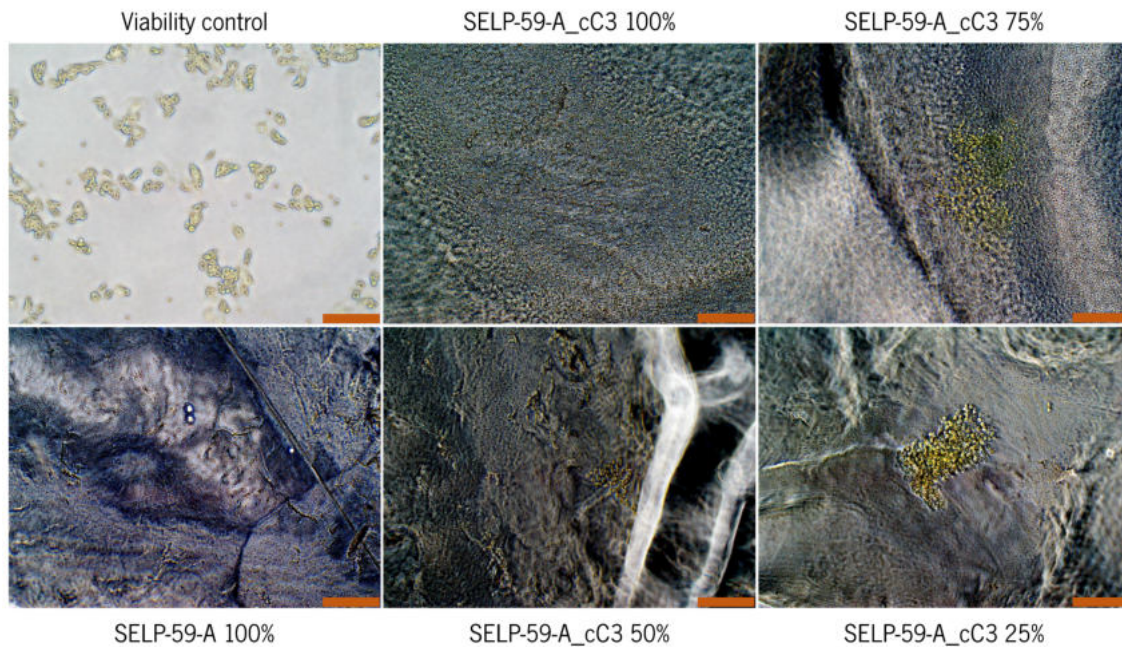


Figure 41. Brightfield micrographs of SH-SY5Y cells seeded and cultured on surface SELP-59-A_cC3 films for 24 h, visualized with 200x amplification. Cells seeded and cultured on surface SELP-59-A 100% films and on surface of a surface treated well for 24 h were used as controls. Scale bar represents 100 μ m.

As observed in SELP-59-A_cC3 films, the number of cells adhered to SELP-59-A_cRGD also does not appear to be related with the amount of adhesion sequence (Figure 42). SELP-59-A_cRGD 25% film promoted the adhesion of a higher number of cells, while the SELP-59-A_cRGD 75% stimulated a more advanced stage of cell adhesion, as the cells seem more spread over the film surface.

Due to several problems in the maintenance of the cell line, the cells were not in the ideal state of viability as can be seen in the viability control. In addition, there were complications with fluorescence observation, although SHSY5Y cells were fixed and stained with Hoechst and Phalloidin. These results will be repeated and validated thoroughly in future experiments.

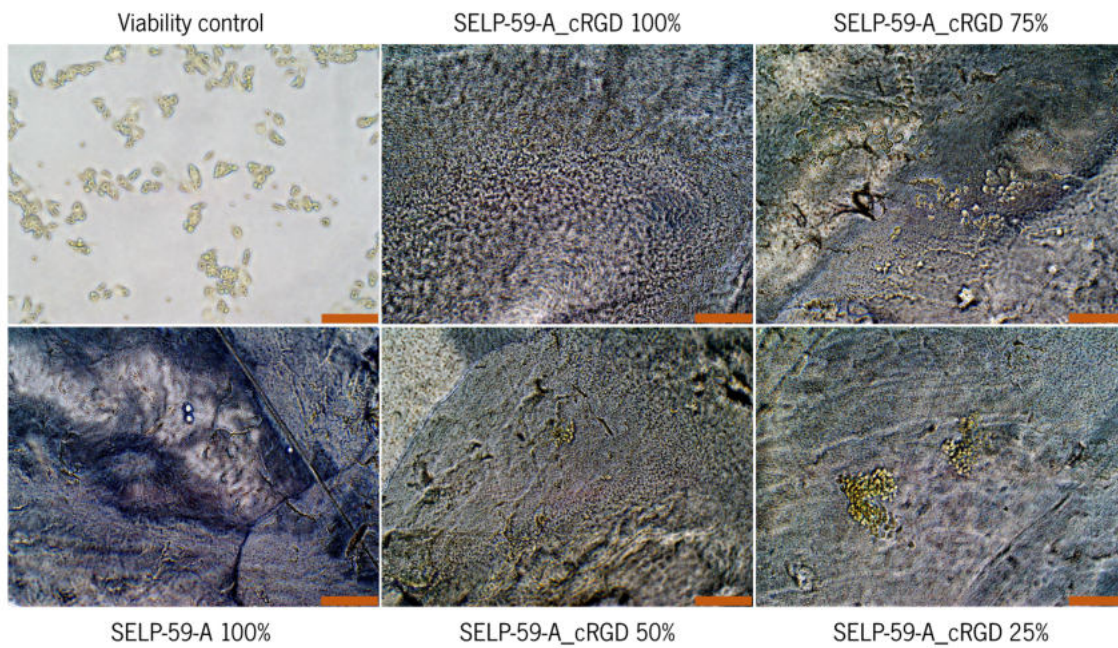


Figure 42. Brightfield micrographs of SH-SY5Y cells seeded and cultured on surface SELP-59-A_cRGD films for 24 h, visualized with 200x amplification. Cells seeded and cultured on surface SELP-59-A 100% films and on surface of a surface treated well for 24 h were used as controls. Scale bar represents 100 μm .

5. Conclusions and Future Perspectives

5. CONCLUSIONS AND FUTURE PERSPECTIVES

Tissue engineering is a growing area that primarily targets the creation of functional constructs for tissue repair, using what is known as the triad of tissue engineering: scaffold, cells and signaling molecules. A considerable number of materials have appeared that have appealing characteristics to be used as a scaffold. However, most of them are non-bioactive and have none or little influence on cellular behavior as they fail to comply with the complex number of requisites such as cell adhesion, growth, differentiation, etc.

Silk-elastin-like proteins, SELPs, are a family of rPBPs composed of tandem repeats of alternated silk- and elastin-like amino acid sequences/blocks, resembling the minimal consensus repeats found in natural silk fibroin and mammalian elastin. These genetically engineered protein polymers combine in the same structure the crystallinity and mechanical strength of silk with the high resilience and water solubility of elastin. Due to its remarkable properties such as biocompatibility, biodegradability and mechanical properties, SELPs are appealing to be used as scaffolds.

The present work targeted the functionalization of a recombinant SELP, namely SELP-59-A, via the introduction of cell-binding motifs by genetically manipulating its structure, in order to obtain a material with improved cell adhesion ability. To achieve this, the main objective was divided in three tasks: i) functionalization with different cell binding motifs by genetic engineering; ii) production and purification of the functionalized materials; iii) evaluation of the biological performance using mammalian cell cultures.

For the first task, two cell-binding motifs were chosen: RGD, which has activity in a broad spectrum of cell lines, and C3, that is specific to cell lines that express NCAM. To increase the probability of success, each of the adhesion sequences was placed at the N- and C-terminus of the SELP-59-A sequence.

In the second task, three of the four designed polymers were successfully produced in *E. coli* BL21 (DE3) by means of auto-induction using TBlac. The purification of the polymers was efficiently achieved using an inexpensive methodology that allowed the recovery of virtually pure protein. The purified polymers were successfully processed into blended formulations by combining SELP-59-A with different percentages of the functionalized polymer (0, 25, 50, 75 and 100 wt%).

Finally, in the third task, for the evaluation of the ability of films to promote cell adhesion, HaCaT and SH-SY5Y cells were cultured on the surface of the methanol-treated films for 24 h. The results show that cell adhesion was dependent not only of the adhesion sequence, but also of the cell line and the content/concentration of the cell-binding motif. The adhesion of HaCaT cells to the films demonstrated

to be influenced by the content of SELP-59-A_cRGD. While cells only marginally adhered to the pristine SELP-59-A films, the incorporation of functionalized SELP-59-A_cRGD demonstrated to have a positive effect in cell adhesion, showing to increase up to a concentration of 50% with no noticeable improvements at higher concentrations. On the other hand, when HaCaT cells were incubated on films functionalized with the C3 sequence (SELP-59-A_nC3 and SELP-59-A_cC3 films), the number of adhered cells showed to increase with increasing concentrations of the cell-binding motif. Similarly, when incubated on SELP-59-A_nC3 films, the number of SH-SY5Y cells adhered to the films demonstrated to increase with increasing concentration of the cell-binding motif. However, when incubated on SELP-59-A_cC3 and SELP-59-A_cRGD films there were no apparent relation between the content of cell-binding motif and the number of adhered cells.

Taken together, the results suggest that the functional SELP-based films have potential to be used as materials for biomedical applications, but further work is needed. For instance, there is the need to increase the number of cell adhesion assays to reach a proper conclusion, and to extend these assays to other cell lines. Also, the evaluation of cell viability through MTT or resazurin reduction assays would be complementary and would provide additional important information. An unexpected and interesting result of the present work is related with the remarkable adhesion of HaCaT cells to the SELP-59-A_nC3 and SELP-59-A_cC3 films. Therefore, it would be interesting to study in more detail the adhesion processes of non-neuronal cells to the C3 cell-binding motif, since there is a lack of knowledge on the possible effects triggered by C3-mediated cell adhesion in these cell lines. A further step would be to evaluate cell adhesion/migration/proliferation in 3D structures by, for instance, inducing the gelation of SELP into hydrogels, as this spatial conformation allow for a better cell infiltration.

6. References

6. REFERENCES

1. Farhadieh, R. D., Bulstrode, N. W. & Cugno, S. *Plastic and reconstructive surgery: approaches and techniques*. (Wiley Blackwell, 2015).
2. Lanza, R., Langer, R. & Vacanti, J. *Principles of Tissue Engineering*. (Academic Press, 2007).
3. Pereira, H. *et al.* Human Meniscus: From Biology to Tissue Engineering Strategies. in 1089–1102 (2015).
4. Kobayashi, M. & Spector, M. In vitro response of the bone marrow-derived mesenchymal stem cells seeded in a type-I collagen-glycosaminoglycan scaffold for skin wound repair under the mechanical loading condition. *Mol. Cell. Biomech.* **6**, 217–227 (2009).
5. Aydemir, I., Öztürk, Ş., Kılıçaslan Sönmez, P. & Tuğlu, M. İ. Mesenchymal stem cells in skin wound healing. *Anatomy* **10**, 228–234 (2016).
6. Yun, E. J., Yon, B., Joo, M. K. & Jeong, B. Cell Therapy for Skin Wound Using Fibroblast Encapsulated Poly(ethylene glycol)-poly(L-alanine) Thermogel. *Biomacromolecules* **13**, 1106–1111 (2012).
7. Liu, G. *et al.* Bone regeneration in a canine cranial model using allogeneic adipose derived stem cells and coral scaffold. *Biomaterials* **34**, 2655–2664 (2013).
8. He, X. *et al.* BMP2 Genetically Engineered MSCs and EPCs Promote Vascularized Bone Regeneration in Rat Critical-Sized Calvarial Bone Defects. *PLoS One* **8**, e60473 (2013).
9. Imaizumi, M. *et al.* Evaluation of the Use of Induced Pluripotent Stem Cells (iPSCs) for the Regeneration of Tracheal Cartilage. *Cell Transplant.* **22**, 341–353 (2013).
10. Xie, X. *et al.* Comparative evaluation of MSCs from bone marrow and adipose tissue seeded in PRP-derived scaffold for cartilage regeneration. *Biomaterials* **33**, 7008–7018 (2012).
11. Xu, J., Chen, Y., Yue, Y., Sun, J. & Cui, L. Reconstruction of epidural fat with engineered adipose tissue from adipose derived stem cells and PLGA in the rabbit dorsal laminectomy model. *Biomaterials* **33**, 6965–6973 (2012).
12. Lequeux, C. *et al.* Subcutaneous fat tissue engineering using autologous adipose-derived stem cells seeded onto a collagen scaffold. *Plast. Reconstr. Surg.* **130**, 1208–1217 (2012).
13. Kuo, Y.-C. & Lin, C.-C. Accelerated nerve regeneration using induced pluripotent stem cells in chitin-chitosan-gelatin scaffolds with inverted colloidal crystal geometry. *Colloids Surf. B. Biointerfaces* **103**, 595–600 (2013).
14. Iwamuro, M. *et al.* A preliminary study for constructing a bioartificial liver device with induced

- pluripotent stem cell-derived hepatocytes. *Biomed. Eng. Online* **11**, 93 (2012).
15. Ravichandran, R., Venugopal, J. R., Sundarrajan, S., Mukherjee, S. & Ramakrishna, S. Cardiogenic differentiation of mesenchymal stem cells on elastomeric poly (glycerol sebacate)/collagen core/shell fibers. *World J. Cardiol.* **5**, 28–41 (2013).
 16. Kc, P., Hong, Y. & Zhang, G. Cardiac tissue-derived extracellular matrix scaffolds for myocardial repair: advantages and challenges. *Regen. Biomater.* **6**, 185–199 (2019).
 17. Ikada, Y. Challenges in tissue engineering. *J. R. Soc. Interface* **3**, 589–601 (2006).
 18. Nikolova, M. P. & Chavali, M. S. Recent advances in biomaterials for 3D scaffolds: A review. *Bioact. Mater.* **4**, 271–292 (2019).
 19. Bryksin, A. V., Brown, A. C., Baksh, M. M., Finn, M. G. & Barker, T. H. Learning from nature - Novel synthetic biology approaches for biomaterial design. *Acta Biomater.* **10**, 1761–1769 (2014).
 20. Vepari, C. & Kaplan, D. L. Silk as a biomaterial. *Prog. Polym. Sci.* **32**, 991–1007 (2007).
 21. Falconnet, D., Csucs, G., Grandin, H. M. & Textor, M. Surface engineering approaches to micropattern surfaces for cell-based assays. *Biomaterials* **27**, 3044–3063 (2006).
 22. Engel, E., Michiardi, A., Navarro, M., Lacroix, D. & Planell, J. A. Nanotechnology in regenerative medicine: the materials side. *Trends Biotechnol.* **26**, 39–47 (2008).
 23. Dhandayuthapani, B., Yoshida, Y., Maekawa, T. & Kumar, D. S. Polymeric scaffolds in tissue engineering application: A review. *Int. J. Polym. Sci.* **2011**, 431–459 (2011).
 24. Bergmann, C. P. & Stumpf, A. Biomaterials. in *Dental Ceramics: Microstructure, Properties and Degradation* 1–84 (Springer, 2013).
 25. O'Brien, F. J. Biomaterials & scaffolds for tissue engineering. *Mater. Today* **14**, 88–95 (2011).
 26. Leukers, B. *et al.* Hydroxyapatite scaffolds for bone tissue engineering made by 3D printing. *J. Mater. Sci. Mater. Med.* **16**, 1121–1124 (2005).
 27. Kang, Y., Kim, S., Fahrenholtz, M., Khademhosseini, A. & Yang, Y. Osteogenic and angiogenic potentials of monocultured and co-cultured human-bone-marrow-derived mesenchymal stem cells and human-umbilical-vein endothelial cells on three-dimensional porous beta-tricalcium phosphate scaffold. *Acta Biomater.* **9**, 4906–4915 (2013).
 28. Tallawi, M. *et al.* Strategies for the chemical and biological functionalization of scaffolds for cardiac tissue engineering: A review. *J. R. Soc. Interface* **12**, (2015).
 29. Migliaresi, C. & Motta, A. *Scaffolds for Tissue Engineering: Biological Design, Materials, and Fabrication.* (Pan Stanford Publishing Pte. Ltd., 2014).

30. Murugan, R. & Ramakrishna, S. Nano-featured Scaffolds for Tissue Engineering: A Review of Spinning Methodologies. *Tissue Eng.* **12**, 435–447 (2006).
31. Parisi, O. I., Curcio, M. & Puoci, F. *Advanced Polymers In Medicine*. (Springer, 2015).
32. Hu, J. *et al.* Porous nanofibrous PLLA scaffolds for vascular tissue engineering. *Biomaterials* **31**, 7971–7977 (2010).
33. Yang, F. *et al.* Fabrication of nano-structured porous PLLA scaffold intended for nerve tissue engineering. *Biomaterials* **25**, 1891–1900 (2004).
34. Sun, T. *et al.* Self-Organization of Skin Cells in Three-Dimensional Electrospun Polystyrene Scaffolds. *Tissue Eng.* **11**, 1023–1033 (2005).
35. Schutte, M. *et al.* Rat Primary Hepatocytes Show Enhanced Performance and Sensitivity to Acetaminophen During Three-Dimensional Culture on a Polystyrene Scaffold Designed for Routine Use. *Assay Drug Dev. Technol.* **9**, 475–486 (2011).
36. Baker, S. C. *et al.* Characterisation of electrospun polystyrene scaffolds for three-dimensional in vitro biological studies. *Biomaterials* **27**, 3136–3146 (2006).
37. Grover, G. N., Rao, N. & Christman, K. L. Myocardial matrix–polyethylene glycol hybrid hydrogels for tissue engineering. *Nanotechnology* **25**, 14011 (2013).
38. Giuliani, A. *et al.* Polyglycolic acid–polylactic acid scaffold response to different progenitor cell in vitro cultures: a demonstrative and comparative X-ray synchrotron radiation phase-contrast microtomography study. *Tissue Eng. Part C. Methods* **20**, 308–316 (2014).
39. Wu, Y., Xia, H., Zhang, B., Zhao, Y. & Wang, Y. Assessment of polyglycolic acid scaffolds for periodontal ligament regeneration. *Biotechnol. Biotechnol. Equip.* **32**, 701–706 (2018).
40. Pan, Z. & Ding, J. Poly(lactide-co-glycolide) porous scaffolds for tissue engineering and regenerative medicine. *Interface Focus* **2**, 366–377 (2012).
41. Liu, H., Slamovich, E. B. & Webster, T. J. Less harmful acidic degradation of poly(lactico-glycolic acid) bone tissue engineering scaffolds through titania nanoparticle addition. *Int. J. Nanomedicine* **1**, 541–545 (2006).
42. Alini, M. *et al.* The potential and limitations of a cell-seeded collagen/hyaluronan scaffold to engineer an intervertebral disc-like matrix. *Spine (Phila. Pa. 1976)*. **28**, 446–453 (2003).
43. Farach-Carson, M. C. & Carson, D. D. Perlecan—a multifunctional extracellular proteoglycan scaffold. *Glycobiology* **17**, 897–905 (2007).
44. Farokhi, M., Jonidi Shariatzadeh, F., Solouk, A. & Mirzadeh, H. Alginate Based Scaffolds for Cartilage Tissue Engineering: A Review. *Int. J. Polym. Mater. Polym. Biomater.* **69**, 230–247

- (2020).
45. Madihally, S. V & Matthew, H. W. T. Porous chitosan scaffolds for tissue engineering. *Biomaterials* **20**, 1133–1142 (1999).
 46. Li, Z., Ramay, H. R., Hauch, K. D., Xiao, D. & Zhang, M. Chitosan-alginate hybrid scaffolds for bone tissue engineering. *Biomaterials* **26**, 3919–3928 (2005).
 47. Ma, L. *et al.* Collagen/chitosan porous scaffolds with improved biostability for skin tissue engineering. *Biomaterials* **24**, 4833–4841 (2003).
 48. Stone, K. R., Steadman, J. R., Rodkey, W. G. & Shu-Tung, L. Regeneration of Meniscal Cartilage with Use of a Collagen Scaffold. *J. Bone Jt. Surg.* **79**, 1770–1777 (1997).
 49. Olatunji, O. *et al.* Natural Polymers: Industry techniques and applications. in *Natural Polymers: Industry Techniques and Applications* (ed. O., O.) 63–91 (Springer, Cham, 2016).
 50. Casal, M., Cunha, A. M. & Machado, R. Future Trends for Recombinant Protein-Based Polymers: The Case Study of Development and Application of Silk-Elastin-Like Polymers. in *Bio-Based Plastics: Materials and Applications* (ed. Kabasci, S.) 311–329 (John Wiley & Sons, Ltd, 2014).
 51. Yang, Y. J., Holmberg, A. L. & Olsen, B. D. Artificially Engineered Protein Polymers. *Annu. Rev. Chem. Biomol. Eng.* **8**, 549–575 (2017).
 52. Numata, K. How to define and study structural proteins as biopolymer materials. *Polym. J.* (2020).
 53. Abascal, N. C. & Regan, L. The past, present and future of protein-based materials. *Open Biol.* **8**, 180113 (2020).
 54. Engel, J. & Bächinger, H. P. Structure, stability and folding of the collagen triple helix. in *Collagen: Primer in Structure, Processing and Assembly* (eds. Jürgen, B., Holger, N. & Müller, P. K.) **247**, 7–33 (Springer, 2005).
 55. Wenger, M. P. E., Bozec, L., Horton, M. A. & Mesquidaz, P. Mechanical properties of collagen fibrils. *Biophys. J.* **93**, 1255–1263 (2007).
 56. Machado, R. *et al.* Electrospun silk-elastin-like fibre mats for tissue engineering applications. *Biomed. Mater.* **8**, (2013).
 57. Hu, X., Cebe, P., Weiss, A. S., Omenetto, F. & Kaplan, D. L. Protein-based composite materials. *Mater. Today* **15**, 208–215 (2012).
 58. Cappello, J. *et al.* Genetic engineering of structural protein polymers. *Biotechnol. Prog.* **6**, 198–202 (1990).
 59. Chow, D., Nunalee, M. L., Lim, D. W., Simnick, A. J. & Chilkoti, A. Peptide-based Biopolymers in Biomedicine and Biotechnology. *Mater. Sci. Eng. R. Rep.* **62**, 125–155 (2008).

60. Kaplan, D. L. Fibrous proteins - silk as a model system. *Polym. Degrad. Stab.* **59**, 25–32 (1998).
61. Li, L. & Kiick, K. L. Resilin-Based Materials for Biomedical Applications. *ACS Macro Lett.* **2**, 635–640 (2013).
62. van Hest, J. C. M. & Tirrell, D. A. Protein-based materials, toward a new level of structural control. *Chem. Commun.* 1897–1904 (2001).
63. Machado, R. *et al.* Exploiting the Sequence of Naturally Occurring Elastin: Construction, Production and Characterization of a Recombinant Thermoplastic Protein-Based Polymer. *J. Nano Res.* **6**, 133–145 (2009).
64. Machado, R. *et al.* Exploring the Properties of Genetically Engineered Silk-Elastin-Like Protein Films. *Macromol. Biosci.* **15**, 1698–1709 (2015).
65. Spiess, K., Lammel, A. & Scheibel, T. Recombinant Spider Silk Proteins for Applications in Biomaterials. *Macromol. Biosci.* **10**, 998–1007 (2010).
66. Hardy, J. G. & Scheibel, T. R. Silk-inspired polymers and proteins. *Biochem. Soc. Trans.* **37**, 677–681 (2009).
67. Qiu, W., Teng, W., Cappello, J. & Wu, X. Wet-Spinning of Recombinant Silk-Elastin-Like Protein Polymer Fibers with High Tensile Strength and High Deformability. *Biomacromolecules* **10**, 602–608 (2009).
68. Dinjaski, N. & Kaplan, D. L. Recombinant protein blends: silk beyond natural design. *Curr. Opin. Biotechnol.* **39**, 1–7 (2016).
69. Pereira, A. M. *et al.* Silk-based biomaterials functionalized with fibronectin type II promotes cell adhesion. *Acta Biomater.* **47**, 50–59 (2016).
70. Paiva dos Santos, B. *et al.* Production, purification and characterization of an elastin-like polypeptide containing the Ile-Lys-Val-Ala-Val (IKVAV) peptide for tissue engineering applications. *J. Biotechnol.* **298**, 35–44 (2019).
71. Quintanilla-Sierra, L., García-Arévalo, C. & Rodríguez-Cabello, J. C. Self-assembly in elastin-like recombinamers: a mechanism to mimic natural complexity. *Mater. Today Bio* **2**, 100007 (2019).
72. Kamata, H., Ashikari-Hada, S., Mori, Y., Azuma, A. & Hata, K. Extemporaneous Preparation of Injectable and Enzymatically Degradable 3D Cell Culture Matrices from an Animal-Component-Free Recombinant Protein Based on Human Collagen Type I. *Macromol. Rapid Commun.* **40**, 1900127 (2019).
73. Mikael, P. E. *et al.* Production and Characterization of Recombinant Collagen-Binding Resilin Nanocomposite for Regenerative Medicine Applications. *Regen. Eng. Transl. Med.* **5**, 362–372

- (2019).
74. Yan, J. *et al.* Preparation of recombinant human-like collagen/fibroin scaffold and its promoting effect on vascular cells biocompatibility. *J. Bioact. Compat. Polym.* **33**, 416–425 (2018).
 75. Barroca, M. *et al.* Antibiotic free selection for the high level biosynthesis of a silk-elastin-like protein. *Sci. Rep.* **6**, 1–11 (2016).
 76. Machado, R. *et al.* High level expression and facile purification of recombinant silk-elastin-like polymers in auto induction shake flask cultures. *AMB Express* **3**, 1–15 (2013).
 77. Gustafson, J. A. & Ghandehari, H. Silk-elastinlike protein polymers for matrix-mediated cancer gene therapy. *Adv. Drug Deliv. Rev.* **62**, 1509–1523 (2010).
 78. Rodriguez-Caballero, J. C., Alonso, M., Díez, M. I., Caballero, M. I. & Herguedas, M. M. Structural investigation of the poly(pentapeptide) of elastin, poly(GVGVP), in the solid state. *Macromol. Chem. Phys.* **200**, 1831–1838 (1999).
 79. Tatham, A. S. & Shewry, P. R. Elastomeric proteins : biological roles , structures and mechanisms. *Trends Biochem. Sci.* **25**, 567–571 (2000).
 80. Ribeiro, A., Arias, F. J., Reguera, J., Alonso, M. & Rodríguez-Cabello, J. C. Influence of the amino-acid sequence on the inverse temperature transition of elastin-like polymers. *Biophys. J.* **97**, 312–320 (2009).
 81. Bessa, P. C. *et al.* Thermoresponsive self-assembled elastin-based nanoparticles for delivery of BMPs. *J. Control. Release* **142**, 312–318 (2010).
 82. Nagapudi, K. *et al.* Protein-based thermoplastic elastomers. *Macromolecules* **38**, 345–354 (2005).
 83. Urry, D. W. & Luan, C.-H. Elastic, Plastic, and Hydrogel Protein-based Polymers. in *Polymer Data Handbook* (ed. M., J. E.) 78–89 (Oxford University Press, 1999).
 84. Rincón, A. C. *et al.* Biocompatibility of elastin-like polymer poly(VPAVG) microparticles: in vitro and in vivo studies. *J. Biomed. Mater. Res. A* **78**, 343–351 (2006).
 85. Cappello, J. *et al.* In-situ self-assembling protein polymer gel systems for administration, delivery, and release of drugs. *J. Control. Release* **53**, 105–117 (1998).
 86. Numata, K., Hamasaki, J., Subramanian, B. & Kaplan, D. L. Gene delivery mediated by recombinant silk proteins containing cationic and cell binding motifs. *J. Control. Release* **146**, 136–143 (2010).
 87. Huang, W., Rollett, A. & Kaplan, D. L. Silk-elastin-like protein biomaterials for the controlled delivery of therapeutics. *Expert Opin. Drug Deliv.* **12**, 779–791 (2015).

88. Qiu, W. *et al.* Complete recombinant silk-elastinlike protein-based tissue scaffold. *Biomacromolecules* **11**, 3219–3227 (2010).
89. Guda, C. *et al.* Hyper expression of an environmentally friendly synthetic polymer gene. *Biotechnol. Lett.* **17**, 745–750 (1995).
90. Teng, W., Huang, Y., Cappello, J. & Wu, X. Optically transparent recombinant silk-elastinlike protein polymer films. *J. Phys. Chem. B* **115**, 1608–1615 (2011).
91. Collins, T., Branca, F., Padrão, J., Machado, R. & Casal, M. High Level Biosynthesis of a Silk-Elastin-like Protein in *E. coli*. *Biomacromolecules* **15**, 2701–2708 (2014).
92. Collins, T. *et al.* Batch production of a silk-elastin-like protein in *E. coli* BL21 (DE3): key parameters for optimisation. *Microb. Cell Fact.* **12**, 1–16 (2013).
93. Fernandes, M. M. *et al.* Multifunctional magnetically responsive biocomposites based on genetically engineered silk-elastin-like protein. *Compos. Part B Eng.* **153**, 413–419 (2018).
94. Correia, D. M. *et al.* Development of bio-hybrid piezoresistive nanocomposites using silk-elastin protein copolymers. *Compos. Sci. Technol.* **172**, 134–142 (2019).
95. Cooper, G. M. *The Cell: a molecular approach*. (Oxford University Press: Sinauer Associates, 2019).
96. McEver, R. P. & Luscinskas, F. W. Chapter 12 - Cell Adhesion. in (eds. Hoffman, R. et al.) 127–134 (Elsevier, 2018).
97. Khalili, A. A. & Ahmad, M. R. A Review of cell adhesion studies for biomedical and biological applications. *Int. J. Mol. Sci.* **16**, 18149–18184 (2015).
98. McEver, R. P. & Zhu, C. Rolling cell adhesion. *Annu. Rev. Cell Dev. Biol.* **26**, 363–396 (2010).
99. Alberts, B., Johnson, A., Lewis, J., Raff, M., Roberts, K., and Walter, P. Cell-Cell Adhesion and Communication. in *Molecular Biology of the Cell* 101–121 (W H Freeman & Co, 2002).
100. Windisch, R. *et al.* Oncogenic Deregulation of Cell Adhesion Molecules in Leukemia. *Cancers (Basel)*. **11**, 311 (2019).
101. Goodwin, K. *et al.* Cell-cell and cell-extracellular matrix adhesions cooperate to organize actomyosin networks and maintain force transmission during dorsal closure. *Mol. Biol. Cell* **28**, 1301–1310 (2017).
102. Chen, Y., Ju, L., Rushdi, M., Ge, C. & Zhu, C. Receptor-mediated cell mechanosensing. *Mol. Biol. Cell* **28**, 3134–3155 (2017).
103. Hersel, U., Dahmen, C. & Kessler, H. RGD modified polymers: Biomaterials for stimulated cell adhesion and beyond. *Biomaterials* **24**, 4385–4415 (2003).

104. Mandai, K., Rikitake, Y., Mori, M. & Takai, Y. Chapter Six - Nectins and Nectin-Like Molecules in Development and Disease. in *Cellular Adhesion in Development and Disease* **112**, 197–231 (Academic Press, 2015).
105. Sumigray, K. D. & Lechler, T. Chapter Twelve - Cell Adhesion in Epidermal Development and Barrier Formation. in *Cellular Adhesion in Development and Disease* (ed. Yap, A. S. B. T.-C. T. in D. B.) **112**, 383–414 (Academic Press, 2015).
106. Andl, C. D., Moustafa, A.-E. Al, Deramaudt, T. B. & O’Neill, G. M. Cell Adhesion Signaling and Its Impact on Tumorigenesis. *J. Oncol.* **2010**, (2010).
107. Tsukita, S., Furuse, M. & Itoh, M. Multifunctional strands in tight junctions. *Nat. Rev. Mol. Cell Biol.* **2**, 285–293 (2001).
108. Niessen, C. M. & Gottardi, C. J. Molecular components of the adherens junction. *Biochim. Biophys. Acta - Biomembr.* **1778**, 562–571 (2008).
109. Lie, P. P. Y., Cheng, C. Y. & Mruk, D. D. The biology of the desmosome-like junction a versatile anchoring junction and signal transducer in the seminiferous epithelium. *Int. Rev. Cell Mol. Biol.* **286**, 223–269 (2011).
110. Kowalczyk, A. P. & Green, K. J. Chapter Five - Structure, Function, and Regulation of Desmosomes. in *The Molecular Biology of Cadherins* (ed. van Roy, F. B. T.-P. in M. B. and T. S.) **116**, 95–118 (Academic Press, 2013).
111. Kagan, H. M. *The Extracellular Matrix: an Overview.* **1**, (Springer, 1998).
112. Kristensen, J. H. & Karsdal, M. A. Chapter 30 - Elastin. in *Biochemistry of Collagens, Laminins and Elastin* (ed. Karsdal Laminins and Elastin, M. A. B. T.-B. of C.) 197–201 (Academic Press, 2016).
113. Ratner, B. D., Hoffman, A. S., Schoen, F. J. & Lemons, J. E. *Biomaterials Science: An Introduction to Materials in Medicine.* (Academic Press, 2004).
114. Martins-Green, M. & Bissell, M. J. Cell-ECM interactions in development. *Semin. Dev. Biol.* **6**, 149–159 (1995).
115. Byron, A. *et al.* Proteomic Analysis of Integrin Adhesion Complexes. *Sci. Signal.* **4**, (2012).
116. Humphries, J. D. Integrin ligands at a glance. *J. Cell Sci.* **119**, 3901–3903 (2006).
117. Mecham, R. P. *Integrins: Molecular and Biological Responses to the Extracellular Matrix.* (Academic Press, 1994).
118. Lodish H, Berk A, Zipursky SL, Matsudaira P, Baltimore D, D. J. Cell-Matrix Adhesion. in *Molecular Cell Biology* 1184 (Media Connected, 2000).

119. Solouk, A. *et al.* The study of collagen immobilization on a novel nanocomposite to enhance cell adhesion and growth. *Iran. Biomed. J.* **15**, 6–14 (2011).
120. Aflori, M. *et al.* Collagen immobilization on polyethylene terephthalate surface after helium plasma treatment. *Mater. Sci. Eng. B* **178**, 1303–1310 (2013).
121. Yoon, J. J., Song, S. H., Lee, D. S. & Park, T. G. Immobilization of cell adhesive RGD peptide onto the surface of highly porous biodegradable polymer scaffolds fabricated by a gas foaming/salt leaching method. *Biomaterials* **25**, 5613–5620 (2004).
122. Ho, M.-H. *et al.* Preparation and Characterisation of RGD-Immobilized Chitosan Scaffolds. *Biomaterials* **26**, 3197–3206 (2005).
123. Tasiopoulos, C. P., Widhe, M. & Hedhammar, M. Recombinant Spider Silk Functionalized with a Motif from Fibronectin Mediates Cell Adhesion and Growth on Polymeric Substrates by Entrapping Cells during Self-Assembly. *ACS Appl. Mater. Interfaces* **10**, 14531–14539 (2018).
124. Girotti, A., Orbanic, D., Ibáñez-Fonseca, A., Gonzalez-Obeso, C. & Rodríguez-Cabello, J. C. Recombinant Technology in the Development of Materials and Systems for Soft-Tissue Repair. *Adv. Healthc. Mater.* **4**, 2423–2455 (2015).
125. Girotti, A. *et al.* Design and bioproduction of a recombinant multi(bio)functional elastin-like protein polymer containing cell adhesion sequences for tissue engineering purposes. *J. Mater. Sci. Mater. Med.* **15**, 479–484 (2004).
126. Pierschbacher, M. D. & Ruoslahti, E. Cell attachment activity of fibronectin can be duplicated by small synthetic fragments of the molecule. *Nature* **309**, 30–33 (1984).
127. Boateng, S. Y. *et al.* RGD and YIGSR synthetic peptides facilitate cellular adhesion identical to that of laminin and fibronectin but alter the physiology of neonatal cardiac myocytes. *Am. J. Physiol. Cell Physiol.* **288**, C30-8 (2005).
128. Barczyk, M., Carracedo, S. & Gullberg, D. Integrins. *Cell Tissue Res.* **339**, 269–280 (2010).
129. Karecla, P. I., Green, S. J., Bowden, S. J., Coadwell, J. & Kilshaw, P. J. Identification of a binding site for integrin alphaEbeta7 in the N-terminal domain of E-cadherin. *J. Biol. Chem.* **271**, 30909–15 (1996).
130. Plow, E. F., Haas, T. A., Zhang, L., Loftus, J. & Smith, J. W. Ligand binding to integrins. *J. Biol. Chem.* **275**, 21785–21788 (2000).
131. Ruoslahti, E. Rgd and Other Recognition Sequences for Integrins. *Annu. Rev. Cell Dev. Biol.* **12**, 697–715 (1996).
132. Zwolanek, D. *et al.* Collagen XXII binds to collagen-binding integrins via the novel motifs GLQGER

- and GFKGER. *Biochem. J.* **459**, 217–227 (2014).
133. Bini, E. *et al.* RGD-functionalized bioengineered spider dragline silk biomaterial. *Biomacromolecules* **7**, 3139–3145 (2006).
 134. Costa, R. R. *et al.* Stimuli-responsive thin coatings using elastin-like polymers for biomedical applications. *Adv. Funct. Mater.* **19**, 3210–3218 (2009).
 135. Hwang, D. S., Sim, S. B. & Cha, H. J. Cell adhesion biomaterial based on mussel adhesive protein fused with RGD peptide. *Biomaterials* **28**, 4039–4046 (2007).
 136. Hwang, D. S., Waite, J. H. & Tirrell, M. Promotion of osteoblast proliferation on complex coacervation-based hyaluronic acid - recombinant mussel adhesive protein coatings on titanium. *Biomaterials* **31**, 1080–1084 (2010).
 137. Kinikoglu, B., Rodríguez-Cabello, J. C., Damour, O. & Hasirci, V. The influence of elastin-like recombinant polymer on the self-renewing potential of a 3D tissue equivalent derived from human lamina propria fibroblasts and oral epithelial cells. *Biomaterials* **32**, 5756–5764 (2011).
 138. Martin, L., Alonso, M., Möller, M., Rodríguez-Cabello, J. C. & Mela, P. 3D microstructuring of smart bioactive hydrogels based on recombinant elastin-like polymers. *Soft Matter* **5**, 1591–1593 (2009).
 139. Morgan, A. W. *et al.* Characterization and optimization of RGD-containing silk blends to support osteoblastic differentiation. *Biomaterials* **29**, 2556–2563 (2008).
 140. Nagaoka, M., Jiang, H. L., Hoshihara, T., Akaike, T. & Cho, C. S. Application of recombinant fusion proteins for tissue engineering. *Ann. Biomed. Eng.* **38**, 683–693 (2010).
 141. Nettles, D. L., Chilkoti, A. & Setton, L. A. Applications of elastin-like polypeptides in tissue engineering. *Adv. Drug Deliv. Rev.* **62**, 1479–1485 (2010).
 142. Smith, E., Yang, J., McGann, L., Sebald, W. & Uludag, H. RGD-grafted thermoreversible polymers to facilitate attachment of BMP-2 responsive C2C12 cells. *Biomaterials* **26**, 7329–7338 (2005).
 143. Widhe, M., Johansson, U., Hillerdahl, C. O. & Hedhammar, M. Recombinant spider silk with cell binding motifs for specific adherence of cells. *Biomaterials* **34**, 8223–8234 (2013).
 144. Widhe, M., Shalaly, N. D. & Hedhammar, M. A fibronectin mimetic motif improves integrin mediated cell binding to recombinant spider silk matrices. *Biomaterials* **74**, 256–266 (2016).
 145. Wohlrab, S. *et al.* Cell adhesion and proliferation on RGD-modified recombinant spider silk proteins. *Biomaterials* **33**, 6650–6659 (2012).
 146. Hubbell, J. A., Massia, S. P., Desai, N. P. & Drumheller, P. D. Endothelial cell-selective materials for tissue engineering in the vascular graft via a new receptor. *Biotechnology. (N. Y.)* **9**, 568–572

- (1991).
147. He, W., Yong, T., Teo, W. E., Ma, Z. & Ramakrishna, S. Fabrication and endothelialization of collagen-blended biodegradable polymer nanofibers: Potential vascular graft for blood vessel tissue engineering. *Tissue Eng.* **11**, 1574–1588 (2005).
 148. Eberhart, A. *et al.* A new generation of polyurethane vascular prostheses: Rara Avis or Ignis Fatuus? *J. Biomed. Mater. Res.* **48**, 546–558 (1999).
 149. Heilshorn, S. C., DiZio, K. A., Welsh, E. R. & Tirrell, D. A. Endothelial cell adhesion to the fibronectin CS5 domain in artificial extracellular matrix proteins. *Biomaterials* **24**, 4245–4252 (2003).
 150. Kambe, Y., Murakoshi, A., Urakawa, H., Kimura, Y. & Yamaoka, T. Vascular induction and cell infiltration into peptide-modified bioactive silk fibroin hydrogels. *J. Mater. Chem. B* **5**, 7557–7571 (2017).
 151. Liu, J. C., Heilshorn, S. C. & Tirrell, D. A. Comparative cell response to artificial extracellular matrix proteins containing the RGD and CS5 cell-binding domains. *Biomacromolecules* **5**, 497–504 (2004).
 152. Martin, L., Alonso, M., Girotti, A., Arias, F. J. & Rodríguez-Cabello, J. C. Synthesis and characterization of macroporous thermosensitive hydrogels from recombinant elastin-like polymers. *Biomacromolecules* **10**, 3015–3022 (2009).
 153. Martínez-Osorio, H. *et al.* Genetically engineered elastin-like polymer as a substratum to culture cells from the ocular surface. *Curr. Eye Res.* **34**, 48–56 (2009).
 154. Berezin, V. *Structure and Function of the Neural Cell Adhesion Molecule NCAM*. **663**, (Springer Science & Business Media, 2010).
 155. Kiryushko, D., Bock, E. & Berezin, V. Pharmacology of Cell Adhesion Molecules of the Nervous System. *Curr. Neuropharmacol.* **5**, 253–267 (2007).
 156. Mie, M., Sasaki, S. & Kobatake, E. Construction of a bFGF-tethered multi-functional extracellular matrix protein through coiled-coil structures for neurite outgrowth induction. *Biomed. Mater.* **9**, 15004 (2014).
 157. Heath, C. A. Cells for tissue engineering. *Trends Biotechnol.* **18**, 17–19 (2000).
 158. Howard, D., Buttery, L. D., Shakesheff, K. M. & Roberts, S. J. Tissue engineering: strategies, stem cells and scaffolds. *J. Anat.* **213**, 66–72 (2008).
 159. Fodor, W. L. Tissue engineering and cell based therapies, from the bench to the clinic: the potential to replace, repair and regenerate. *Reprod. Biol. Endocrinol.* **1**, 102 (2003).
 160. Vig, K. *et al.* Advances in Skin Regeneration Using Tissue Engineering. *Int. J. Mol. Sci.* **18**, 789

- (2017).
161. Pietrzak, W. *Musculoskeletal Tissue Regeneration: Biological Materials and Methods*. (Humana Press, 2008).
 162. Patience, C., Takeuchi, Y. & Weiss, R. A. Infection of human cells by an endogenous retrovirus of pigs. *Nat. Med.* **3**, 282–286 (1997).
 163. Shambloott, M. J. *et al.* Derivation of pluripotent stem cells from cultured human primordial germ cells. *Proc. Natl. Acad. Sci.* **95**, 13726 LP – 13731 (1998).
 164. Solter, D. & Gearhart, J. Putting Stem Cells to Work. *Science (80-)*. **283**, 1468–1470 (1999).
 165. Thomson, J. A. *et al.* Embryonic Stem Cell Lines Derived from Human Blastocysts. *Science (80-)*. **282**, 1145–1147 (1998).
 166. Hentze, H. *et al.* Teratoma formation by human embryonic stem cells: evaluation of essential parameters for future safety studies. *Stem Cell Res.* **2**, 198–210 (2009).
 167. Prokhorova, T. A. *et al.* Teratoma formation by human embryonic stem cells is site dependent and enhanced by the presence of Matrigel. *Stem Cells Dev.* **18**, 47–54 (2009).
 168. Wagers, A. J. & Weissman, I. L. Plasticity of Adult Stem Cells. *Cell* **116**, 639–648 (2004).
 169. Kotobuki, N., Hirose, M., Takakura, Y. & Ohgushi, H. Cultured Autologous Human Cells for Hard Tissue Regeneration: Preparation and Characterization of Mesenchymal Stem Cells from Bone Marrow. *Artif. Organs* **28**, 33–39 (2004).
 170. Altman, J. & Das, G. D. Autoradiographic and histological evidence of postnatal hippocampal neurogenesis in rats. *J. Comp. Neurol.* **124**, 319–335 (1965).
 171. Kajstura, J. *et al.* Myocyte proliferation in end-stage cardiac failure in humans. *Proc. Natl. Acad. Sci.* **95**, 8801 LP – 8805 (1998).
 172. Altman, J. Autoradiographic and histological studies of postnatal neurogenesis. IV. Cell proliferation and migration in the anterior forebrain, with special reference to persisting neurogenesis in the olfactory bulb. *J. Comp. Neurol.* **137**, 433–457 (1969).
 173. Lois, C. & Alvarez-Buylla, A. Proliferating subventricular zone cells in the adult mammalian forebrain can differentiate into neurons and glia. *Proc. Natl. Acad. Sci.* **90**, 2074 LP – 2077 (1993).
 174. Kovalevich, J. & Langford, D. Considerations for the Use of SH-SY5Y Neuroblastoma Cells in Neurobiology BT - Neuronal Cell Culture: Methods and Protocols. in (eds. Amini, S. & White, M. K.) 9–21 (Humana Press, 2013).
 175. Biedler, J. L., Helson, L. & Spengler, B. A. Morphology and growth, tumorigenicity, and

- cytogenetics of human neuroblastoma cells in continuous culture. *Cancer Res.* **33**, 2643–2652 (1973).
176. Schoop, V. M., Fusenig, N. E. & Mirancea, N. Epidermal Organization and Differentiation of HaCaT Keratinocytes in Organotypic Coculture with Human Dermal Fibroblasts. *J. Invest. Dermatol.* **112**, 343–353 (1999).
177. Ruoslahti, E. *Cell Biology of Extracellular Matrix*. **1**, (Springer, 1991).
178. Pierschbacher, M. D. & Ruoslahti, E. Influence of stereochemistry of the sequence Arg-Gly-Asp-Xaa on binding specificity in cell adhesion. *J. Biol. Chem.* **262**, 17294–17298 (1987).
179. Ruoslahti, E. & Pierschbacher, M. D. New perspectives in cell adhesion: RGD and integrins. *Science* **238**, 491–497 (1987).
180. Patel, P. R. *et al.* Synthesis and Cell Adhesive Properties of Linear and Cyclic RGD Functionalized Polynorbornene Thin Films. *Biomacromolecules* **13**, 2546–2553 (2012).
181. Zhu, J., Tang, C., Kottke-Marchant, K. & Marchant, R. E. Design and Synthesis of Biomimetic Hydrogel Scaffolds with Controlled Organization of Cyclic RGD Peptides. *Bioconjug. Chem.* **20**, 333–339 (2009).
182. Leahy, D. J., Aukhil, I. & Erickson, H. P. 2.0 Å Crystal Structure of a Four-Domain Segment of Human Fibronectin Encompassing the RGD Loop and Synergy Region. *Cell* **84**, 155–164 (1996).
183. Menorca, R. M. G., Fussell, T. S. & Elfar, J. C. Nerve physiology: mechanisms of injury and recovery. *Hand Clin.* **29**, 317–330 (2013).
184. Burnett, M. G. & Zager, E. L. Pathophysiology of peripheral nerve injury: a brief review. *Neurosurg. Focus* **16**, E1 (2004).
185. Yang, F., Murugan, R., Wang, S. & Ramakrishna, S. Electrospinning of nano/micro scale poly(l-lactic acid) aligned fibers and their potential in neural tissue engineering. *Biomaterials* **26**, 2603–2610 (2005).
186. Yao, L. *et al.* Effect of functionalized micropatterned PLGA on guided neurite growth. *Acta Biomater.* **5**, 580–588 (2009).
187. Chew, S. Y., Mi, R., Hoke, A. & Leong, K. W. Aligned Protein-Polymer Composite Fibers Enhance Nerve Regeneration: A Potential Tissue-Engineering Platform. *Adv. Funct. Mater.* **17**, 1288–1296 (2007).
188. Schmidt, C. E. & Leach, J. B. Neural Tissue Engineering: Strategies for Repair and Regeneration. *Annu. Rev. Biomed. Eng.* **5**, 293–347 (2003).
189. Kim, Y.-T., Haftel, V. K., Kumar, S. & Bellamkonda, R. V. The role of aligned polymer fiber-based

- constructs in the bridging of long peripheral nerve gaps. *Biomaterials* **29**, 3117–3127 (2008).
190. Corey, J. M. *et al.* The design of electrospun PLLA nanofiber scaffolds compatible with serum-free growth of primary motor and sensory neurons. *Acta Biomater.* **4**, 863–875 (2008).
191. Corey, J. M. *et al.* Aligned electrospun nanofibers specify the direction of dorsal root ganglia neurite growth. *J. Biomed. Mater. Res. A* **83**, 636–645 (2007).
192. Schnell, E. *et al.* Guidance of glial cell migration and axonal growth on electrospun nanofibers of poly-epsilon-caprolactone and a collagen/poly-epsilon-caprolactone blend. *Biomaterials* **28**, 3012–3025 (2007).
193. Gertz, C. C. *et al.* Accelerated neuritogenesis and maturation of primary spinal motor neurons in response to nanofibers. *Dev. Neurobiol.* **70**, 589–603 (2010).
194. Flynn, K. C. The cytoskeleton and neurite initiation. *Bioarchitecture* **3**, 86–109 (2013).
195. Sachana, M., Flaskos, J. & Hargreaves, A. J. Chapter 15 - In Vitro Biomarkers of Developmental Neurotoxicity. in (ed. Gupta, R. C. B. T.-R. and D. T. (Second E.) 255–288 (Academic Press, 2017).
196. Cohen-Cory, S. The developing synapse: construction and modulation of synaptic structures and circuits. *Science* **298**, 770–776 (2002).
197. Ronn, L. C. B. *et al.* Characterization of a novel NCAM ligand with a stimulatory effect on neurite outgrowth identified by screening a combinatorial peptide library. *Eur. J. Neurosci.* **16**, 1720–1730 (2002).
198. Rønn, L. C. B., Doherty, P., Holm, A., Berezin, V. & Bock, E. Neurite outgrowth induced by a synthetic peptide ligand of neural cell adhesion molecule requires fibroblast growth factor receptor activation. *J. Neurochem.* **75**, 665–671 (2000).
199. Kiryushko, D. *et al.* A synthetic peptide ligand of neural cell adhesion molecule (NCAM), C3d, promotes neuritogenesis and synaptogenesis and modulates presynaptic function in primary cultures of rat hippocampal neurons. *J. Biol. Chem.* **278**, 12325–12334 (2003).
200. Rønn, L. C. B. *et al.* Identification of a neuritogenic ligand of the neural cell adhesion molecule using a combinatorial library of synthetic peptides. *Nat. Biotechnol.* **17**, 1000–1005 (1999).
201. Ditlevsen, D. K. *et al.* The role of phosphatidylinositol 3-kinase in neural cell adhesion molecule-mediated neuronal differentiation and survival. *J. Neurochem.* **84**, 546–556 (2003).
202. Klementiev, B. *et al.* A peptide agonist of the neural cell adhesion molecule (NCAM), C3, protects against developmental defects induced by a teratogen pyrimethamine. *Int. J. Dev. Neurosci.* **20**, 527–536 (2002).

203. Xu, R. *et al.* Screening of bioactive peptides using an embryonic stem cell-based neurodifferentiation assay. *AAPS J.* **16**, 400–412 (2014).
204. Kulahin, N. *et al.* Modulation of the homophilic interaction between the first and second Ig modules of neural cell adhesion molecule by heparin. *J. Neurochem.* **95**, 46–55 (2005).
205. Neiiendam, J. L. *et al.* An NCAM-derived FGF-receptor agonist, the FGL-peptide, induces neurite outgrowth and neuronal survival in primary rat neurons. *J. Neurochem.* **91**, 920–935 (2004).
206. Cambon, K. *et al.* A synthetic neural cell adhesion molecule mimetic peptide promotes synaptogenesis, enhances presynaptic function, and facilitates memory consolidation. *J. Neurosci.* **24**, 4197–4204 (2004).
207. Dallerac, G. *et al.* The neural cell adhesion molecule-derived peptide FGL facilitates long-term plasticity in the dentate gyrus in vivo. *Learn. Mem.* **18**, 306–313 (2011).
208. Knafo, S. *et al.* Facilitation of AMPA receptor synaptic delivery as a molecular mechanism for cognitive enhancement. *PLoS Biol.* **10**, e1001262 (2012).
209. Downer, E. J. *et al.* A synthetic NCAM-derived mimetic peptide, FGL, exerts anti-inflammatory properties via IGF-1 and interferon-gamma modulation. *J. Neurochem.* **109**, 1516–1525 (2009).
210. Hansen, R. K. *et al.* Identification of NCAM-binding peptides promoting neurite outgrowth via a heterotrimeric G-protein-coupled pathway. *J. Neurochem.* **103**, 1396–1407 (2007).
211. Pedersen, M. V. *et al.* Neuritogenic and survival-promoting effects of the P2 peptide derived from a homophilic binding site in the neural cell adhesion molecule. *J. Neurosci. Res.* **75**, 55–65 (2004).
212. Li, S. *et al.* Triple effect of mimetic peptides interfering with neural cell adhesion molecule homophilic cis interactions. *Biochemistry* **44**, 5034–5040 (2005).
213. Kohler, L. B., Soroka, V., Korshunova, I., Berezin, V. & Bock, E. A peptide derived from a trans-homophilic binding site in neural cell adhesion molecule induces neurite outgrowth and neuronal survival. *J. Neurosci. Res.* **88**, 2165–2176 (2010).
214. Kraev, I. *et al.* A peptide mimetic targeting trans-homophilic NCAM binding sites promotes spatial learning and neural plasticity in the hippocampus. *PLoS One* **6**, e23433 (2011).
215. Jacobsen, J., Kiselyov, V., Bock, E. & Berezin, V. A peptide motif from the second fibronectin module of the neural cell adhesion molecule, NCAM, NLIKQDDGGSPIRHY, is a binding site for the FGF receptor. *Neurochem. Res.* **33**, 2532–2539 (2008).
216. Hansen, S. M. M. *et al.* NCAM-derived peptides function as agonists for the fibroblast growth factor receptor. *J. Neurochem.* **106**, 2030–2041 (2008).

217. Hinsby, A. M., Berezin, V. & Bock, E. Molecular mechanisms of NCAM function. *Front. Biosci.* **9**, 2227–2244 (2004).
218. Francavilla, C. *et al.* Neural cell adhesion molecule regulates the cellular response to fibroblast growth factor. *J. Cell Sci.* **120**, 4388 LP – 4394 (2007).
219. Pedersen, S. *et al.* Fast Translation within the First 45 Codons Decreases mRNA Stability and Increases Premature Transcription Termination in *E. coli*. *J. Mol. Biol.* **431**, 1088–1097 (2019).
220. Hanson, G. & Collier, J. Codon optimality, bias and usage in translation and mRNA decay. *Nat. Rev. Mol. Cell Biol.* **19**, 20–30 (2018).
221. Tats, A., Remm, M. & Tenson, T. Highly expressed proteins have an increased frequency of alanine in the second amino acid position. *BMC Genomics* **7**, 28 (2006).
222. Lipońska, A., Ousalem, F., Aalberts, D. P., Hunt, J. F. & Boël, G. The new strategies to overcome challenges in protein production in bacteria. *Microb. Biotechnol.* **12**, 44–47 (2019).
223. Shemesh, R., Novik, A. & Cohen, Y. Follow the leader: preference for specific amino acids directly following the initial methionine in proteins of different organisms. *Genomics. Proteomics Bioinformatics* **8**, 180–189 (2010).
224. Christensen, T. *et al.* Fusion order controls expression level and activity of elastin-like polypeptide fusion proteins. *Protein Sci.* **18**, 1377–1387 (2009).
225. Hess, A.-K., Saffert, P., Liebeton, K. & Ignatova, Z. Optimization of Translation Profiles Enhances Protein Expression and Solubility. *PLoS One* **10**, e0127039 (2015).
226. Varshavsky, A. The N-end rule pathway and regulation by proteolysis. *Protein Sci.* **20**, 1298–1345 (2011).
227. Tobias, J. W., Shrader, T. E., Rocap, G. & Varshavsky, A. The N-end rule in bacteria. *Science* **254**, 1374–1377 (1991).
228. Teng, W., Cappello, J. & Wu, X. Recombinant silk-elastinlike protein polymer displays elasticity comparable to elastin. *Biomacromolecules* **10**, 3028–3036 (2009).
229. Lyons, R. E. *et al.* Design and facile production of recombinant resilin-like polypeptides: gene construction and a rapid protein purification method. *Protein Eng. Des. Sel.* **20**, 25–32 (2007).
230. McPherson, D. T., Xu, J. & Urry, D. W. Product purification by reversible phase transition following *Escherichia coli* expression of genes encoding up to 251 repeats of the elastomeric pentapeptide GVGVP. *Protein Expr. Purif.* **7**, 51–57 (1996).
231. Nakamura, M., Mie, M., Mihara, H., Nakamura, M. & Kobatake, E. Construction of a multi-functional extracellular matrix protein that increases number of N1E-115 neuroblast cells having

- neurites. *J. Biomed. Mater. Res. B. Appl. Biomater.* **91**, 425–432 (2009).
232. Culbertson, M. R. RNA surveillance. Unforeseen consequences for gene expression, inherited genetic disorders and cancer. *Trends Genet.* **15**, 74–80 (1999).
233. Dumon-Seignovert, L., Cariot, G. & Vuillard, L. The toxicity of recombinant proteins in *Escherichia coli*: a comparison of overexpression in BL21(DE3), C41(DE3), and C43(DE3). *Protein Expr. Purif.* **37**, 203–206 (2004).
234. Rogulin, E. A., Perevyazova, T. A., Zheleznyaya, L. A. & Matvienko, N. I. Plasmid pRARE as a Vector for Cloning to Construct a Superproducer of the Site-Specific Nickase N.BspD6I. *Biochem.* **69**, 1123–1127 (2004).
235. Lefebvre, J., Boileau, G. & Manjunath, P. Recombinant expression and affinity purification of a novel epididymal human sperm-binding protein, BSPH1. *Mol. Hum. Reprod.* **15**, 105–114 (2008).
236. Studier, F. W. & Moffatt, B. A. Use of bacteriophage T7 RNA polymerase to direct selective high-level expression of cloned genes. *J. Mol. Biol.* **189**, 113–130 (1986).
237. Hu, M.-C. & Chung, B. Expression of Human 21-Hydroxylase (P450c21) in Bacterial and Mammalian Cells: A System to Characterize Normal and Mutant Enzymes. *Mol. Endocrinol.* **4**, 893–898 (1990).
238. Moffatt, B. A. & Studier, F. W. T7 lysozyme inhibits transcription by T7 RNA polymerase. *Cell* **49**, 221–227 (1987).
239. O'Mahony, D. J. *et al.* The effect of phage T7 lysozyme on the production of biologically active porcine somatotropin in *Escherichia coli* from a gene transcribed by T7 RNA polymerase. *Gene* **91**, 275–279 (1990).
240. Chen, L., Zhou, M.-L., Qian, Z.-G., Kaplan, D. L. & Xia, X.-X. Fabrication of Protein Films from Genetically Engineered Silk-Elastin-Like Proteins by Controlled Cross-Linking. *ACS Biomater. Sci. Eng.* **3**, 335–341 (2017).
241. Pelton, J. T. & McLean, L. R. Spectroscopic Methods for Analysis of Protein Secondary Structure. *Anal. Biochem.* **277**, 167–176 (2000).
242. Barth, A. Infrared spectroscopy of proteins. *Biochim. Biophys. Acta - Bioenerg.* **1767**, 1073–1101 (2007).
243. Surewicz, W. K., Mantsch, H. H. & Chapman, D. Determination of protein secondary structure by Fourier transform infrared spectroscopy: a critical assessment. *Biochemistry* **32**, 389–394 (1993).

244. Hu, X., Kaplan, D. & Cebe, P. Determining Beta-Sheet Crystallinity in Fibrous Proteins by Thermal Analysis and Infrared Spectroscopy. *Macromolecules* **39**, 6161–6170 (2006).
245. Goormaghtigh, E., Ruyschaert, J.-M. & Raussens, V. Evaluation of the Information Content in Infrared Spectra for Protein Secondary Structure Determination. *Biophys. J.* **90**, 2946–2957 (2006).
246. Valentiner, U., Muhlenhoff, M., Lehmann, U., Hildebrandt, H. & Schumacher, U. Expression of the neural cell adhesion molecule and polysialic acid in human neuroblastoma cell lines. *Int. J. Oncol.* **39**, 417–424 (2011).
247. Eltoun, I., Fredenburgh, J., Myers, R. B. & Grizzle, W. E. Introduction to the Theory and Practice of Fixation of Tissues. *J. Histotechnol.* **24**, 173–190 (2001).
248. Wang, X., Ye, K., Li, Z., Yan, C. & Ding, J. Adhesion, proliferation, and differentiation of mesenchymal stem cells on RGD nanopatterns of varied nanospacings. *Organogenesis* **9**, 280–286 (2013).
249. Wang, X. *et al.* Effect of RGD nanospacing on differentiation of stem cells. *Biomaterials* **34**, 2865–2874 (2013).
250. Le Saux, G., Magenau, A., Böcking, T., Gaus, K. & Gooding, J. J. The Relative Importance of Topography and RGD Ligand Density for Endothelial Cell Adhesion. *PLoS One* **6**, e21869 (2011).
251. Le Saux, G. *et al.* Spacing of Integrin Ligands Influences Signal Transduction in Endothelial Cells. *Biophys. J.* **101**, 764–773 (2011).
252. Cavalcanti-Adam, E. A. *et al.* Cell Spreading and Focal Adhesion Dynamics Are Regulated by Spacing of Integrin Ligands. *Biophys. J.* **92**, 2964–2974 (2007).
253. Arnold, M. *et al.* Activation of integrin function by nanopatterned adhesive interfaces. *Chemphyschem* **5**, 383–388 (2004).
254. Cavalcanti-Adam, E. A. *et al.* Lateral spacing of integrin ligands influences cell spreading and focal adhesion assembly. *Eur. J. Cell Biol.* **85**, 219–224 (2006).
255. Cavallaro, U., Niedermeyer, J., Fuxa, M. & Christofori, G. N-CAM modulates tumour-cell adhesion to matrix by inducing FGF-receptor signalling. *Nat. Cell Biol.* **3**, 650–657 (2001).
256. Kos, F. J. & Chin, C. S. Costimulation of T cell receptor-triggered IL-2 production by Jurkat T cells via fibroblast growth factor receptor 1 upon its engagement by CD56. *Immunol. Cell Biol.* **80**, 364–369 (2002).
257. Sanchez-Heras, E., Howell, F. V., Williams, G. & Doherty, P. The fibroblast growth factor receptor acid box is essential for interactions with N-cadherin and all of the major isoforms of neural cell

- adhesion molecule. *J. Biol. Chem.* **281**, 35208–16 (2006).
258. Francavilla, C. *et al.* The binding of NCAM to FGFR1 induces a specific cellular response mediated by receptor trafficking. *J. Cell Biol.* **187**, 1101–1116 (2009).
259. Sørensen, H. P. & Mortensen, K. K. Advanced genetic strategies for recombinant protein expression in *Escherichia coli*. *J. Biotechnol.* **115**, 113–128 (2005).
260. Chung, C. T., Niemela, S. L. & Miller, R. H. One-step preparation of competent *Escherichia coli*: transformation and storage of bacterial cells in the same solution. *Proc. Natl. Acad. Sci.* **86**, 2172–2175 (1989).

Este trabalho foi financiado por fundos nacionais através da FCT – Fundação para a Ciência e a Tecnologia, I.P., no âmbito do projeto "FunBioPlas - Novel synthetic biocomposites for biomedical devices" com referência ERA-IB-2-6/0004/2014.



7. Annexes and Appendixes

Annex I – Competent cells

Protocol for *E. coli* XL1-Blue

- From an overnight culture (10 mL), inoculate 400 μ L in 10 μ L of LB medium. Incubate at 37 °C, 180 rpm until an $OD_{600} = 0.3$;
- Inoculate 4 ml from previous culture into 10 ml LB medium. Incubate at 37 °C, 180 rpm until reach $OD_{600} = 0.3$;
- Incubate on ice for 5 min;
- Discard the supernatant and gently resuspend the pellet in 20 ml cold TFBI;
- Centrifuge at 2500 rpm for 5 min at 4 °C;
- Discard supernatant and gently resuspend pellet in 20 mL cold TFBI;
- Incubate on ice for 5 min;
- Store cells in 100 μ L aliquots in previously cooled microtubes;
- Freeze cells in liquid nitrogen and store at -80 °C.

TFBI (50 mL)

- 0.147 g KOAc
- 0.495 g $MnCl_2$
- 0.06 g RbCl
- 0.735 g $CaCl_2$
- 7.5 g glycerol
- Optimize the pH to 5.8 with CH_3COOH
- Adjust volume to 50 mL with dH_2O

TFBII (50 mL)

- 0.105 g NaMOPS
- 0.551 g $CaCl_2$
- 0.060 g RbCl
- 7.5 g glycerol
- Optimize the pH to 6.5 with NaOH
- Adjust volume to 50 mL with dH_2O

Protocol for *E. coli* BL21 (DE3)

- Grow 5 mL of desired *E. coli* strain overnight at 37 °C in LB medium (supplemented with antibiotics if necessary) to stationary phase;
- Dilute the overnight culture 1:100 in fresh LB and grow with vigorous shaking at 37 °C until $OD_{600nm}=0.6$;
- Incubate on ice for 10 min;
- Spin down cells at 15000 x g for 10 min at 4 °C;
- Resuspend the pellet gently in 32 mL of ice-cold TB buffer (considering 100 mL of culture volume) and incubate for 10 min on ice;
- Spin down cells at 15000 x g for 10 min at 4 °C;
- Resuspend the pellet gently in 8 mL of ice-cold TB buffer and add DMSO to final concentration of 7 % with gently swirling;
- Incubate on ice for 10 min;
- Dispense cell suspension in 200 μ L aliquots and immediately flash-freeze in liquid N₂.

TB buffer (50 mL)

- 0.119 g HEPES
- 0.110 g CaCl₂
- 0.932 g KCl
- 0.544 g MnCl₂
- Optimize the pH to 6.7 with KOH
- Adjust volume to 50 mL with dH₂O

Annex II - Plasmids

pET25b(+) plasmid

Created with SnapGene®

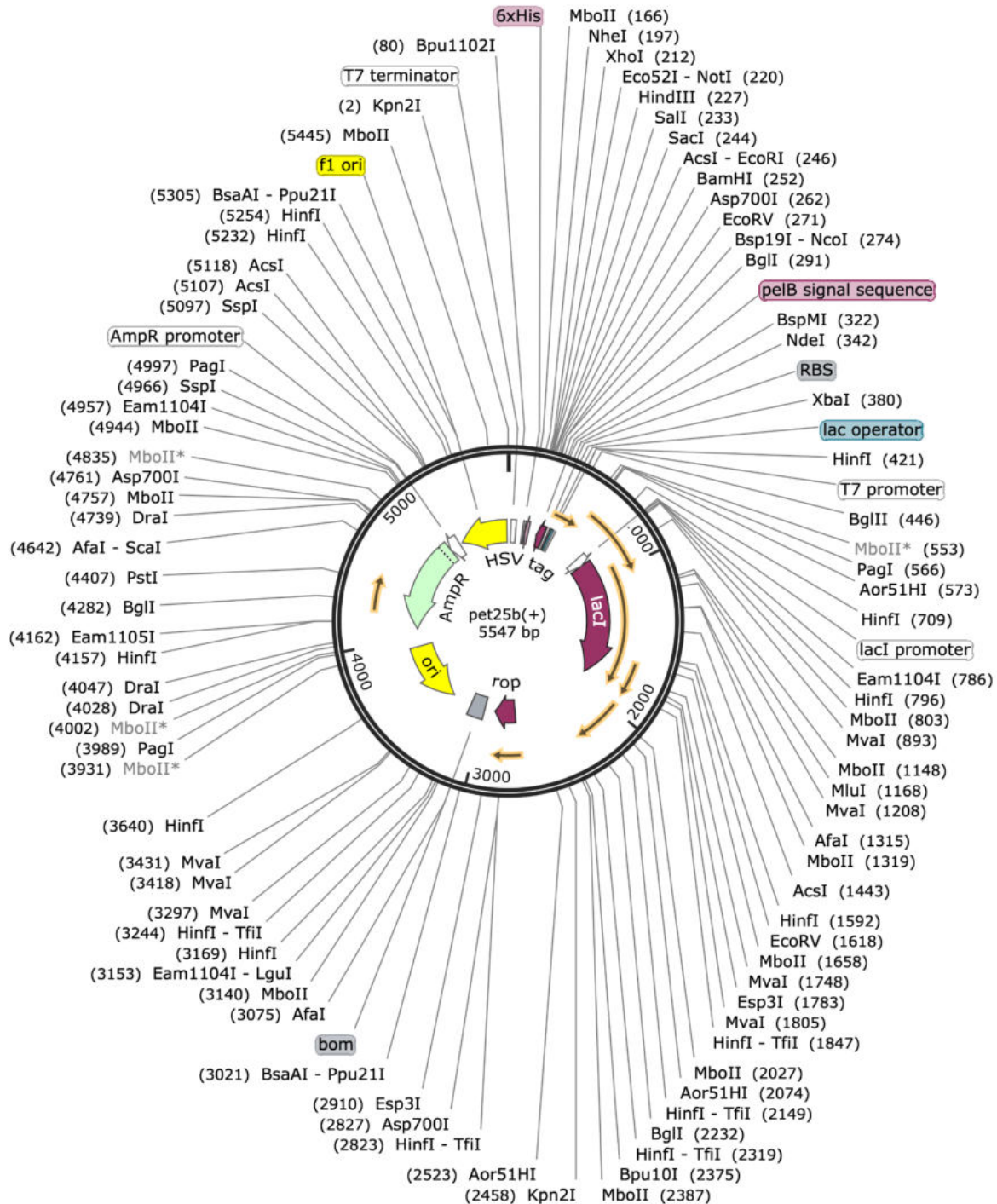


Figure 43. Schematic representation of pET25b(+) plasmid.

pCM13::*SELP-59A* plasmid

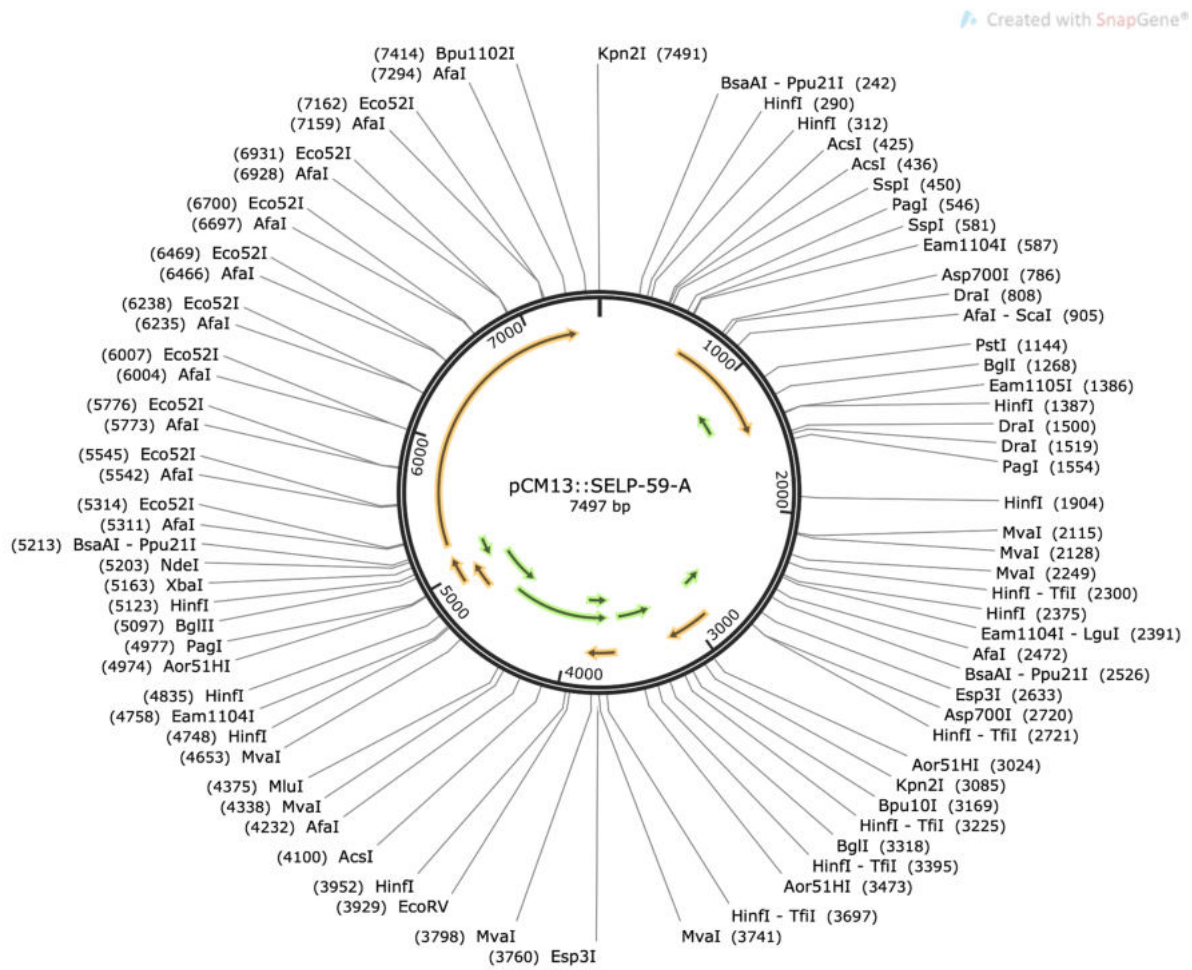


Figure 44. Schematic representation of pCM13::*SELP-59A* plasmid.

pLysE plasmid

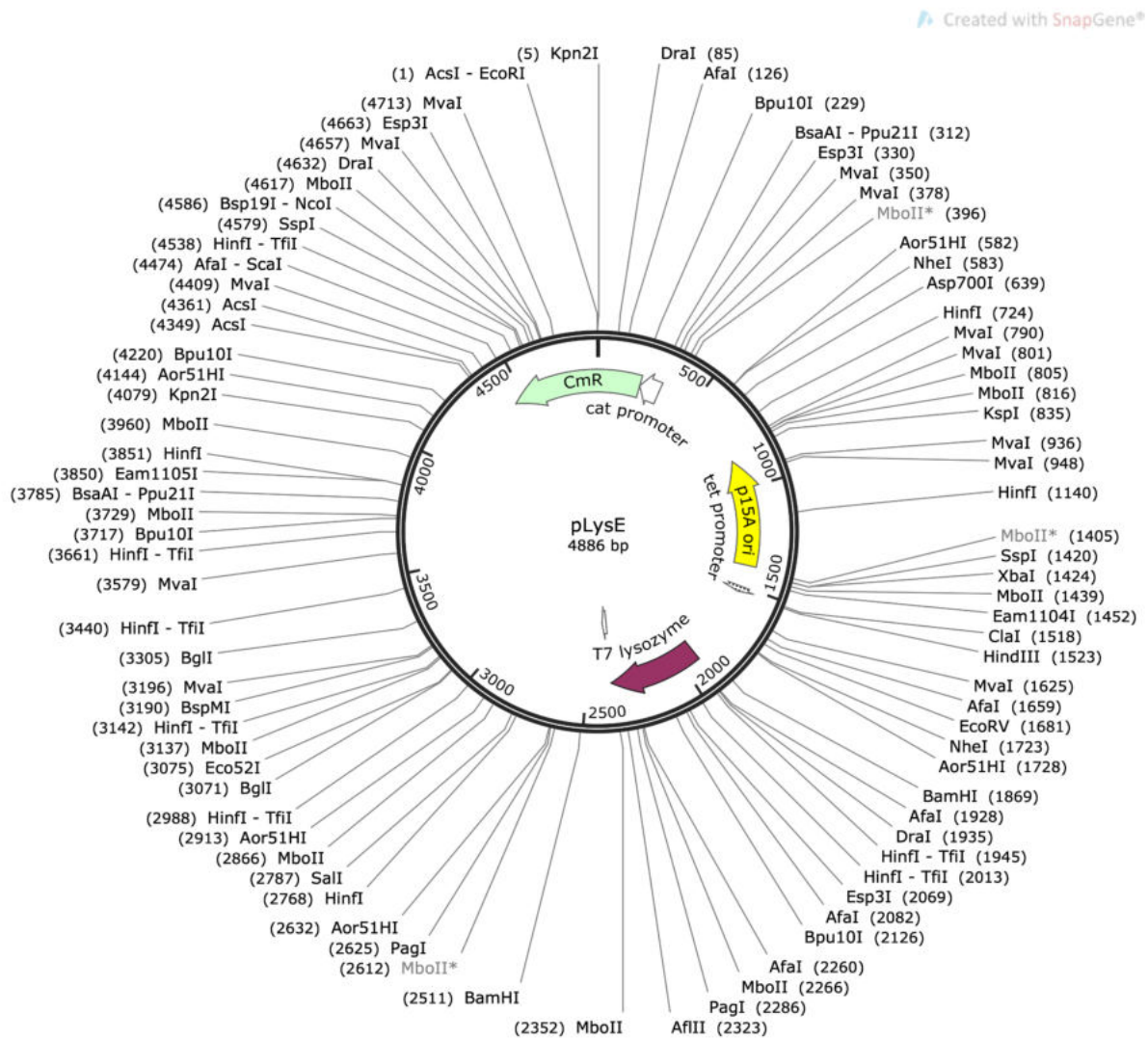


Figure 45. Schematic representation of pLysE plasmid.

pRARE plasmid

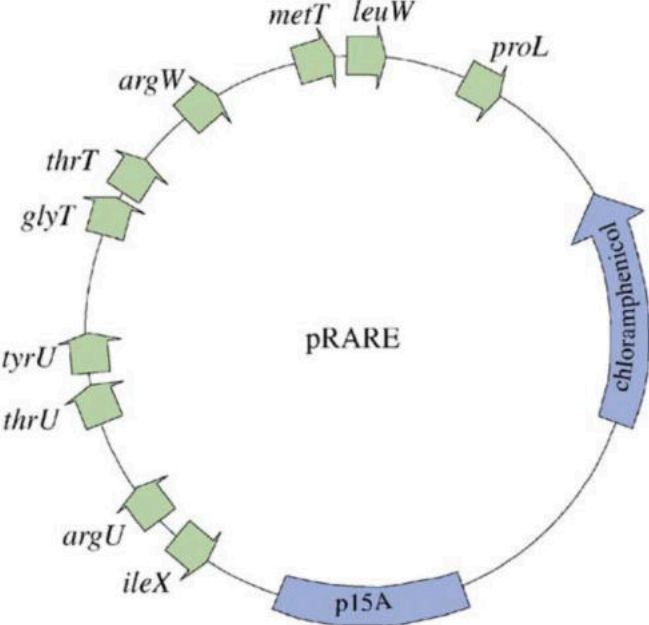


Figure 46. Schematic representation of pRARE plasmid. Reproduced from ²⁵⁹.

pDrive::*SELP-59A* plasmid

Created with SnapGene®

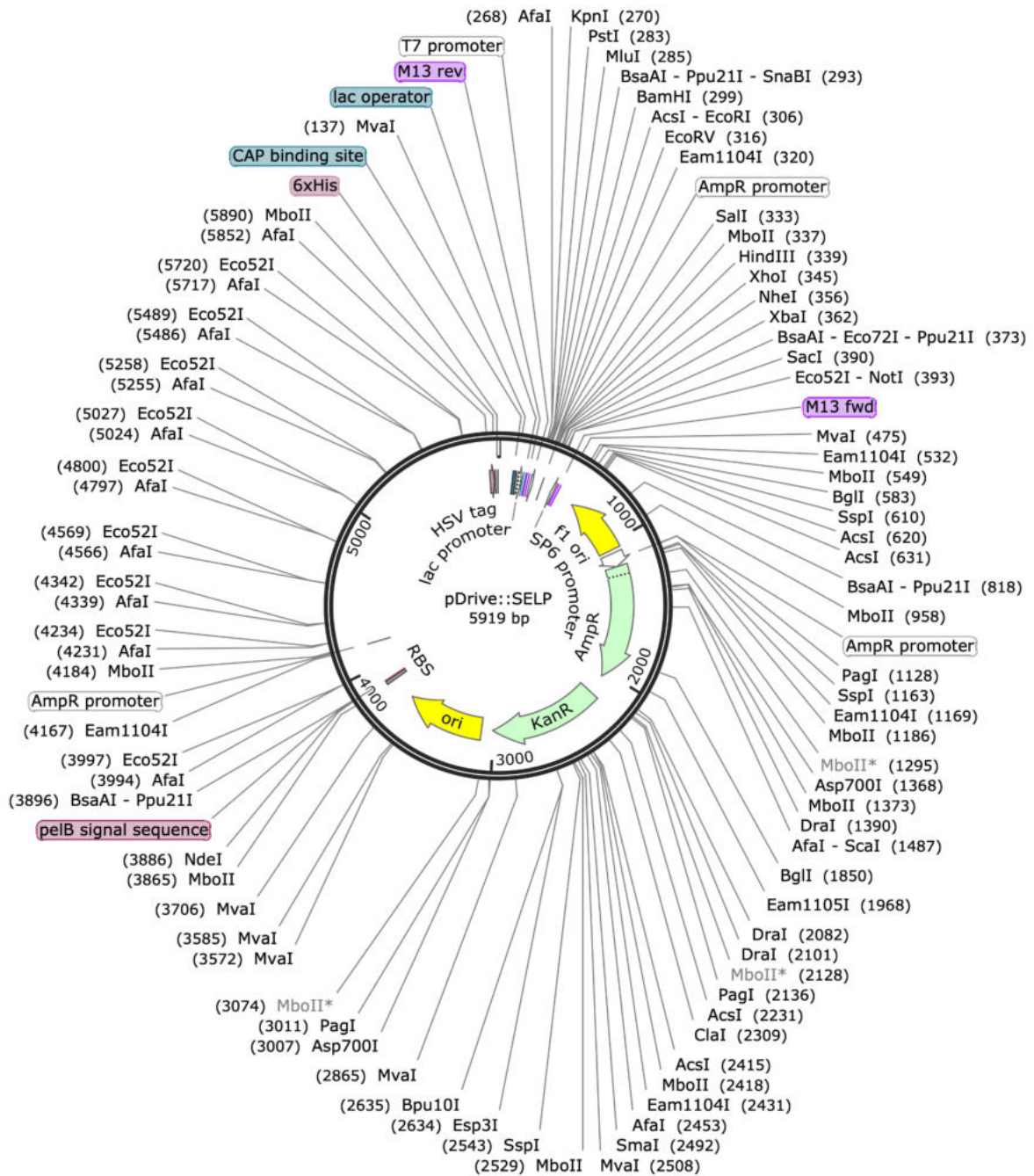


Figure 47. Schematic representation of pDrive::*SELP-59A* plasmid.

pET25::*adapter* plasmid

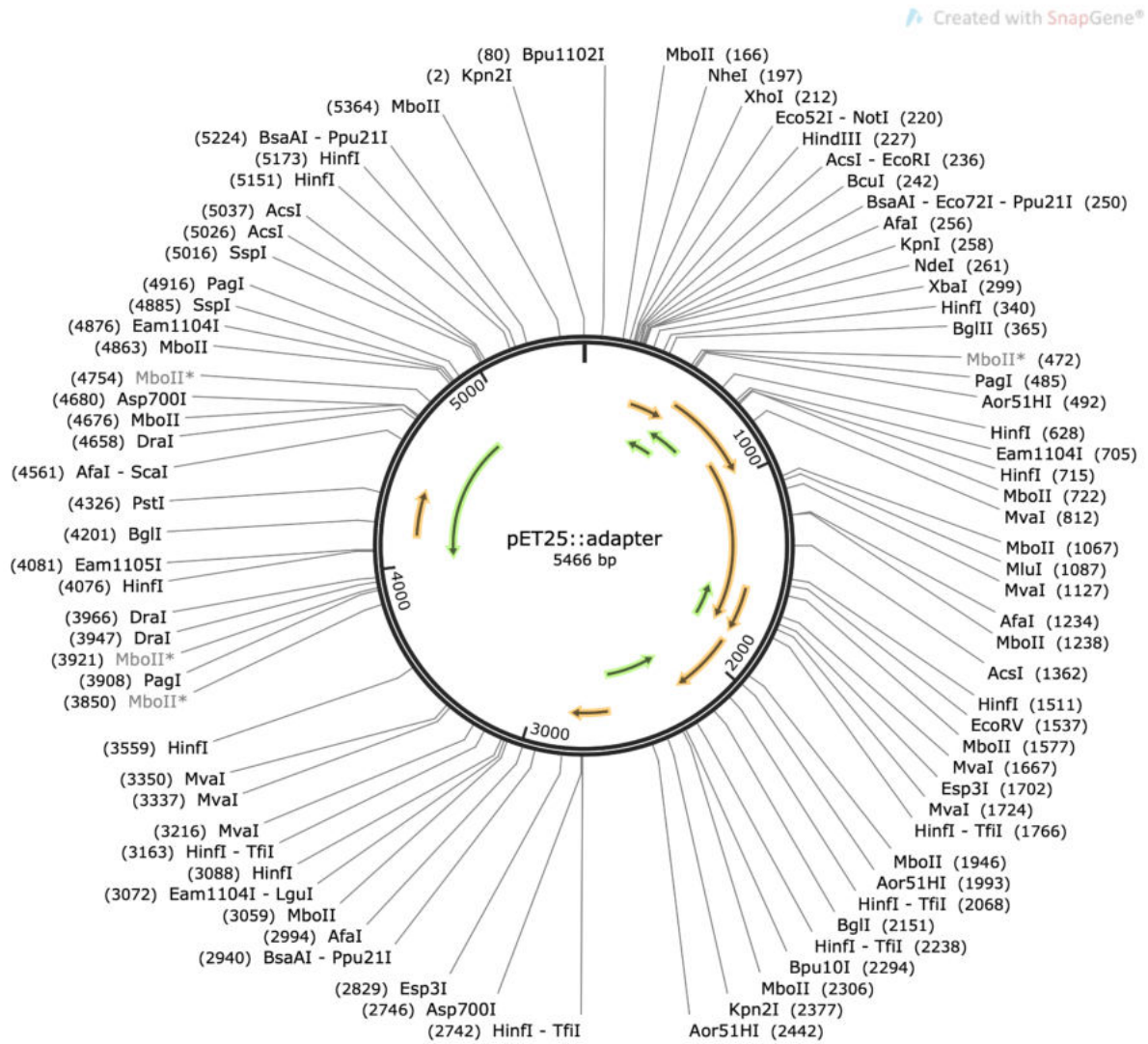


Figure 48. Schematic representation of pET25::*adapter* plasmid.

pET25::*SELP-59-A* plasmid

Created with SnapGene®

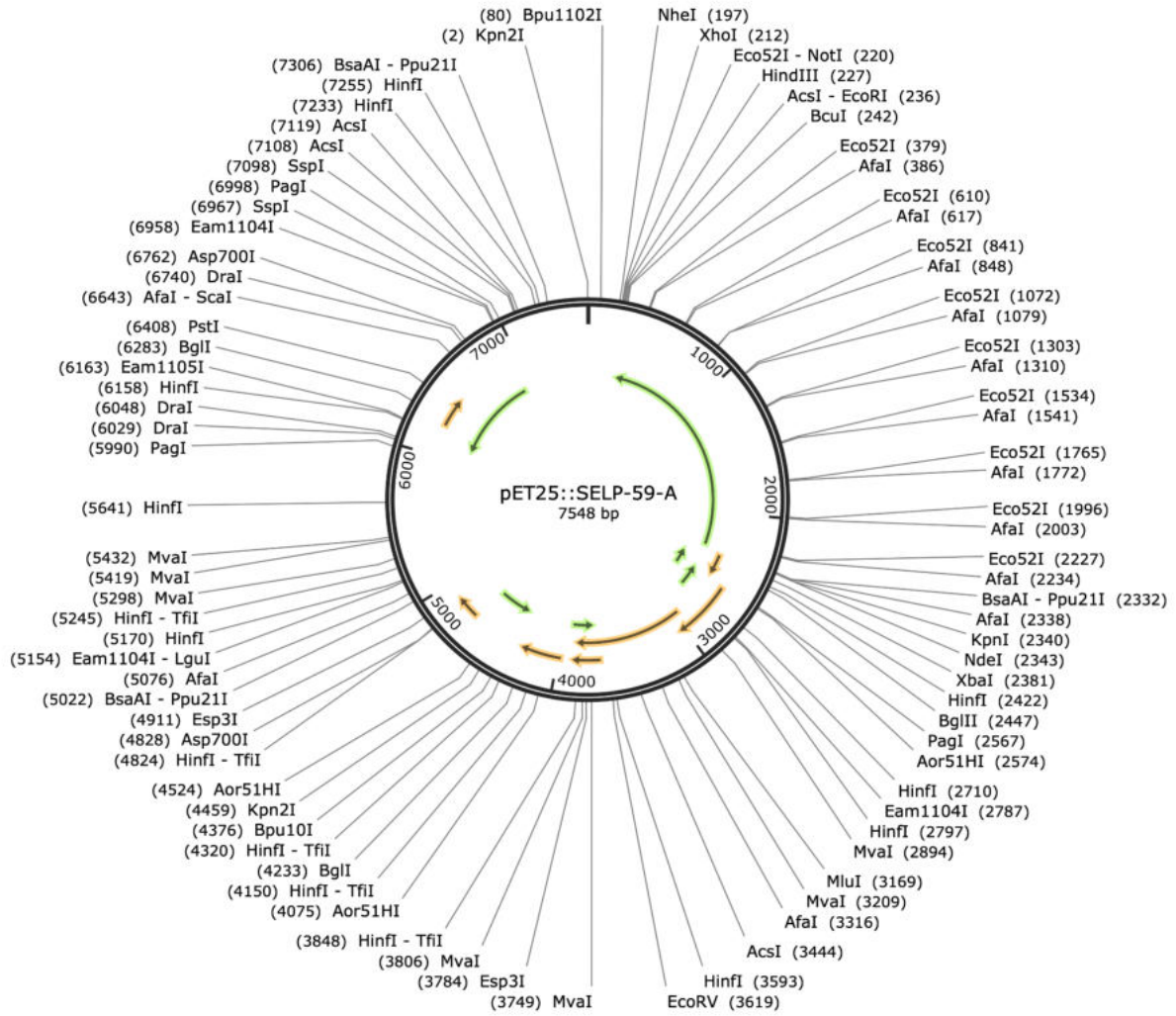


Figure 49. Schematic representation of pET25::*SELP-59-A* plasmid.

pET25::*SELP-59-A+SELP-59-A* plasmid

Created with SnapGene®

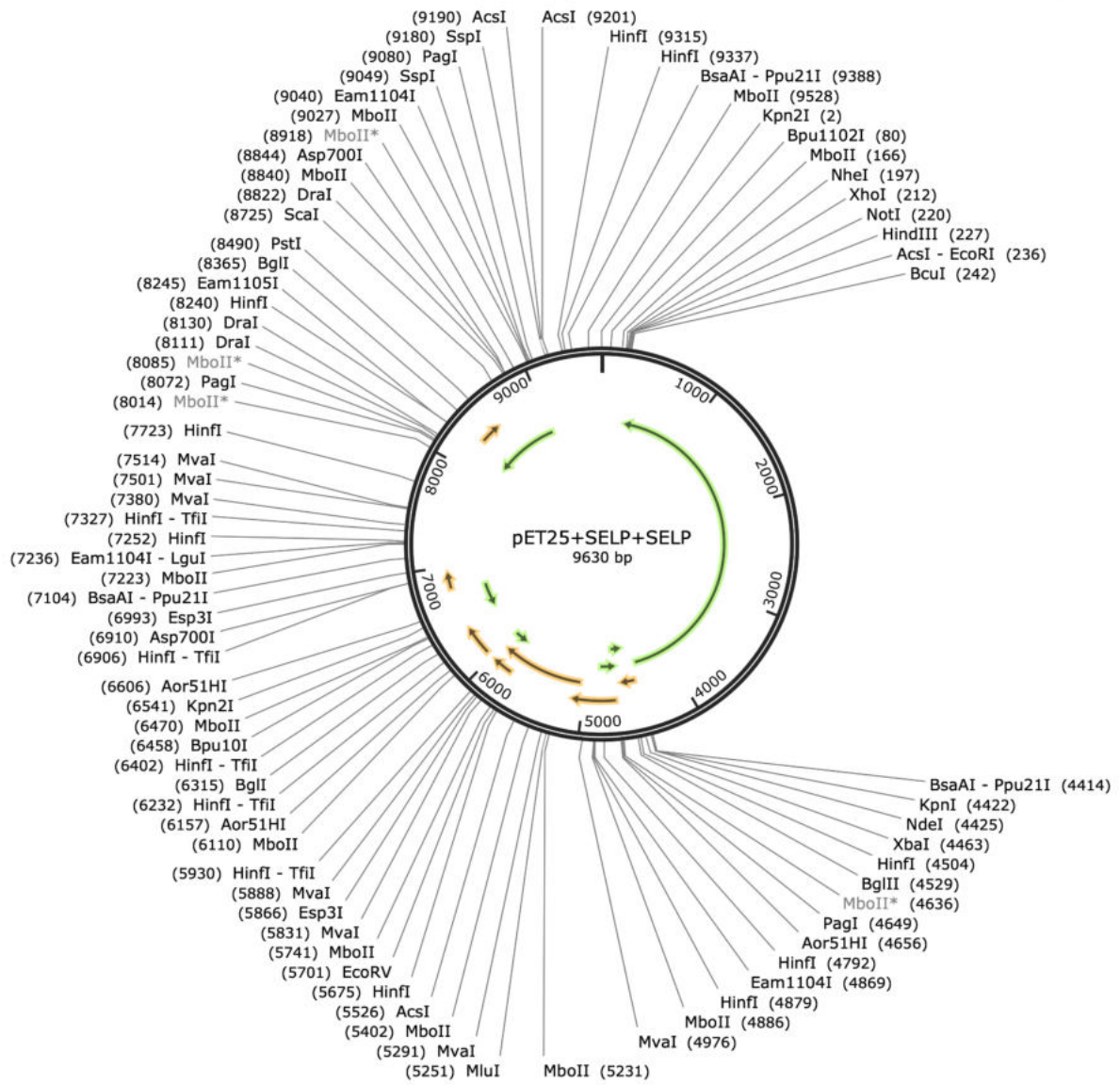


Figure 50. Schematic representation of pET25::*SELP-59-A+SELP-59-A* plasmid.

pET25::*SELP-59-A_nC3* plasmid

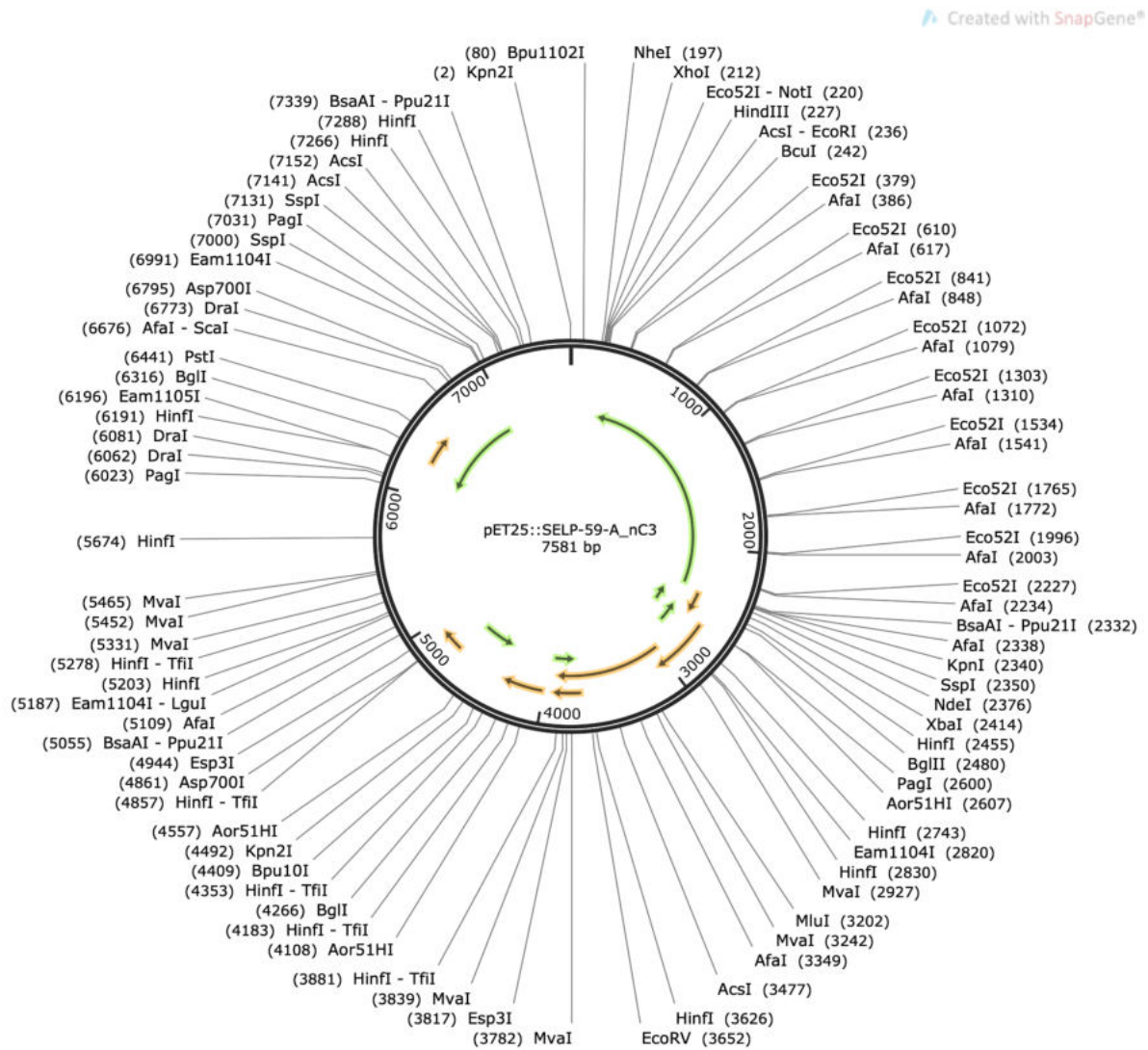


Figure 51. Schematic representation of pET25::*SELP-59-A_nC3* plasmid.

pET25::*SELP-59-A_c3* plasmid

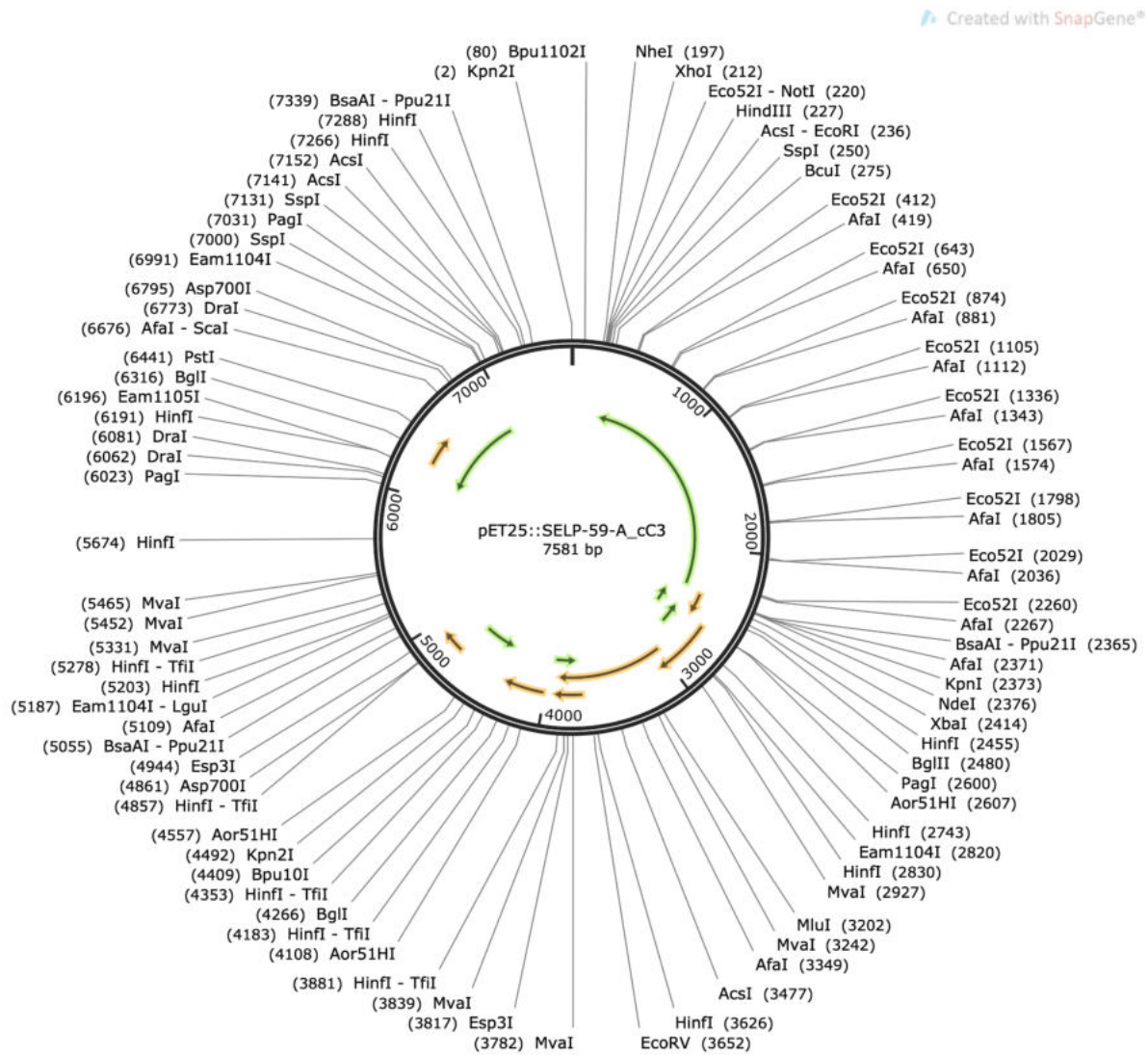


Figure 52. Schematic representation of pET25::*SELP-59-A_c3* plasmid.

pET25::*SELP-59-A_nRGD* plasmid

Created with SnapGene®

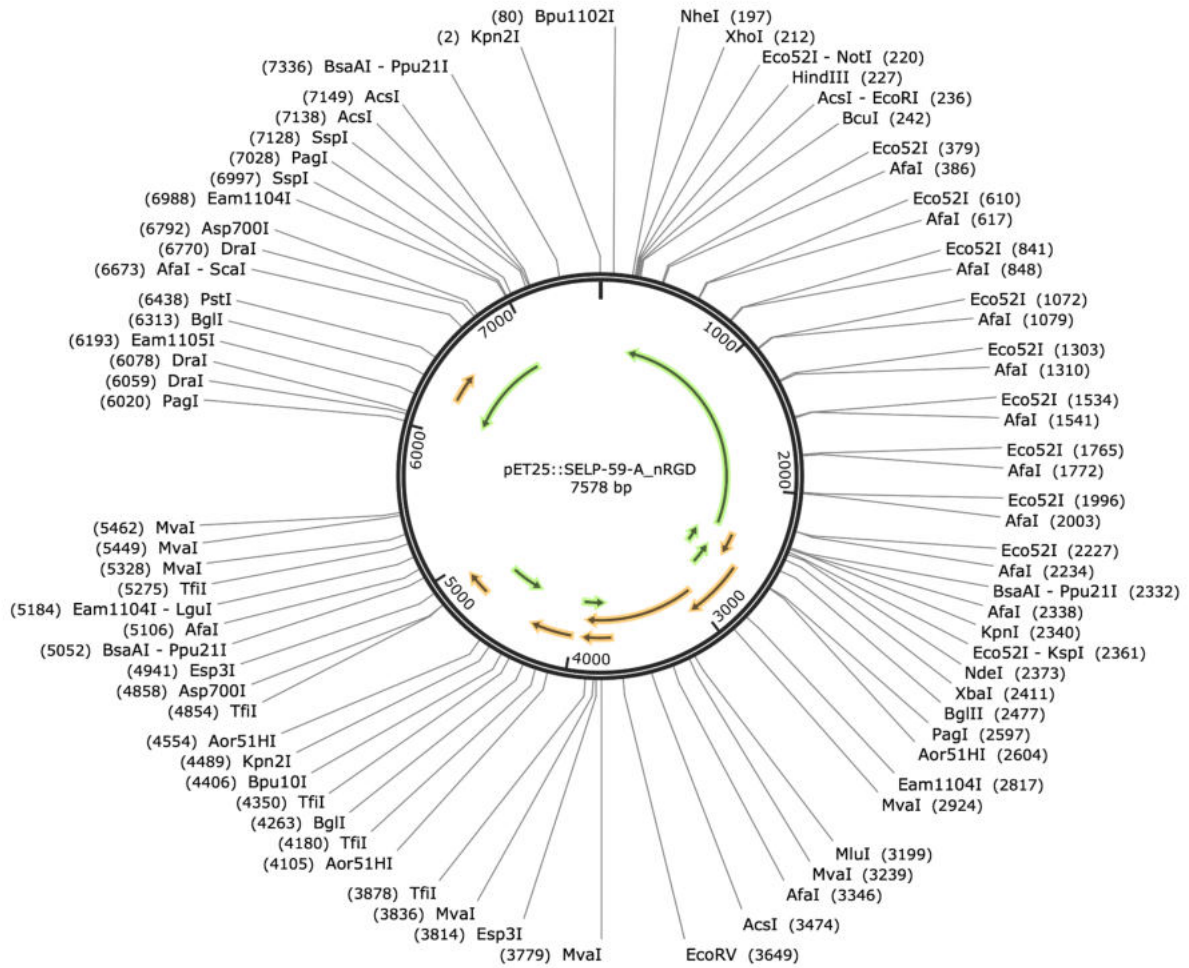


Figure 53. Schematic representation of pET25::*SELP-59-A_nRGD* plasmid.

pET25::*SELP-59-A_cRGD* plasmid

Created with SnapGene®

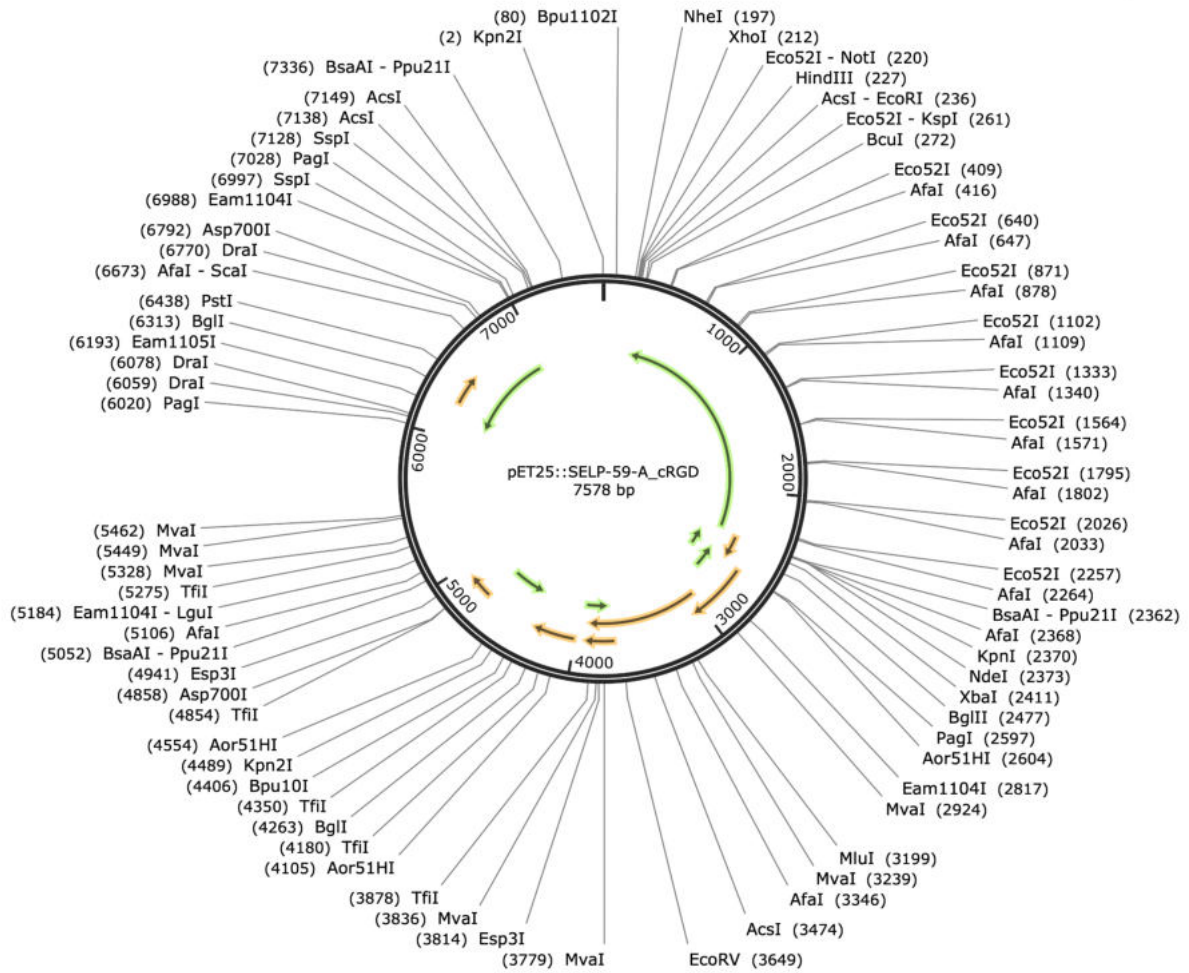


Figure 54. Schematic representation of pET25::*SELP-59-A_cRGD* plasmid.

Annex III – Culture media and solutions

LB medium

- 10 g tryptone
- 5 g yeast extract
- 5 g NaCl
- Adjust volume to 1 L with dH₂O

TB medium

- 12 g tryptone
- 24 g yeast extract
- 8 g glycerol
- 50 mL phosphate solution 20x
- Adjust volume to 950 mL dH₂O

Phosphate solution 20x (500 mL)

- 23.14 g KH₂PO₄
- 125.41 g K₂HPO₄
- Adjust volume to 500 mL with dH₂O

TBlac medium

- 12 g tryptone
- 24 g yeast extract
- 8 g glycerol
- 50 mL phosphate solution 20x
- 50 mL lactose solution 20x
- 900 mL dH₂O

Phosphate solution 20x (500 mL)

- 23.14 g KH_2PO_4
- 125.41 g K_2HPO_4
- Adjust volume to 500 mL with dH_2O

Lactose solution 20x (500 mL)

- 20 g lactose
- Adjust volume to 500 mL with dH_2O

TAE 50x (1L)

- 242 g Tris
- 57.1 mL Glacial acetic acid
- 18.6 g EDTA
- Adjust volume to 1 L with dH_2O

PBS 10x (1 L)

- 12.0 g Na_2HPO_4
- 2.4 g KH_2PO_4
- 80 g NaCl
- 2 g KCl
- Adjust volume to 1 L with dH_2O

Annex IV – Cell transformation protocols

TSS method (adapted from ²⁶⁰)

- Pre-inoculum of bacterium at 37 °C 200 rpm, overnight;
- In the next day, read the optical density (OD_{600nm}) and optimize the OD to 0.1 in tubes of 50 mL containing 10 mL of LB medium;
- Put the tubes at 37 °C, 200 rpm until achieve the $OD_{600nm} = 0.3-0.4$. Here, put the tubes on ice for 5 min;
- Transfer culture for a 2 mL microtube;
- Centrifuge the cultures at 1100 x g, 10 min at 4 °C. Reject the supernatant and resuspend the pellet in 1 mL of 4 °C TSS 1x;
- Add 1 μ L of plasmid (1-10 ng). Wait 1 h on ice;
- Give a heat shock at 42 °C for 2 min;
- Stop heat shock by immersion on ice for 2 min;
- After, 1 mL of warm LB is added, and the suspension is incubated 1 h at 37 °C at 200 rpm;
- 50-200 μ L of the transformation mix is plated in LB agar plus the antibiotic (see table 6);
- Incubate for 16-20 h at 37 °C.

TSS 1x (20 mL)

- 2 g PEG MW 3350;
- 1 mL DMSO pure for molecular biology;
- 95 mg $MgCl_2$;
- 19 mL LB medium;
- Optimize the pH to 6.5
- Sterilize by filtration.

Heat shock protocol

- Defrost competent cells on ice;
- Add 100 ng of DNA to the competent cells and left for 30 min at 4 °C;
- Give a heat shock at 42 °C for 1 min;
- Take off samples from bath and place them into ice for 10 min;
- Then, using flame to create a sterile atmosphere, add 800 µL of LB medium into each microtube;
- After that, microtubes incubate at 37 °C, 200 rpm, for 1 h;
- Centrifuge samples for 1 min at 14000 x g;
- Discard 900 µL of supernatant. Resuspend the volume left using up-down pipette move;
- Pipette 100 µL of final sample and spread into plates. Incubate for an overnight period at 37 °C.

Annex V – DNA sequencing

pET25::adapter sequencing

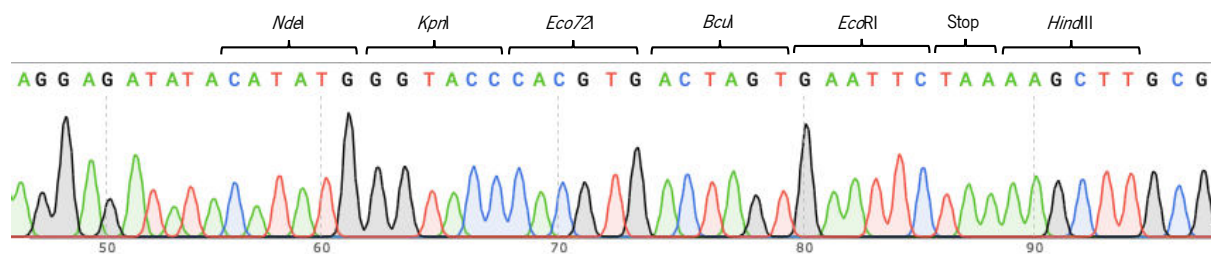


Figure 55. pET25::adapter sequencing chromatogram using T7 promoter primer.

pET25::*SELP-59-A* sequencing

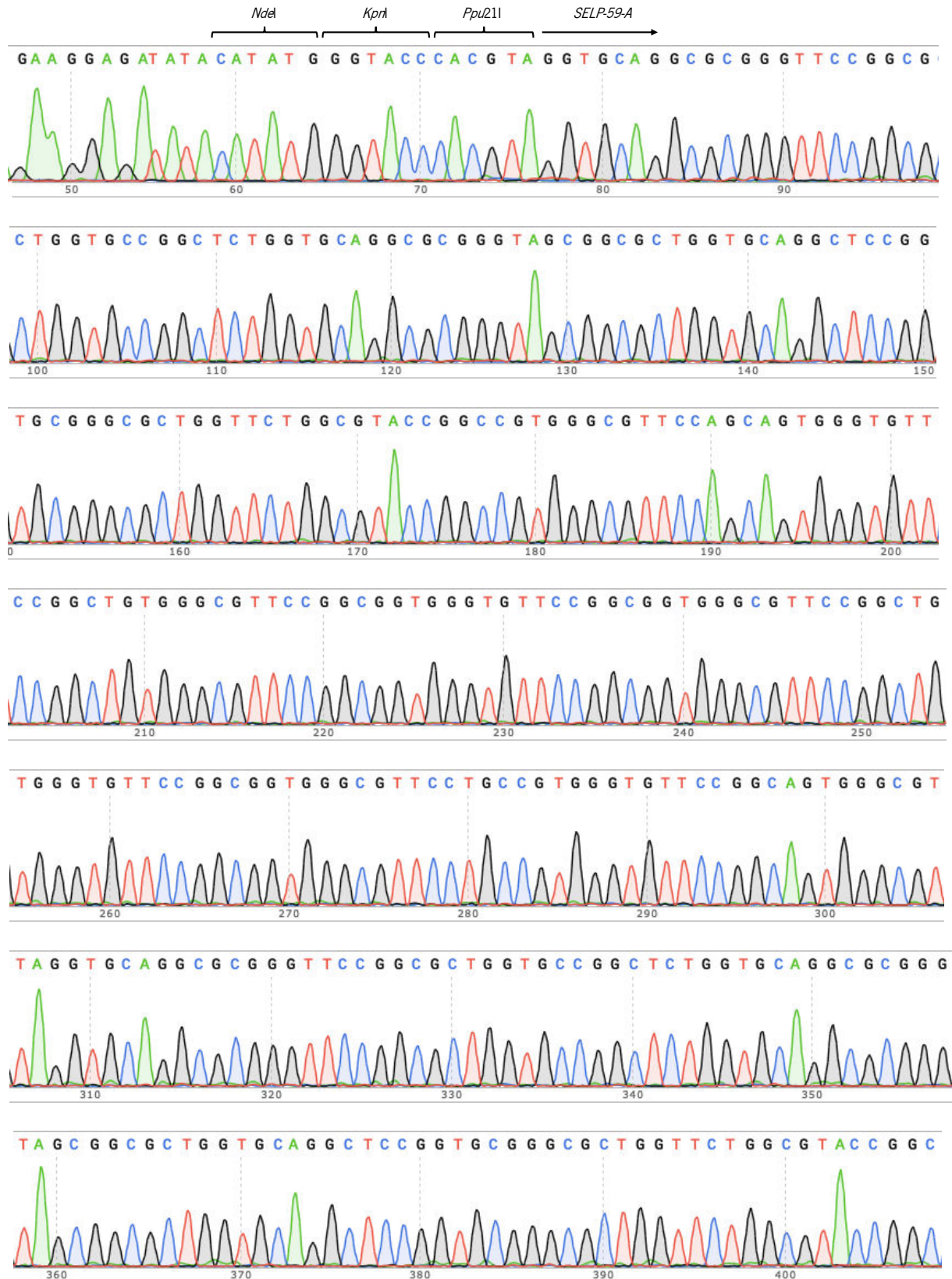


Figure 56. pET25::*SELP-59-A* sequencing chromatogram using T7 promoter primer.

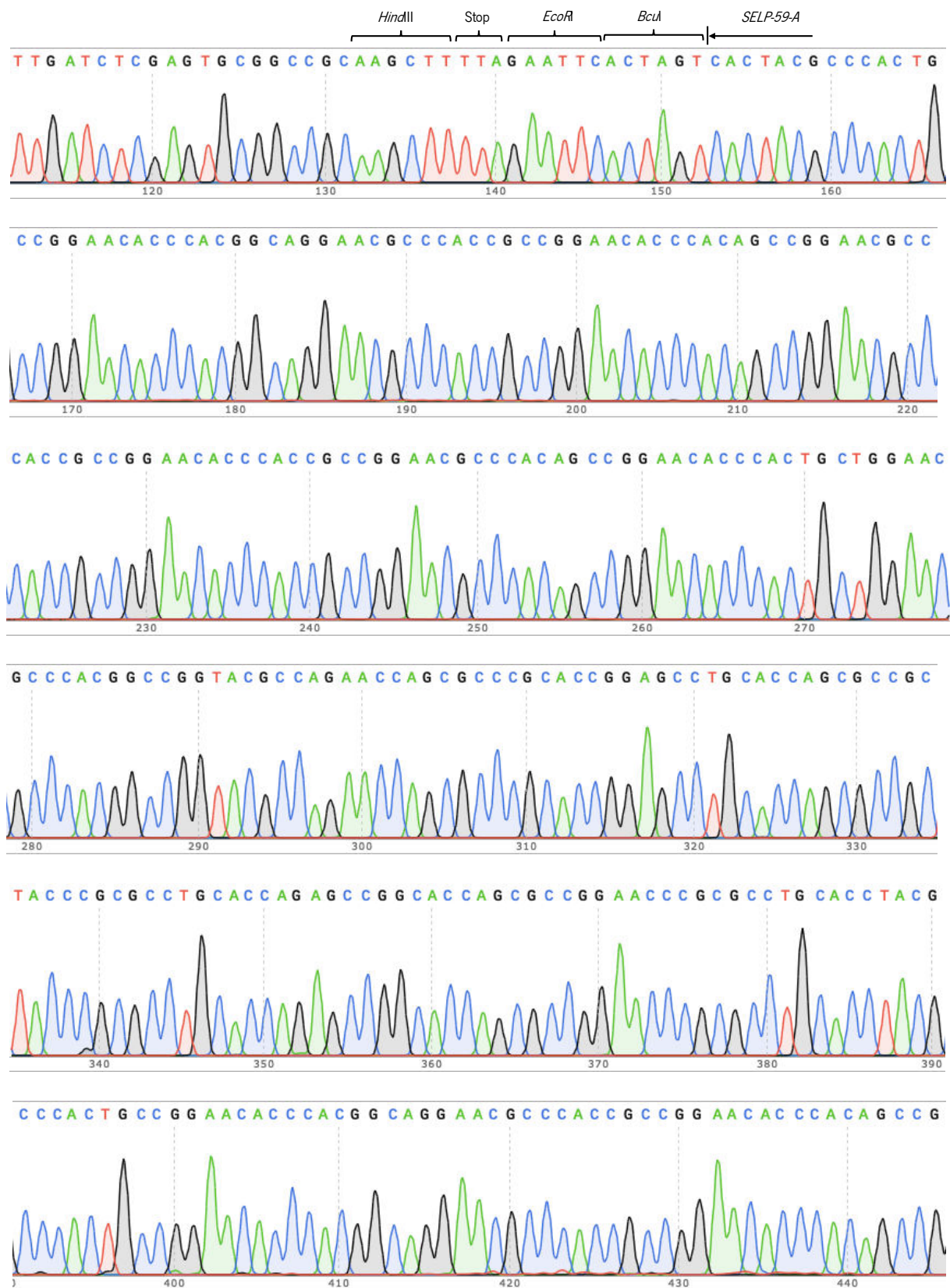


Figure 57. pET25::*SELP-59A* sequencing chromatogram using T7 terminator primer.

SELP-59-A double insertion (pET25::*SELP-59-A+SELP-59-A*) sequencing

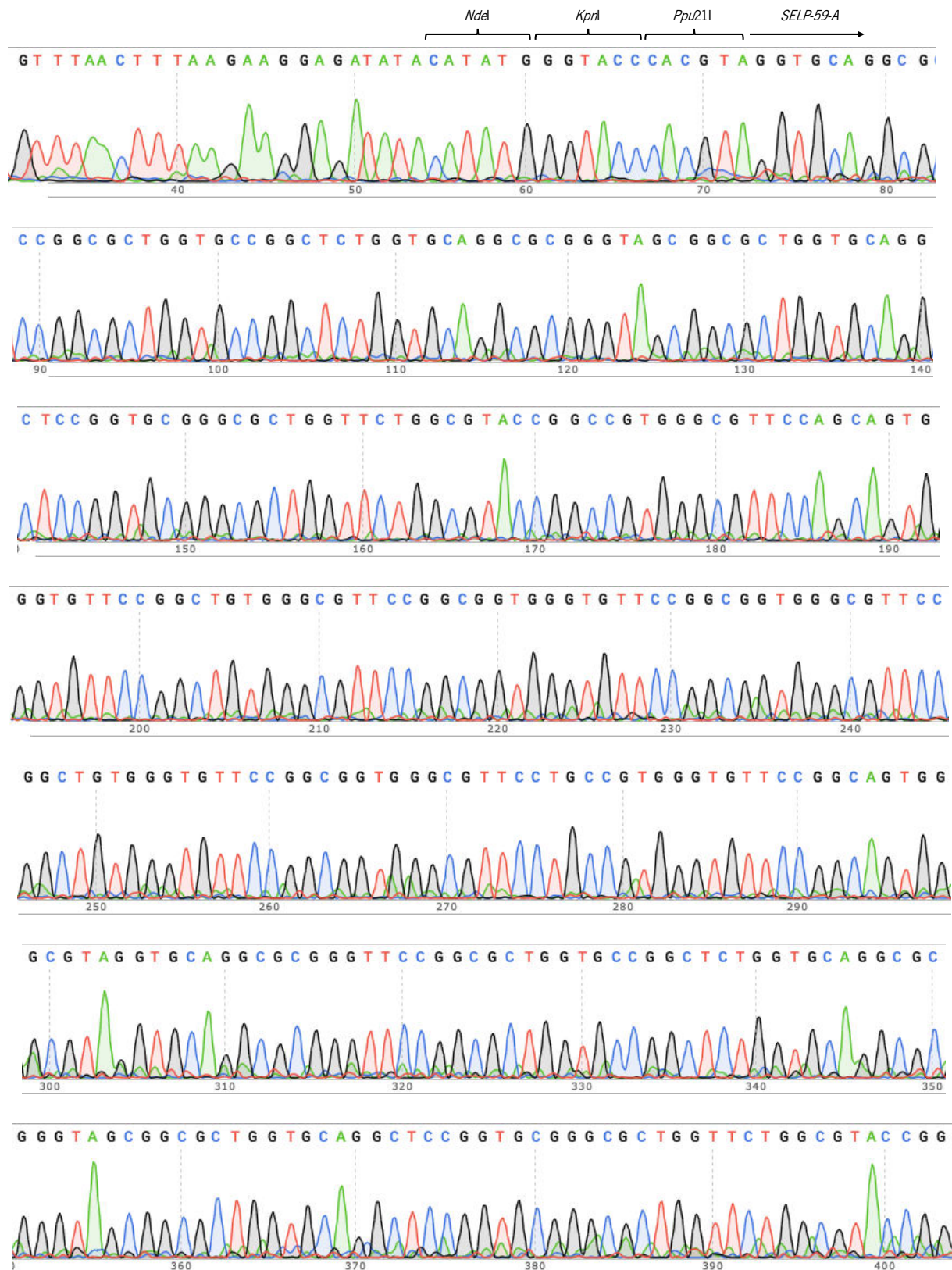


Figure 58. pET25::*SELP-59-A+SELP-59-A* (double insertion) sequencing chromatogram using T7 promoter primer.

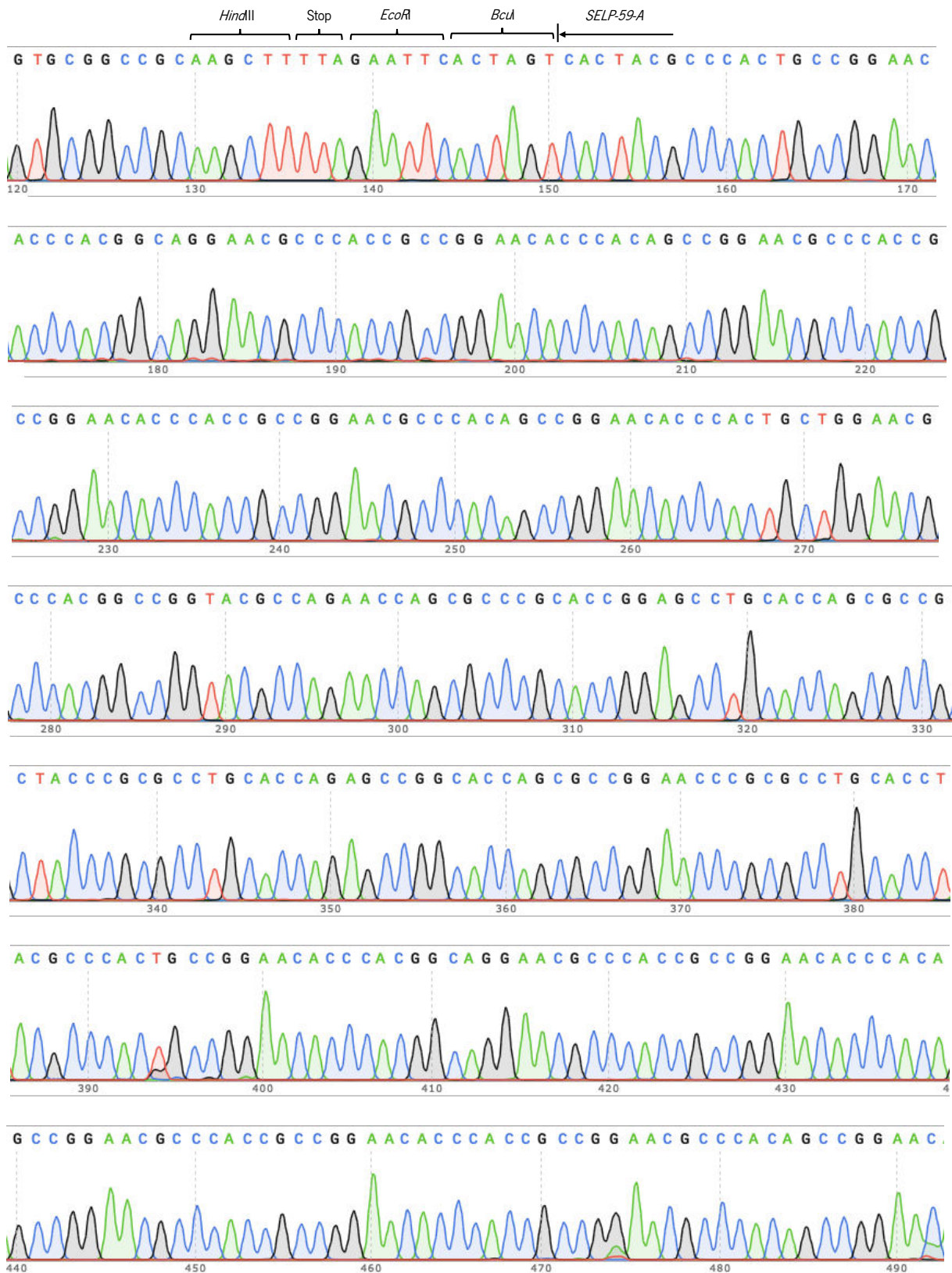


Figure 59. pET25::*SELP-59-A*+*SELP-59-A* (double insertion) sequencing chromatogram using T7 terminator primer.

pET25::*SELP-59-A_nC3* sequencing

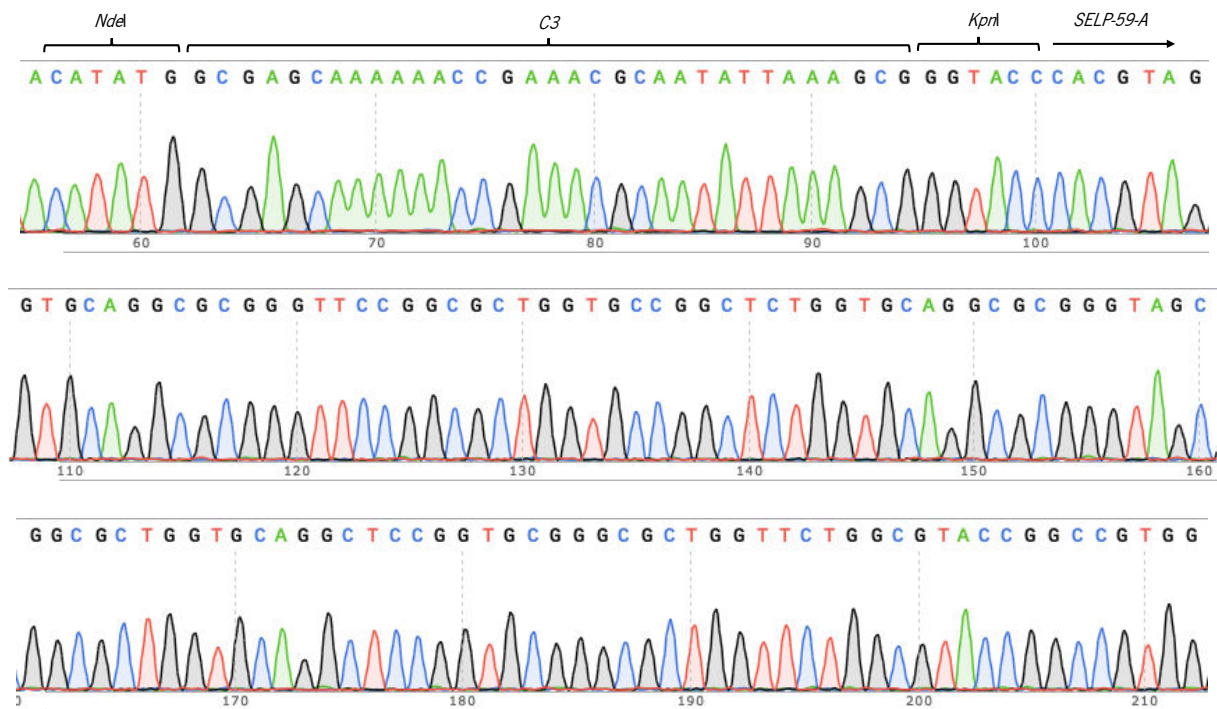


Figure 60. pET25::*SELP-59-A_nC3* sequencing chromatogram using T7 promotor primer.

pET25::*SELP-59A_cC3* sequencing

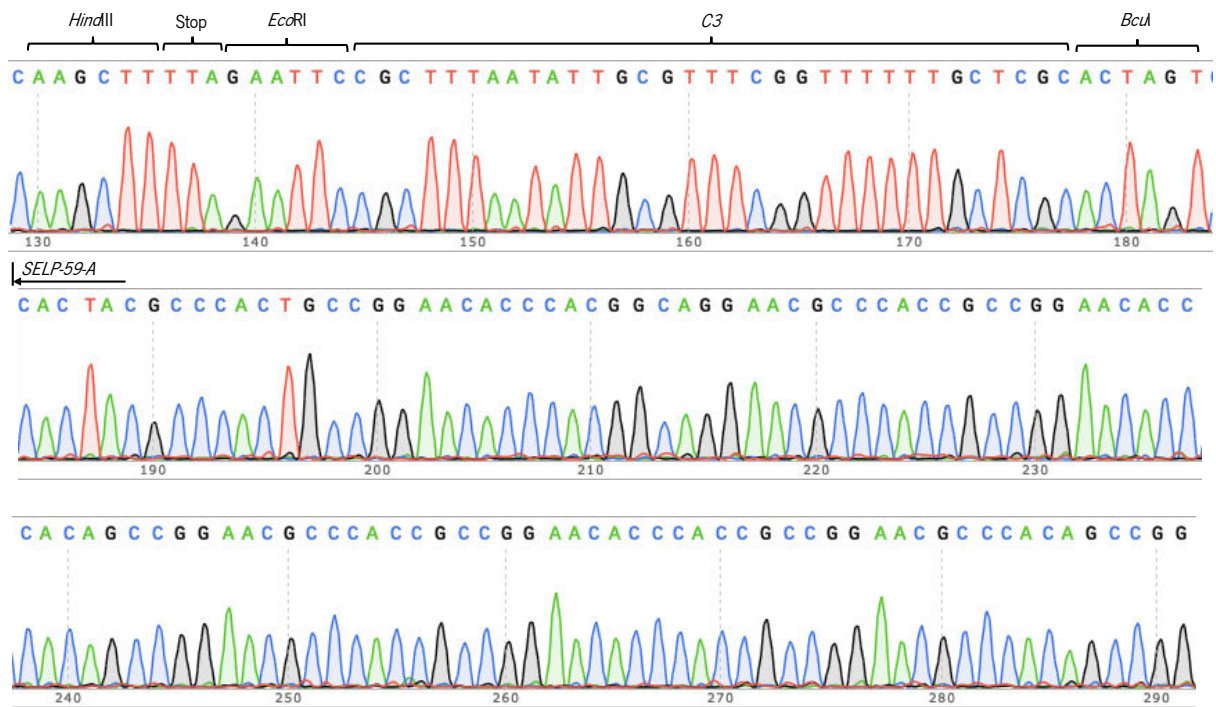


Figure 61. pET25::*SELP-59A_cC3* sequencing chromatogram using T7 terminator primer.

pET25::*SELP-59-A_nRGD* sequencing

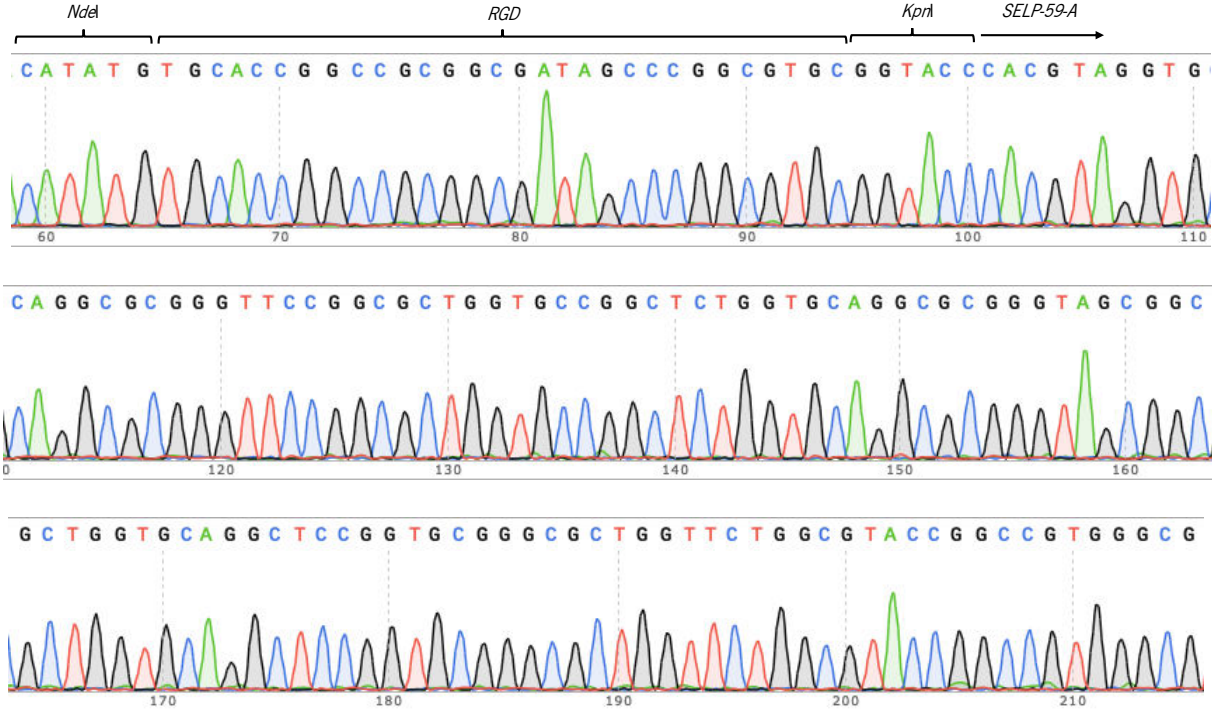


Figure 62. pET25::*SELP-59-A_nRGD* sequencing chromatogram using T7 promotor primer.

pET25::*SELP-59-A_cRGD* sequencing

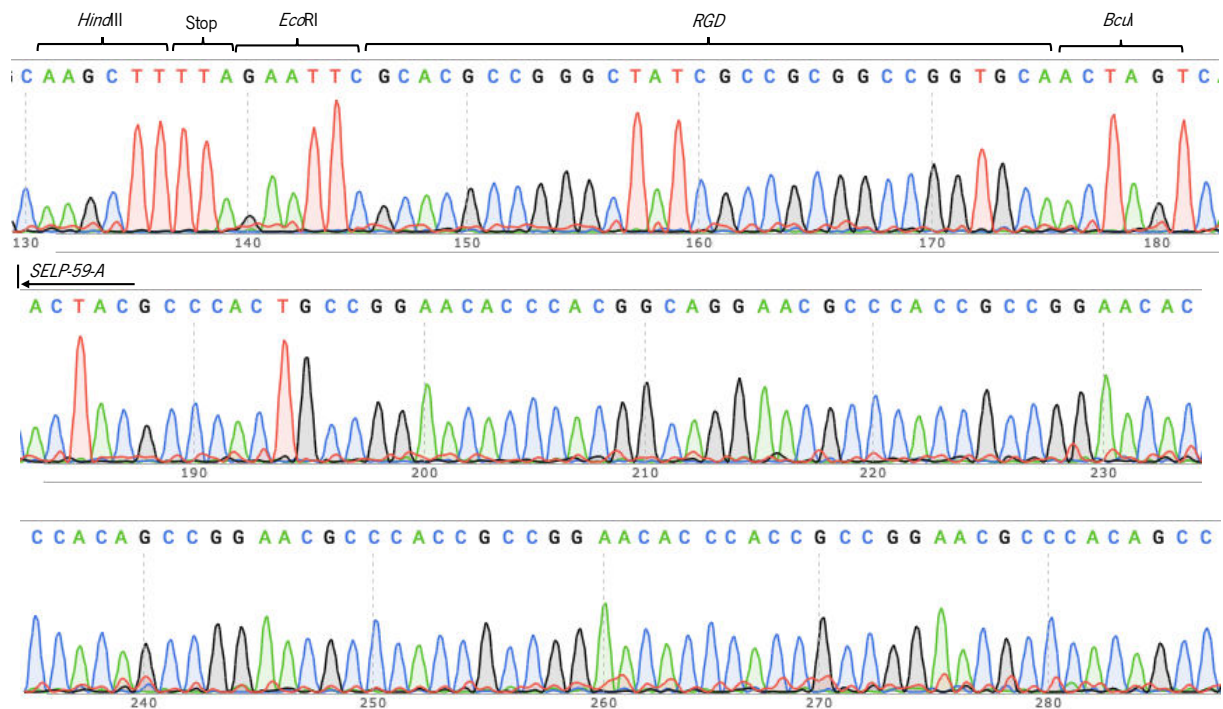


Figure 63. pET25::*SELP-59-A_cRGD* sequencing chromatogram using T7 terminator primer.

Appendix I – ATR-FTIR absorbance spectra

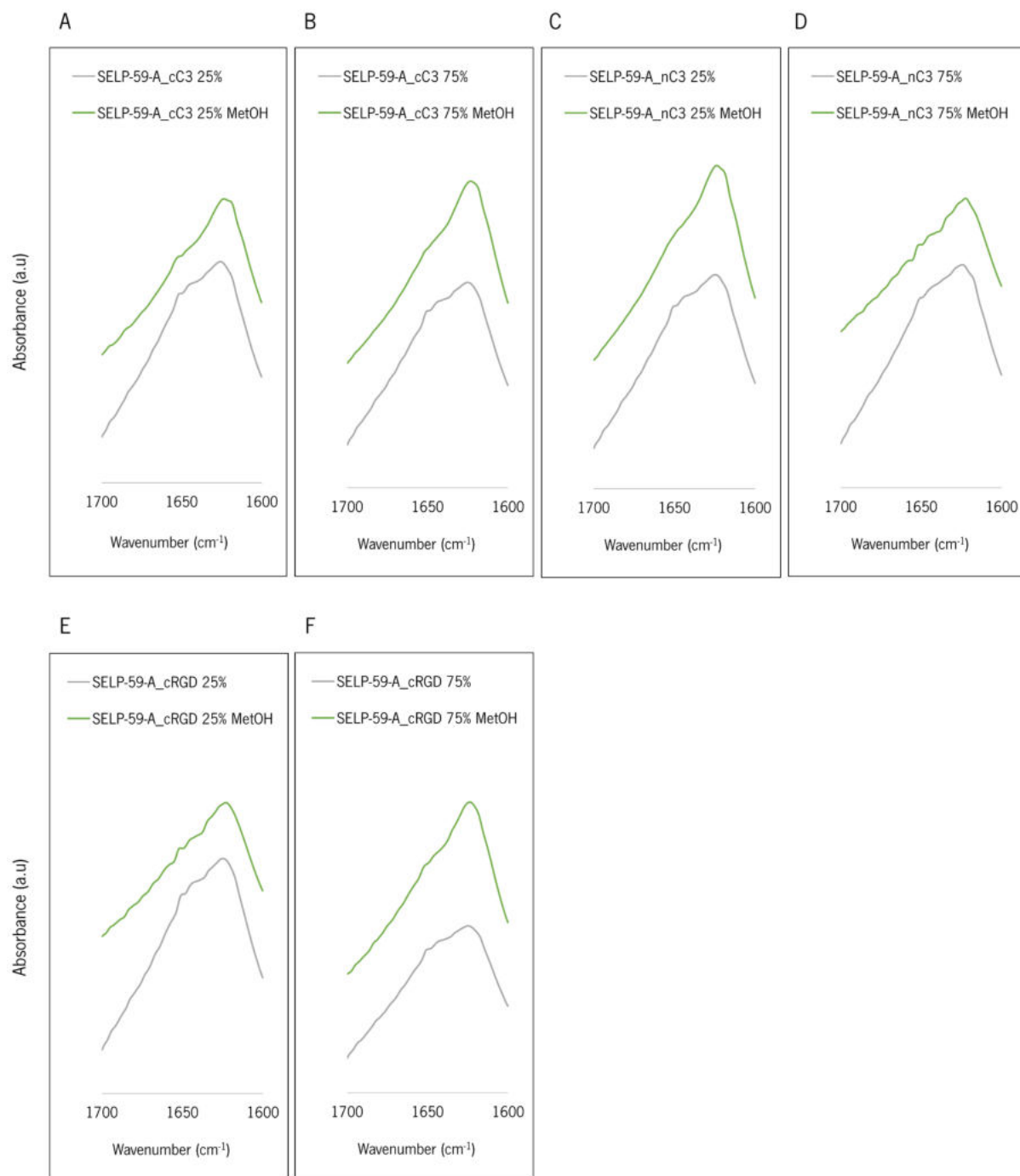


Figure 64. Experimentally determined ATR-FTIR absorbance spectra for amide I region for the non-treated and methanol saturated air-treated SELP-59-A_CAM 75%, SELP-59-A_CAM 25% films.